NONLINEARLY REGENERATED LONG HAUL DATA TRANSMISSION

ASHLEY GRAY

Doctor of Philosophy

ASTON UNIVERSITY

January 2006

ASTON UNIVERSITY

NONLINEARLY REGENERATED LONG HAUL DATA TRANSMISSION

ASHLEY GRAY

Doctor of Philosophy

January 2006

Thesis Summary

This thesis experimentally examines the use of different techniques for optical fibre transmission over ultra long haul distances. Its format firstly examines the use of dispersion management as a means of achieving long haul communications. Secondly, examining the use concatenated NOLMs for DM autosoliton ultra long haul propagation, by comparing their performance with a generic system without NOLMs. Thirdly, timing jitter in concatenated NOLM system is examined and compared to the generic system and lastly issues of OTDM amplitude non-uniformity from channel to channel in a saturable absorber, specifically a NOLM, are raised.

Transmission at a rate of 40Gbit/s is studied in an all-Raman amplified standard fibre link with amplifier spacing of the order of 80km. We demonstrate in this thesis that the detrimental effects associated with high power Raman amplification can be minimized by dispersion map optimization. As a result, a transmission distance of 1600 km (2000km including dispersion compensating fibre) has been achieved in standard single mode fibre.

The use of concatenated NOLMs to provide a stable propagation regime has been proposed theoretically. In this thesis, the observation experimentally of autosoliton propagation is shown for the first time in a dispersion managed optical transmission system. The system is based on a strong dispersion map with large amplifier spacing. Operation at transmission rates of 10, 40 and 80Gbit/s is demonstrated. With an insertion of a stabilizing element to the NOLM, the transmission of a 10 and 20Gbit/s data stream was extended and demonstrated experimentally. Error-free propagation over 100 and 20 thousand kilometers has been achieved at 10 and 20Gbit/s respectively, with terrestrial amplifier spacing.

The monitoring of timing jitter is of importance to all optical systems. Evolution of timing jitter in a DM autosoliton system has been studied in this thesis and analyzed at bit rates from 10Gbit/s to 80Gbit/s. Non-linear guiding by in-line regenerators considerably changes the dynamics of jitter accumulation.

As transmission systems require higher data rates, the use of OTDM will become more prolific. The dynamics of switching and transmission of an optical signal comprising individual OTDM channels of unequal amplitudes in a dispersion-managed link with in-line non-linear fibre loop mirrors is investigated.

Acknowledgements

Whilst I was at Aston University, I found the people there helpful, friendly and willing to accommodate any situation. I would like to thank Zhijian Huang for his friendship and by being my mentor, as he took time to show me many of the techniques involved in optical communications engineering. Thanks go to my supervisor Igor Khrushchev.

I must also thank work colleagues and friends Dave Norman, Jim Harrison, Keith Blow, Ian Bennion, Sergei Turisyn, Robin Ibbottson and Yak Wan Andy Lee for advice and counselling.

Special thanks go to Kim for her support over the last four years.

Contents

List of Tables

List of Figures

GLOSSARY

AOM Acoustic Optical Modulator

AM Amplitude Modulation

ASK Amplitude-Shift Keying

ASEF Amplified Spontaneous Emission Filter

BPF Band Pass Filter

BER Bit Error Rate

BERT Bit Error Rate Tester

CW Continuous Wave

XPM Cross Phase Modulation

dB Decibels

DEMUX Demultiplexer

DPSK Differential-Phase Shift Keying

DSO Digital Sampling Oscilloscope

DCF Dispersion Compensating Fibre

DMS Dispersion Managed Solitons

DSF Dispersion Shifted Fibre

DRA Distributed Raman Amplification

DRBS Double Rayleigh Back-Scattering

ESA Electrical Spectrum Analyizer

EAM Electro Absorption Modulator

EDFA Erbium Doped Fibre Amplifier

FWM Four Wave Mixing

FWHM Full Width at Half Maximum

GH Gordon-Haus timing jitter

GVD Group Velocity Dispersion

ISI Inter-Symbol Interference

ISO Isolator

MZ Mach-Zender interferometer

MUX Multiplexer

MPI Multi-Path Interference

NOLM Non-Linear Optical Loop Mirror

NLSE Non-Linear Schrödinger Equation

NRZ Non-Return-to-Zero

OSA Optical Spectral Analyizer

OSNR Optical Signal to Noise Ratio

OTDM Optical Time Division Multiplexing

PSK Phase-Shift Keying

PC Polarization Controller

PMD Polarization-Mode Dispersion

RF Radio Frequency

RIN Relative Intensity Noise

RZ Return-to-Zero

RMS Root Mean Squared

SHG Second Harmonic Generation

SPM Self Phase Modulation

SMF Single Mode Fibre

SBS Stimulated Brillouin Scattering

SRS Stimulated Raman Scattering

VOA Variable Optical Attenuator

WDM Wavelength Division Multiplexing

Chapter 1 Introduction

The expansion of the Internet has resulted in greater bandwidth being demanded from the telecom industry. The need for extra bandwidth is highlighted acutely at the metro area networks, long-haul area networks and the transoceanic optical fibre links, as these are the main arteries of the telecommunication network. These core level optical fibre links are generally hundreds to thousands of kilometres long spanning cities, continents and oceans.

There are standard techniques that can be utilized to gain extra bandwidth in the optical fibre, such as wavelength division multiplexing (WDM) or optical time division multiplexing (OTDM). OTDM is used in all the experiments discussed in this thesis.

The design of long haul communications systems depend on the amplification type and spacing, dispersion map and the need to maintain pulse integrity throughout the fibre span. The regeneration of optical pulses is usually achieved electronically, but the increased demand for higher rates of data regeneration means this will need to be achieved optically if the expansion of the Internet is to reach its full potential.

The most cost effective type of optical regeneration is re-amplification and re-shaping, (2R regeneration). This method of regeneration can employ passive optical components, such as fibre or semiconductor based saturable absorbers. 3R regeneration is the more costly option as complex retiming solutions are needed. The cost of achieving clock recovery using electronic means may become prohibitive at higher data rates, over longer distances, as many regenerators may be required.

The work presented in this thesis is based on the concepts of linear and non-linear optics, propagation, and transmission theory. The main body of the work is experimental long haul quasi-linear pulse propagation with Raman amplification and in later chapters non-linear elements are used to guide propagation. All these systems are then tested with the resultant effects documented.

1.1 Historical Background

The first quasi-digital transmission system was Morse code, where the duration of an electrical signal was used to distinguish between 'on' and 'off'. It was by this method that the worlds first transatlantic telecommunication link was produced.

The transmission of light along a waveguide through the phenomenon of total internal reflection (Snell's Law) was discovered by J. Tyndall in 1854. However, until the 1950s there was neither a suitable transmission medium nor a coherent source, such as a laser, which would enable this process to be exploited. In 1954, A. C. S. van Heel's proposal of cladding the guiding core, resulted in a suitable transmission medium being achieved. T. H. Maiman invented the laser in 1960 and this provided the coherent source. The loss in the early optical fibres was high; at roughly 1000dB/km, this made them useless for long distance communications. However, a breakthrough in 1970 by F. P. Kapron changed this limiting factor with a novel low loss optical fibre with losses of 0.2dB/km. Compact coherent sources became available around the same time making the prospect of optical communications a reality.

The fundamental loss limit, which is set by Rayleigh scattering, is almost reached in today's optical fibre; the fibre can be routinely manufactured, with losses of 0.18dB/km at certain wavelengths. This means that the signal can be propagated over long distances before it needs to be recovered. Prior to 1990, in commercial submarine systems, this was done electronically by repeaters spaced every 60 to 70km. In 1990, the erbium doped fibre amplifier became commercially available thus replacing many of the electronic repeaters. Today there are many submarine optical cable systems connecting countries and continents, but as with the expansion of the Internet the need for increased bandwidth is always on the rise.

Transoceanic optical systems routinely carry Gigabits bit per second per channel, but with higher data rates per channel arising from the increased bandwidth, there is a drive to deliver these signals over trans-oceanic distances without the need for electronic

regeneration. Re-amplification of the signal is only one of the issues surrounding high bit rate communications. As the degradation of the pulse shape due to non-linear interactions, over the amplified optical spectrum also causes concern. However, it is re-timing or reducing the effects of timing jitter that poses one of the biggest problems in optical communications at speeds of 40Gbit/s and above.

2R (Re-shaping and Re-amplification) and 3R (2R plus Re-timing) optical regenerators have been studied extensively for the last decade and a half, and with the miniaturization of components, it is likely that they may be incorporated into a long-haul transmission systems in the next decade, to provide low jitter stable pulse propagation over transoceanic submarine cables.

1.2 Overview and aims of thesis

The aim of the thesis is to evaluate different options for ultra and long haul optical fibre communication systems. Extensive experimental work is complimented with theoretical analysis where appropriate. An operational wavelength of 1553nm is used and the utilization of Raman amplification for the optical gain is used for each of the experiments discussed in this thesis.

The theoretical background to the thesis is discussed in Chapter 2. Specifically, the linear effects of pulse propagation in optical fibre are described and the non-linear phenomena that can cause deleterious and advantageous pulse propagation at both short and long distances are discussed.

The procedures and measurements used in long-haul recirculating loop experiments are described in Chapter 3. The differences involved in pulse propagation, such as data format and dispersion maps, are discussed in the initial sections of chapter 3, whilst the theoretical background and experimental techniques associated with the recirculating loop are discussed in the remainder of the chapter. The chapter finishes with a description of the

autocorrelator, detailing the experimental set up and theoretical analysis that are needed for successful operation of the device.

The transmission system described in Chapter 4, utilizes standard single mode fibre, since single mode fibre contributes to the majority of the fibre used in commercial transmission systems. A comparison is then made between four different types of standard fibre dispersion map. In all four maps, the gain is provided by Raman amplification. Within the bandwidth of the signal, Raman amplification produces noise that increases with pump power, which cannot be determined by Optical Signal-to-Noise Ratio (OSNR) values alone. One such component to the noise is a phenomenon called Double Rayleigh Backscattering (DRBS). The amount of noise that originates from double Rayleigh backscattering is dependent on which type of map is used, and this evaluation with the aide of various techniques leads to an optimum map. The total transmission length at a data rate of 40Gbit/s was 2000km.

Within Chapter 5 a quasi-linear generic system, similar to the one described in chapter 4, is compared with a non-linearly guided system. The non-linearly guided system utilizes the saturable absorption effects of the Non-linear Optical Loop Mirror (NOLM), which effectively filters out noise and dispersive wave radiation. The localized non-linearity and the quasi-linear nature of the transmission line also allows a new stable propagation regime called DM autosoliton to be initiated after a couple of hundred kilometres; this is in direct comparison to a dispersion managed soliton system where the non-linearity is provided by the fibre.

The transmission system in Chapter 5 uses standard fibre with dispersion compensation that results in a strong dispersion map, similar to commercial transmission systems. It is shown in this chapter that with the insertion of a saturable absorber it is possible to extend the propagation distance to the point where it becomes physically limited.

In Chapter 6 the theory involved with timing jitter is discussed and the most important issues concerning dispersion-managed systems are focussed on. The timing jitter measurements were taken on a gated autocorrelator for data rates above 20Gbit/s and a

digital sampling oscilloscope for comparison at 10 and 20Gbit/s. The timing jitter measurements at 10, 20, 40, and 80Gbit/s were taken and then the generic system is compared with the non-linearly guided system. The results obtained for the DM autosoliton system show a dramatic decrease in the timing jitter at all data rates. The results are discussed for each data rate with allocations to be made to differing forms of timing jitter.

In Chapter 7 it is shown that the insertion of a Gaussian shaped filter can improve the stability of the NOLM, thus proving that the transmission distance is physically limited by propagating error free over 100,000km at 10Gbit/s. When the timing jitter for this distance is compared to that for the theoretical plot for polarization mode dispersion, it is shown that this system is limited by Polarization Mode Dispersion (PMD). The insertion over the filter also improved propagation at 20Gbit/s, which achieved an error free distance of over 20,000km.

The discussion in Chapter 8 concentrates on the passive effects of 2R regeneration on optical time division multiplexing. OTDM channels of different amplitudes will experience differing transformations. The effect of channel inequality on non-linear signal switching in a NOLM, incorporated into a 40Gbit/s transmission system is also discussed in this chapter.

Finally, in Chapter 9 the results of the research are discussed and the conclusions summarized.

Chapter 2 Single mode Fibre characteristics and transmission theory

2.1 Introduction

In this chapter the background theory to this research is presented. The linear characteristics of single mode optical fibre are discussed in Section 2.2, such as optical fibre loss or attenuation, dispersive effects of optical fibre and fibre birefringence.

The optical fibre non-linear characteristics are presented in Section 2.3. Topics included are: the Non-Linear Schrödinger Equation (NLSE), Group Velocity Dispersion (GVD), chirp, Self Phase Modulation (SPM), optical Solitons, Cross Phase Modulation (XPM), Four-Wave Mixing (FWM), Stimulated Brillouin Scattering (SBS) and Stimulated Raman Scattering (SBS). The chapter is summarized in Section 2.4.

2.2 Linear single mode fibre characteristics

Optical fibres used in telecommunications are manufactured from silica and consist of a core and a cladding with differing refractive indices. For long-haul communications Single Mode Fibre (SMF) is used which has a core diameter of typically 8 to 10-μm. Light propagates along the fibre, via a mechanism known as total internal reflection, which arises when the refractive index of the cladding is less than the refractive index of the core. A propagation mode in an optical fibre corresponds to a specific solution to the wave equation, depending on the boundary conditions (diameter of the fibre optic core in this case). Therefore, as the name suggests, for multimode fibre the boundary conditions mean that there are many solutions to the wave equation, and hence many propagation modes. Single mode fibre is weakly guiding due to the small difference between the refractive indices, and the boundary conditions mean that there is only one propagation mode, which is the only linearly polarized (LP_{mn}) mode. The notation LP is just a different means of expressing the Transverse Electric (TE) and Transverse Magnetic (TM) modes.

An important characteristic of optical fibre is the normalized frequency or the V parameter, which determines the number of modes that can propagate down the fibre. The V parameter is dimensionless and is given as [1]:

$$V = \frac{2\pi}{\lambda} r n_1 (2\Delta)^{1/2}. \qquad (2.1)$$

This equation contains four important design variables associated with single mode fibres, the fibre radius r, the refractive index of the core n_1, and the operating wavelength λ. The refractive index difference is denoted by Δ and is given as [1]:

$$\Delta = \frac{n_1^2 - n_2^2}{2n_1^2} \approx \frac{n_1 - n_2}{n_1} \quad \text{for } \Delta \ll 1, \qquad (2.2)$$

where n_2 is the refractive index of the cladding of the optical fibre.

For the optical fibre to be single mode the V parameter, whose origins arise from the eigenvalues of the core and the cladding, has to be between 0 and 2.405, as for these cases only the LP_{01} mode will propagate. For multimode fibre V is greater than 2.405, then the LP_{11} mode and higher modes will propagate. The work discussed in this thesis was only concerned with the properties of the single mode optical fibre characteristics associated with long-haul communications.

2.2.1 Optical fibre loss

Optical fibre loss or attenuation of a fibre link is one of the most important factors associated with optical transmission. There are numerous contributing factors to optical fibre loss, which can be grouped into intrinsic losses and extrinsic losses [2]. Intrinsic losses are due to pure silica's (SiO_2) molecular construction. SiO_2 molecules exhibit vibrational resonances in the infrared region, which lead to absorption bands [2].

Extrinsic losses result from the amount of impurities in the fibre core. Rayleigh scattering is a dominant contributor to the losses; it is due to microscopic fluctuations in density of the core [2] and is proportional to λ^{-4}.

Waveguide imperfections such as *Mie scattering* are due to inhomogeneities in the fibre, but by employing good design and construction these types of losses can reduced to insignificant levels [2].

Attenuation in optical fibres, α_{dB}, is generally expressed in Decibels per unit length (dB km^{-1}), and is given by [2]:

$$\alpha_{dB} = -\frac{10}{L}\log_{10}\left(\frac{P_{out}}{P_{in}}\right) = 4.343\alpha \text{ , (2.3)}$$

where L (μm) is the length of the fibre, P_{in} (Watts) is the power in and P_{out} (Watts) is the power out. The power at any given point along the fibre is given by [2]:

$$P_{out} = P_{in}\exp(-\alpha_{dB}L), \qquad (2.4)$$

2.2.2 Dispersion

Dispersion is a result of the variation of refractive index with frequency, and arises because waves of different wavelengths move through transparent media, such as silica, at different speeds [3]. Pure monochromatic waves do not exist in nature. However, groups of monochromatic waves with very similar frequencies clustered narrowly around the main frequency do, and these are known collectively as a *wave group*. The group velocity of the wave group is given by [4]:

$$\upsilon = \frac{c}{n(\omega)}, \qquad (2.5)$$

where v is velocity of the pulse, c is the speed of light in a vacuum and $n(\omega)$ is the distribution of refractive index with frequency. This equation illustrates the effect that the distribution of frequencies in the wave group has on the propagation of the wave group (optical pulse) along the fibre.

For optical communications systems one of the most unfavourable effects is temporal pulse broadening of the wave group. If ω_0 is the centre frequency of a nearly monochromatic wave, then taking the Taylor series expansion of the mode-propagation constant $\beta = 2\pi n/\lambda$ gives [4]:

$$\beta(\omega) = n(\omega)\frac{\omega}{c} = \beta_0 + \beta_1(\omega - \omega_0) + \frac{1}{2!}\beta_2(\omega - \omega_0)^2 + \frac{1}{3!}\beta_3(\omega - \omega_0)^3 + \ldots\ldots, \quad (2.6)$$

where β_0 is the propagation mode at the central wavelength and this undergoes no change, β_1 is the group velocity which dictates the speed of the pulse envelope as it propagates through the optical fibre, and β_2 and β_3 are responsible for pulse broadening within the fibre.

In optical fibre telecommunications the dispersion is commonly referred to as the parameter D, which is related β_2 by the equation [4]:

$$D = -\frac{2\pi c}{\lambda^2}\beta_2, \quad (2.7)$$

where λ is the operating wavelength.

In telecommunications λ is usually in the 1550nm region, and for standard single mode fibre the value of D is typically $17ps/(nm.km)$. D can be positive or negative as defined by the inverse sign of β_2. A positive value of D indicates the dispersion is in the anomalous region whereas a negative value indicates dispersion in the normal region. The zero dispersion wavelength λ_D, in step index silica fibres is in the 1300nm region, and corresponds to $\beta_2 = 0ps^2/nm$.

There are speciality fibres and devices that can invert the sign of the dispersion associated with the system being used; the magnitude of the dispersion of these devices and fibre can be fixed or variable. These can then be used to compensate for the dispersion [5] that can accrue in an optical fibre system. The most commonly used fibres are known as dispersion-compensating fibres (DCF) [6] whilst fibre Bragg gratings (FBG) [7], have a similar effect.

2.2.3 Fibre Birefringence

Single mode fibre is not truly single mode because this mode has two polarization states. Due to imperfections in the optical fibres cylindrical core, this can lead to a temporal walk off (the change in time of an optical pulse between the two polarization states from the beginning to the end of a length of fibre) of the optical pulse in the different polarization states. This walk off is due to the group velocity of each of the two polarization states being different. This is termed as the birefringence of the fibre, and this leads to a periodic power exchange between the two polarization states called *beat length* (L_B), which is given by [4]:

$$L_B = \frac{\lambda}{B}. \qquad (2.8)$$

Here B is the birefringence and λ is the operating wavelength. The state of polarization changes over L_B from linear to elliptical then back to linear again. The walk off of the pulse that comes from fibre birefringence leads to an additional dispersion term, which is known as polarization mode dispersion (PMD) and is of importance to periodically amplified optical telecommunication systems [8].

Research into polarization mode dispersion is currently a topic of interest, as the majority of the fibre currently operational is old and unfortunately has a high value of polarization mode dispersion (typically 1ps/km$^{1/2}$). Compensators for polarization mode

dispersion are currently being sought to utilize the best performance from the already installed optical fibre.

2.3 Non-linearity in single mode fibre

The previous section discussed the linear fibre characteristics that have a detrimental impact on the performance of an optical transmission system. Within this section fibre non-linearity is discussed, as this can cause pulse distortion and a degradation of transmission performance over long-haul transmission distances [9]. Thus every effort must be made to keep fibre non-linearity to a minimum. However, there are circumstances where fibre non-linearity could be beneficial to transmission, producing phenomenon, such as pulse compression [10], regeneration [11], amplification [11][12] (Raman, Parametric etc), wavelength conversion [13] and propagation of optical solitons [14].

The response of a dielectric medium (silica fibre) under a low intensity optical field is given by the equation [15]:

$$P(\omega) = \varepsilon_0 \chi(\omega) E\,, \qquad (2.9)$$

where $\boldsymbol{P}$ is the induced polarization from the electric field $\boldsymbol{E}$, χ is the linear susceptibility of the medium and $\boldsymbol{e_0}$ is the permittivity of the dielectric. The frequency of the optical wave causes a dipole oscillatory motion of each atom and establishes polarization through the displacement of electrons relative to the nuclei. With small fields the oscillations of each atom are harmonic and the displacement of electrons is small, thus χ stays constant.

Optical fibre becomes non-linear under intense illumination of light. This phenomenon is due to the anharmonic motion of bound electrons under the influence of an applied optical field. The induced polarization from the electric dipoles is given as [16]:

$$P = \varepsilon_0 \left(\chi E + \chi_2 E^2 + \chi_3 E^3 + ... \right), \qquad (2.10)$$

where χ is the linear susceptibility and χ_2, χ_3,... are the non-linear optical coefficients, and the applied field is in the form $E = e_0 \cos(\omega t - kz)$. For a non-crystalline media such silica fibre, where $\chi_2 = 0$, the non-linearity is due to the next lowest term χ_3. This term is responsible for phenomena, such as self phase modulation, cross phase modulation and four wave mixing. The non-linear susceptibility leads to an intensity dependent refractive index, n, change through the relation [17]:

$$n = n_1 + \frac{3\chi_3}{4c\varepsilon_0 n_1^2} I = n_1 + \eta \frac{P}{A_{eff}}, \qquad (2.11)$$

where the power, P is given in Watts, A_{eff} is the effective area of the optical fibre, n_1 is the refractive index of the core of the fibre, and η is the Kerr coefficient or non-linear index coefficient. In fused silica n_1 and η, are approximately 1.46 and $3.2.10^{-20}$ m^2/W respectively. The change in refractive index is small for short propagation distances, as low optical power is used in optical communications. However, for long propagation distances the accumulated effects of non-linearity can become substantial.

2.3.1 The non-linear Schrödinger equation

Non-linear effects in optical fibres have been an area of interesting study for many decades, and the effects of short pulses, typically with pulse durations in the range of 1ps to 100ps, are of particular interest to optical telecommunications.

An optical pulse propagating down an optical fibre obeys the generalized non-linear Schrödinger equation and with all higher order terms included, this equation is given by [17]:

$$\frac{\partial A}{\partial z}+\frac{i}{2}\beta_2\frac{\partial^2 A}{\partial T^2}-\frac{1}{6}\beta_3\frac{\partial^3 A}{\partial T^3}+\frac{\alpha}{2}A=i\gamma\left[|A|^2A+\frac{i}{\omega_0}\frac{\partial}{\partial T}\left(|A|^2A\right)-T_R A\frac{\partial|A|^2}{\partial T}\right], \quad (2.12)$$

where $A(z,t)$ is the pulse envelope and it is a slowly varying function with time (it is obtained by performing a inverse Fourier transform) and $|A|^2$ is the optical power. T is a transformation of t and corresponds to a frame of reference that is moving with the pulse at the group velocity, and z represents the change in distance along the direction of propagation. The first term on the LHS is the pulse envelope moving with regard to the z-axis; the next term on the LHS is the group velocity dispersion β_2, which causes pulse broadening due to different frequencies of light within the pulse envelope travelling at dissimilar speeds (section 2.2.2). The second to last term on the LHS is the third order dispersion term, β_3: this term becomes the dominant mechanism for pulse broadening if the propagation wavelength is at the zero dispersion wavelength of the fibre i.e. $\beta_2=0$. For ultra-short pulses (less than 0.1ps) with a wide optical bandwidth the effect of the third order dispersion, β_3, is to distort the pulse shape. Unlike the second order dispersion that broadens the pulse symmetrically, third order dispersion distorts asymmetrically by producing oscillations on the leading or trailing edge of the pulse (for negative and positive dispersion values respectively), temporally. The last term on the LHS, α, determines the amount of attenuation the propagating pulse will undergo and is defined in Section 2.2.1.

The multiplying factor on the RHS of equation 2.12, γ is the non-linear coefficient, which originates from the Kerr effect. The second term on the RHS originates from non-linear polarization, which leads to self-steeping, and shock formation at the pulse edge. The last term on the RHS is due to an ultra-short pulse having a wide optical bandwidth; if the bandwidth is sufficiently wide then the pulse will undergo Raman gain from the higher frequency components. This phenomenon causes the self-frequency shift. Finally, ω_0 is the central frequency of the optical pulse.

The non-linear coefficient, γ, is expressed as [18] [19]:

$$\gamma = \frac{\eta k_0}{A_{eff}} = \frac{\eta \omega_0}{c A_{eff}}, \qquad (2.13)$$

where η is the Kerr coefficient, $\gamma|A|^2$ (RHS in equation 2.12) is expressed in units m^2/W and k_0 is the propagation constant for light in a vacuum. For special circumstances $a = 0$, where there are no losses the equation (2.12) becomes the non-linear Schrödinger (NLS) equation.

For silica fibre where the zero dispersion wavelength can be greater or less than the wavelength of the optical pulse, this then alters the sign of the second order dispersion parameter, which greatly affects the propagation behaviour.

2.3.2 Group Velocity Dispersion (GVD)

Group velocity dispersion is an induced temporal effect, which is dependent on the frequency of an optical pulse, and its effect is to change the phase of each spectral component in that optical pulse. These phase changes can affect the pulse shape temporally, but they do not alter the pulse spectrally.

Either the non-linear or the dispersive effects, depending on the initial peak power and pulse duration, can dominate pulse evolution along the fibre. Two length scales can be introduced here that are useful for categorizing the propagation regimes. These are the dispersion length (L_D) and non-linear length (L_{NL}) and are given by [20] [21]:

$$L_D = \frac{T_0^2}{|\beta_2|}, \qquad (2.14)$$

$$L_{NL} = \frac{1}{\gamma P_0}, \qquad (2.15)$$

where T_0 is the initial pulse duration at the 1/e-intensity point, P_0 is the initial power, γ is the non-linear coefficient and β_2 is the second order dispersion constant. The following four categories of pulse propagation exist as defined by the optical fibre length L, L_D and L_{NL} [20].

1. The non-linear and dispersive effects are negligible when $L << L_{NL}$ and $L << L_D$.
2. The pulse propagation is governed by the GVD if $L << L_{NL}$ and $L = L_D$.
3. The pulse propagation is governed by the non-linear effects when $L = L_{NL}$ and $L << L_D$.
4. Both GVD and non-linear effects act on the propagating pulse if $L = L_{NL}$ and $L = L_D$.

The propagation regime defined in point one is the most desirable regime for optical communications. However, at data rates of 10Gbit/s and higher this regime is not easily obtained: this is because the shorter pulse durations associated with data rates in excess of 10Gbit/s are more susceptible to GVD and have a higher non-linearity that arises from a higher optical peak pulse power. In point two, the propagation regime can viewed as quasi-linear, since GVD is dominant and the optical pulse will spread temporally as it propagates down the fibre. Non-linear effects will be dominant in point three leading to spectral distortion and pulse shape distortion. The propagation regime described in point four can lead to the propagation of optical solitons due to the combined effects of GVD and self phase modulation (this is discussed in Section 2.3.5).

Dispersion acts on all pulses regardless of the temporal profile, as the pulse maintains its shape but broadens with propagation. For a Gaussian pulse without chirp (discussed in

Section 2.3.3), that is propagating along a length of fibre the 1/e intensity pulse width, T_0, will broaden to T_1, where T_1 is given by [20] [21]:

$$T_1 = T_0\left[1+\left(\frac{z}{L_D}\right)^2\right]^{1/2}, \qquad (2.16)$$

Here z is the length along the fibre the incident pulse has travelled. T_0 is usually expressed in terms of the Full Width Half Maximum (T_{FWHM}) and for a Gaussian pulse the relationship is $T_{FWHM} = 1.665T_0$. For a hyperbolic-secant pulse $T_{FWHM} = 1.763T_0$.

2.3.3 Chirp

Chirp is defined as a change in the central frequency, ω_0, of an optical pulse with time. Chirp can be either positive or negative, giving the two terms up chirp and down chirp respectively. An optical pulse that undergoes some form of phase modulation is chirped, this means the instantaneous frequency varies (from the central frequency) across the spectral range of an incident optical pulse. As shown in equation 2.16 an optical pulse broadens due to dispersion along a length of optical fibre. When a chirped pulse is considered, the pulse duration, T_1, after a propagation distance, z, is given by [20].

$$T_1 = T_0\left[\left(1+\frac{Cz}{L_D}\right)^2+\left(\frac{z}{L_D}\right)^2\right]^{1/2}, \quad (2.17)$$

where C is the linear frequency chirp.

A pulse is chirped if its carrier frequency changes with time [21] and the time dependent frequency shift, $\delta\omega(t)$, is related to the chirp by:

$$\partial\omega(t) = -\frac{\partial\phi}{\partial t} = \frac{C}{T_0^2}t, \qquad (2.18)$$

where F is the phase. Chirp is important because most lasers produce linear chirp.

GVD can cause chirp because it can cause the different frequency components within an optical pulse spectrum to travel at different speeds along the fibre, which leads to a time delay between the frequencies at the end of the fibre. This time delay alters the shape of the pulse making it broader. The red frequency components travel faster in the normal regime of optical fibre (as discussed in section 2.2.2) and blue frequency components in the anomalous regime.

A chirped pulse has a broader Fourier spectrum than that of an un-chirped pulse and the spectral half width is expressed as $\Delta\omega_0 = (1+C^2)^{1/2}/T_0$. A pulse is said to be transform limited in the absence of chirp ($C=0$), as then $\Delta\omega_0 T_0 = 1$.

A pulse may broaden or compress depending on whether β_2 and C have the same or opposing signs. If $\beta_2 C > 0$ then a Gaussian pulse will broaden at a quicker rate than if the chirp was zero, if $\beta_2 C < 0$ then the pulse duration will compress then broaden. The distance at which the compression reaches a maximum, z_{min}, is given by [21]:

$$z_{\min} = \left[\frac{|C|}{(1+C^2)}\right] L_D, \qquad (2.19)$$

After a distance of z_{min}, the pulse duration has reduced to its minimum, T^{min}, which is given by:

$$T_1^{\min} = \frac{T_0}{(1+C^2)^{1/2}}, \qquad (2.20)$$

When $\beta_2 C<0$ then the pulse is initially chirped, and the initial linear chirp can have a opposite sign to that of the dispersion-induced chirp. This gives a reduction in the net chirp causing a narrowing of the temporal pulse shape; the point at which the pulse duration reaches a minimum, T_1^{min}, is where the two chirps cancel each other out. Dispersion-induced chirp begins to dominate over initial linear chirp with increasing propagation distance, such as an optical pulse experiences in a transmission system.

2.3.4 Self Phase Modulation (SPM)

This section describes Self Phase Modulation (SPM), which occurs when the phase of an optical carrier wave changes. High intensity optical fields within a confined area and time induce SPM.

The non-linear relationship between the refractive index and optical field intensity leads to a frequency change in the spectral profile of an optical pulse. This is a time dependent process, which can be viewed as chirp. It follows that if the refractive index is affected by spatial and temporal variations of optical power, then a pulse propagating with a radial Gaussian intensity distribution will see differing refractive indices according to its radial intensity. If the power of the pulse is steadily increased then the phase change will cease to be negligible. In fused silica, the sign of η (non-linear coefficient) is positive, thus increasing the refractive index with increasing optical power. In this circumstance the pulse will experience a phase change, F, due to self phase modulation, which is given as [22]:

$$\Phi = \frac{\omega\eta}{c}\left|\hat{E}\right|^2 L = \frac{2\pi\eta PL}{\lambda A_{eff}}, \qquad (2.21)$$

where L is the length of fibre that the pulse is propagated over.

Various parts of the pulse undergo different phase shifts, which lead to a shift in frequency (or chirp), and this is due to the optical intensity as it varies throughout the pulse

with respect to the Gaussian distribution profile. In optical fibre, attenuation limits the distance where the non-linear phase shift effects are significant. The length, L_{eff}, after which the non-linear phase shift effects are negligible, is given by [23]:

$$L_{eff} = \frac{1}{\alpha}[1 - \exp(-\alpha L)]. \qquad (2.22)$$

For single mode fibre with a = 0.2dB/km and L = 80 km, L_{eff} is approximately 21km, therefore the non-linear effects are only significant for the first 21km. The dependence of the propagation constant (as discussed in section 2.2) on the refractive index can is given in the equation below [24]:

$$\beta(\omega, I) = \frac{\omega n(\omega, I)}{c}, \qquad (2.23)$$

where the propagation constant, $\beta(\omega,I)$, varies with time due to the variation of intensity with time, $I(t)$. The time derivative propagation constant is proportional to the instantaneous optical frequency and this causes pulse intensity variations in which new frequency components are generated within the pulse envelope. This effect then broadens the pulse spectrally as it is propagating in an optical fibre, whilst not affecting the temporal pulse shape. However, when used in conjunction with group velocity dispersion it can cause pulse duration narrowing or pulse shape distortion.

2.3.5 Optical solitons

Light pulses that utilize the non-linearity of the refractive index of optical fibres to produce non-dispersive light pulses are called solitons. The propagation in fibres of non-linear pulses was proposed by [25] and the first experimental demonstration was presented by [26].

When loss and higher order dispersive terms are ignored, normalized Non-Linear Schrödinger Equation (NLSE) takes the form of [27][28]:

$$-i\frac{\partial u}{\partial \xi} = \frac{1}{2}\frac{\partial^2 u}{\partial s^2} + |u|^2 u, \qquad (2.24)$$

where u is the normalized pulse envelope, s is the normalized time and ξ is the normalized length. All these variables are in soliton units and which given by [27][28]:

$$s = T/T_0 = (t - \beta_2 z)/T_0 \qquad \xi = z/z_c \qquad u = \left(\gamma T_0^2/|\beta_2|\right)^{1/2}. \qquad (2.25)$$

Equation (2.24) can be understood by considering the expansion of the pulse envelope *u* to obtain the dispersive elements around the central frequency such that only the leading terms are kept. Equation (2.24) gives a good approximation of the propagation of a pulse in optical fibre, as long as the pulse duration is greater than 1ps, so that the higher order terms can be ignored. If a pulse envelope propagates along an optical fibre in the anomalous region (negative β_2) with a wavelength significantly different than the zero dispersion wavelength then the pulse envelope will experience no changes to its shape. This pulse is known as the fundamental soliton.

To solve equation (2.24) the inverse scattering method [29] has to be applied to the non-linear Schrödinger equation [30]. The solution to equation (2.24) which gives the fundamental soliton is a hyperbolic secant in the form $u(\xi,s) = sech(s)exp(i\xi/2)$. The form of this equation indicates that the pulse keeps its shape through propagation. This means that the term that produces non-linearity induced up-chirp cancels with the term that causes the dispersion induced down-chirp in equation (2.24), specifically in the anomalous region of the fibre (as discussed in section 2.2.2). This leaves only the part of the term that

produces the change in phase (***sech(s)***). This result shows that a distortion-less propagation at high data rates over long distances is feasible [31].

For higher order solitons when ***(ξ = 0)*** then ***u(0,s) = N Sech(s)*** where the soliton order ***N*** is an integer [28]. The power, P_1, required to produce a fundamental soliton (***N=1***) is given by:

$$P_1 = \frac{3.11|\beta_2|}{\gamma T_{FWHM}^2}. \qquad (2.26)$$

The Full Width Half Maximum (FWHM) for a hyperbolic secant shaped pulse with a pulse duration of T_0 (1/e intensity point) is $T_{FWHM} = 1.76T_0$. The peak power for N^{th} order solitons is given by $P_N = N^2 P_1$. The soliton repeats its shape both spectrally and temporally along a length of fibre returning to its original shape at, z_0, which is known as the soliton period and is the length scale for higher order solitons. z_0 is given as [32]:

$$z_0 = \left(\frac{\pi T_{FWHM}}{\lambda_0}\right)^2 \frac{c}{D}, \qquad (2.27)$$

where ***D*** is the dispersion parameter, ***c*** the speed of light in a vacuum and λ_0 is the zero dispersion wavelength.

The effects of group velocity dispersion and self phase modulation combine in higher order solitons ***N>1*** to produce an oscillatory motion that results in a soliton period or length of z_0, and multiples of thereafter. Producing a higher order soliton can lead to phenomenon such as pulse compression. Where the interplay of SPM induced chirp and GVD leads to a reduction of the pulse duration before the GVD starts to dominate and increase the pulse duration. By using a fibre whose length coincides with maximum compression enables the pulse durations to be specified.

A major problem with soliton transmission is that the attenuation in the fibre causes the soliton to collapse as it propagates down the fibre. To overcome this a solution to the soliton form has to be introduced called the averaged soliton [33]. The averaged soliton was experimentally demonstrated [34], with the loss compensated by the Raman effect. There are other important effects which limit the performance of a soliton based communication system such as the interaction between adjacent pulses and the initial chirp imposed by the source.

Early loss compensation by stimulated Raman scattering was not practical for use in optical telecommunications, due to the size and power requirement of the Raman lasers. It wasn't until the advent of the erbium doped fibre amplifier in the late eighties [35], that the soliton was considered practical for optical communications [36], due to the lower pump power needed. With the use of lumped amplification the induced phase shift over a fibre span needs to be small enough to ensure a stable propagation: this is achieved by setting the amplifiers spacing less than the soliton period $z_a << z_0$. In a soliton system the amplifier spacing is usually a factor of ten less that the full soliton period, however, the limit is $z_a < 4/5 z_0$ [37].

To achieve an ideal soliton, as in the loss-less fibre case, the average non-linear phase shift has to be balanced with the average dispersion. This is achieved by launching a pulse with a mean power over the fibre span that is equal to the loss-less case. As the loss in an optical fibre system decreases exponentially with propagation distance, the intensity dependant non-linearity diminishes, leading to the fundamental soliton not propagating in an optical fibre for long distances and reverting temporally to a Gaussian shape. This can be overcome by increasing the peak power of the soliton. The implication of this is that a new scaling factor is needed to replace N, by the soliton number M, which is not an integer. So, the peak power of the soliton is increased by M times N. The linear gain, G, required is described by loss rate $G = exp(aL_a)$, with L_a being the amplifier spacing in kilometres (km). This leads to M and the peak power for the average soliton being [38]:

$$M = \frac{G \ln G}{G-1} \qquad P_0 = M_0^2 \frac{|\beta_2|}{\gamma T_{FWHM}^2}. \qquad (2.28)$$

Lumped amplification (large gain over a short distance), however, introduces large variations of soliton peak power; this limits the amplifier spacing to a fraction of the dispersion length. The large variations in soliton peak power cause the soliton to shed any excess energy in the form of dispersive radiation; this builds up over successive amplification and is detrimental to the system. At high data rates where the pulse duration is being constantly reduced, the dispersion length becomes so small that the amplifier spacing becomes impractical.

The introduction of Raman fibre lasers and diode lasers in the 1450nm region, (that were small and high-powered) in the late 1990s, could provide the distributed amplification, which was needed to extend the constraints of amplifier spacing imposed by the average soliton regime, at data rates of 20Gbit/s and above. The use of distributed amplification allows an almost loss-less propagation owing to the fact that each section of fibre is compensated for. The scaled power needed for a launched soliton is approximately the same for the lumped amplifier case, but there is a relaxation of the amplifier spacing and less build up of dispersive radiation.

The relaxation of the amplifier spacing is solely dependent on the rate of loss of the Raman pump, if this is zero then the amplifier spacing would be infinite [39] in standard optical fibre this loss is ~0.3dB/km. It was found [39] that the non-adiabatic nature of the pump that excites the intrinsic soliton dynamics is what controls the amplifier spacing. The inhomogeneous pump intensity causes dispersive wave radiation to be radiated out, due to the non-adiabatic nature of the pump. To still provide stable soliton transmission the requirement of a universal amplifier spacing of 2p in soliton units holds [39]. Distributed amplification allows a smaller soliton power excursion, as there is a smaller power fluctuation along the fibre thus leading too less dispersive radiation. In addition the output

power is the same as the input power in a distributed amplification scenario, which leads to a reduced soliton broadening when compared to the lumped amplification case.

2.3.6 Cross Phase Modulation (XPM)

When two or more signals are co-propagating along the same length of fibre, the signals have a non-linear effect on each other due to Cross Phase Modulation (XPM) coupling. Self Phase Modulation (SPM) occurs when the intensity modulation of a signal has a non-linear effect on the refractive index, which in turn causes a phase shift. The intensity modulation will also cause a phase shift in the other co-propagating signal (and visa versa) and this is called XPM. This phenomenon has many applications in signal processing [40], [41], [42].

Cross phase modulation is twice as effective at phase modulating the other co-propagating signal of the same intensity, than the other signals self phase modulation. In SPM the frequencies in the propagated pulse act on themselves, this is a degenerate process, and in XPM the other signal or pump have a different frequency that act on the original signal frequencies.

If one of the propagated waves ($wave_1$) has a greater power than that of the other propagated wave ($wave_2$). Then the phase shift, f, seen by $wave_2$ is evaluated using the slowly varying envelope approximation [43]. The phase shift is given as [44]:

$$\phi = \frac{2\omega_2}{\omega_1} P_{pump}\left(tL - \Delta\beta L^2\right), \qquad (2.29)$$

where $\Delta\beta = \beta_1 - \beta_2$, and is the difference in the group delays for the two pulses, and ω_1 and ω_2 are the respective frequencies of the two waves; P_{pump} is the power in $wave_1$ and L is the length over which the interaction takes place. The amount of interaction between the two waves reaches a maximum when $\Delta\beta = 0$, since the phase shift is largest at this point.

2.3.7 Four-Wave Mixing (FWM)

The third order non-linear susceptibility of silica (discussed in Section 2.3) that leads to such phenomenon as self phase modulation and cross phase modulation also causes another non-linear phenomenon called four wave mixing. Four-wave mixing in a wave-guide has been studied extensively [45].

During scattering, two photons with energies $h\omega_1$ and $h\omega_2$ by means of a scattering process create two new photons, with energies $h\omega_3$ and $h\omega_4$. Through the process of conservation of momentum the net energy is maintained then the phase matching condition occurs (which is the matching of frequencies and wave vectors) [46].

A process of parametric gain [47], can occur when the four wave mixing is partially degenerate, that is when the frequency of pump 1 (ω_1) and pump 2 (ω_2) are equal. The net effect is that energy is transferred from the high power to the low power signal. If three optical fields with carrier frequencies ω_1, ω_2 and ω_3 are co propagating along the same optical fibre simultaneously, then a fourth optical field with a carrier frequency $\omega_4 = \omega_1 \pm \omega_2 \pm \omega_3$, is created as a result of the third order non-linear susceptibility and the intensity dependence of the refractive index.

Four-wave mixing can also be used as a means to achieve 2R regeneration [48], however, as with cross phase modulation, four-wave mixing is detrimental to wavelength division multiplexed systems [49].

2.3.8 Stimulated Brillouin Scattering (SBS)

R. Y. Chiao, C. H. Townes, and B. P. Stoicheff first observed stimulated Brillouin scattering in 1964. SBS occurs in optical fibres at low powers and it is a non-linear process, where the majority of the power of an incident optical wave is converted to a Stokes wave. The Stokes wave has a downshifted frequency that conserves energy and momentum.

Stimulated Brillouin scattering is dependent on the spectral width of the input signal and the pulse duration.

For stimulated Brillouin scattering, the interaction of the pump with a Stokes wave and an acoustic wave is said to be a parametric process. This can be viewed as modulation of the light through thermal molecular vibrations in the fibre. The scattering process of the incident photon produces a phonon of acoustic frequency (acoustic wave); this then sets up a periodic modulation of the refractive index. The periodic modulation of the refractive index is caused by electrostriction, and this produces a grating within the fibre. This periodic modulation of the refractive index has a frequency and a velocity, because of the gratings velocity within the fibres, which Doppler shifts the scattered light to higher or lower frequencies (Stokes wave) called sidebands, through the process of Bragg diffraction. In stimulated Brillouin scattering the frequency shift of the Stokes wave depends on the scattering angle (in an optical fibre the confinement of the optical signal dictates only two possible directions: forwards and backwards). The power and intensity of the Stokes wave is zero for the forward direction and a maximum for the backward direction.

When the pump wave is propagated through the fibre the Stokes wave grows exponentially in the backward direction. However, if there is any loss to the pump wave in the optical fibre then the distance along the length of optical fibre over which the power of the pump wave is effectively converted to a Stokes wave, which is known as the effective length, L_{eff}, and is given by [50]:

$$L_{eff} = \frac{1}{\alpha_p}\left[1 - \exp\left(-\alpha_p L\right)\right], \qquad (2.30)$$

where α_p is the attenuated pump power.

Noise and spontaneous Brillouin scattering that occur in the fibre cause the Stokes wave to develop. This phenomenon occurs when the pump power reaches a critical level, P^{cr}, and it is approximated by the following equation [50]:

$$P^{cr} = \frac{21\rho A_{eff}}{g_{SBS} L_{eff}}, \qquad (2.31)$$

where A_{eff} is the effective area of the fibre, g_{SBS} is the gain of the stimulated Brillouin scattering and ρ is the polarization between the pump and the Stokes wave.

For a standard optical fibre communication system the Brillouin threshold is approximately 1-mW. This however is drastically increased for fast phase changing laser with a sufficiently large bandwidth (>100-MHz), where the phase change is shorter than the phonon lifetime. If the optical pulse is shorter in duration than 10-ns then the stimulated Brillouin scattering is reduced to insignificant levels. This occurs for high bit rate systems where the pulse duration is reduced below than that of the phonon lifetime, which is typically less than 1-ns. For high data rate systems (typically greater than 10Gbit/s) with a laser bandwidth of approximately 1nm (125GHz) the effects of stimulated Brillouin scattering can be neglected and stimulated Raman scattering becomes the dominant effect.

2.3.9 Stimulated Raman Scattering (SRS)

Spontaneous Raman Scattering occurs in all non-linear mediums converting a small amount of the incident optical intensity (typically 10^{-6}) to lower frequency by conversion to a Stokes wave. Only a small amount of the incident radiation gets Stokes downshifted by this mechanism, which is called spontaneous Raman scattering.

Stimulated Raman scattering [51] occurs when a dielectric has a high intensity optical field passed through it, so that the majority of the fields optical power is converted to the Stokes wave, through scattering. This process is intensified in optical fibres [52] because of the small cross sectional area, which increases scattering. This process over long fibre lengths, SRS leads to increased non-linear effects.

The mechanism by which SRS occurs is that of inelastic scattering. The incident pump photon is in-elastically scattered, and this photon is Stokes downshifted (frequency conversion) to a lower frequency. The excess energy that arises from such an event goes to form an optical phonon [53] of a high frequency, unlike stimulated Brillouin scattering, which produces an acoustic phonon. This process in optical fibres was first observed and measured by [54].

Raman amplification is a non-resonant non-linear phenomenon [55]. The amount of Raman amplification is governed by the Raman gain coefficient g_{SRS}, which is related to the cross section of Raman scattering events. The amorphous nature of silica means that the vibration energy levels that occur in such materials, are bonded together. This bonding together of the vibration energy states results in a wide frequency bandwidth of 20THz [56]. In silica optical fibre the Raman gain is typically of the order 10^{-12}cm/W. The Stokes wave is downshifted by 13THz (also called the Raman frequency shift).

The constraints of the fibre only allow the Stokes wave, which has been 'downshifted', to propagate in the forward or backward directions in relation to the fibre core. Otherwise the downshifted stokes wave would propagate isotropically. However, as the threshold for the forward-stimulated Raman scattering is reached first, as shown in equation (2.32), backwards stimulated Raman scattering in optical fibre is generally not observed. One such effect can cause optical amplification if a probe signal is used at the downshifted frequency [57], to that of the pump so that the build up of the optical power in the Stokes wave is passed on to the probe signal.

This type of amplification does not require population inversion, which is the mechanism under which erbium doped fibre amplifiers operate. The wide frequency bandwidth that is characteristic of Raman amplification means that many signals can be amplified simultaneously and this makes Raman amplification very attractive to the telecommunications market.

When the pump power reaches a certain threshold value (the Raman scattering threshold), this leads to an exponential growth in the Stokes wave at the Raman frequency shift [58].

L_{eff} is the effective interaction length of the pump along the optical fibre and is given by [53]:

$$L_{eff} = \frac{[1-\exp(-\alpha_p L)]}{\alpha_p}, \qquad (2.32)$$

where L is the length of the fibre over which the Raman pump is propagated and a_p is the losses incurred by the pump wave over the fibre. For a typical terrestrial fibre span of L = 80km and a_p = 0.24dB/km, the effective length is L_{eff} = 17.9km.

The stimulated Raman scattering threshold occurs when the pump power reaches P^{cr}, which is defined as the point where the Stokes wave has the same power as the pump power at the input: P^{cr} is given by [53]:

$$P^{cr} = \frac{\kappa \rho A_{eff}}{g_{SRS} L_{eff}}, \qquad (2.33)$$

where ρ is the state of polarization between the Raman pump laser and the probe wave, and is either 1 for completely polarized or 2 for a completely random; A_{eff} is the effective area of the fibre core given as ($A_{eff} = pr^2$); g_{SRS} is the Raman gain coefficient and κ the threshold condition is either 16 for forward scattering or 20 for backward scattering.

Raman amplification is independent of the relative directions of the pump and probe waves. For example if ρ = 1, A_{eff} = 50μm^2, g_{SRS} =1.10^{-13}m/W, κ = 16 and L_{eff} = 17.9km, then P^{cr} = 0.446W.

2.4 Summary

Within this chapter the fundamental theoretical topics on which this research is based have been discussed. Sections 2.2 onwards described linear pulse propagation and the problems

thereof, whilst Sections 2.3 detailed the problems associated with non-linearity and pulse propagation within an optical fibre.

Chapter 3 Procedures and measurements for long-haul recirculating loop experiments

3.1 Introduction

In this chapter the procedures and measurements utilized in the recirculating loop experiments described in this thesis are presented. The fundamental aspects of long-haul optical transmission systems, such as amplification processes, transmission formats and dispersion management techniques are presented in Section 3.2. In Section 3.3, the two methods used to investigate transmission system performance are described, namely: measurement of optical pulses and burst measurement techniques. The set up of the transmitter, receiver and fibre loop in the recirculating loop are described in detail in Section 3.4. The details of how the autocorrelator can be used to resolve ultra-fast pulses are given in Section 3.5. Finally, the chapter is summarized in section 3.6.

3.2 Optical transmission

Optical transmission was widely studied in the last decade, but with the economic slow-down in the late 1990's, interest in the topic had diminished particularly in the private sector. The emphasis prior to 1999 was to increase the transmission capacity, whereas from 2000 the focus has been to look at novel ways to improve data transmission.

Optical transmission research covers various techniques, including Optical Time Division Multiplexing (OTDM) [59], Wavelength Division Multiplexing (WDM) [60], differing modulation formats [61] and Dispersion Management (DM) [62].

3.2.1 Erbium doped fibre amplifier

The development of the Erbium Doped Fibre Amplifier (EDFA) was one of the most

important breakthroughs in optical transmission [63]. It is the most common and convenient way to amplify an optical signal with a wavelength of 1550nm and this is widely used in both commercial and research optical telecommunication systems [64].

In this thesis, the main signal recovery mechanism used is Raman amplification, but the use of EDFA's is still beneficial. This is because Raman amplifiers operate under a distributed amplification regime that spans over many kilometres, whilst the EDFA can amplify the signal over short lengths (metres) of fibre. The EDFA is used in all the experiments before the coupler in the recirculating loop (Section 3.4), to compensate for the loss associated with the coupler. To cover the loss by the coupler with the Raman amplifier would mean driving the pump lasers at higher powers, which would lead to signal distortion and added non-linear effects. EDFA's are also utilized in the transmitter (Section 3.4.1), receiver (Section 3.4.2), before the non-linear optical loop-mirror (Chapter 5, 6, 7 and 8) and prior to the autocorrelator (Section 3.5).

The basic principle of an EDFA is the same as a laser, where a pump laser excites a larger proportion of electrons from the ground state to a higher energy level by absorption of a photon, thus obtaining population inversion. The wavelength of the pump laser will dictate how many energy levels an EDFA will have, with a two level system being the simplest. Stimulated emission occurs when a photon enters the fibre amplifier stimulating an inverted electron to emit a photon in coherence with the original photon and causing the electron to return to its ground state. If the inverted electron returns to its ground state via spontaneous emission, then the emitted photon will contribute to noise in the system: this is known as Amplified Spontaneous Emission (ASE). The higher the number of energy levels that the EDFA has, the slower the decay time will be, thus reducing the noise contributed by spontaneous emission. To achieve population inversion in the EDFA used in this work, a diode pump laser is used, with a wavelength at ~980nm or ~1480nm.

The main draw back of using an EDFA is the noise, which can become considerable over successive spans, inevitably leading to deterioration of system performance. In an optical transmission system the Optical Signal to Noise Ratio (OSNR) is a good indicator of

whether there will be an excessive amount of data errors in the system. If the mean Signal to Noise Ratio (SNR) is less than 15.6dB then the required Bit Error Rate (BER) of 1.10^{-9} will not be reached. The Bit Error Rate is discussed in Section 3.3 and is generally used in the transmission industry to evaluate a systems performance.

The noise accumulated by a cascaded optical amplifier system, P_{sp}, with a gain G, can be approximated to [63]:

$$P_{sp} = 2N\left(\frac{hc}{\lambda}\right)(G-1)n_{sp}\delta f\,, \qquad (3.1)$$

where N is the number amplifiers in the system, df is the bandwidth over which the noise is measured, n_{sp} is the population inversion parameter, λ is the operating wavelength, h is Planks constant and c is the speed of light in a vacuum. Equation 3.1 was obtained by assuming the gain of the system equals the loss. The population inversion parameter, n_{sp}, is related to the noise figure of an amplifier, NF, by:

$$NF = 10\log_{10}(2n_{sp}). \qquad (3.2)$$

The two beat noise terms within the EDFA are the most dominant (signal-spontaneous and spontaneous-spontaneous noise), as discussed in Section 3.4.2, with signal-spontaneous noise being the most prolific. By placing a narrow band filter before the receiver, as shown in Section 3.4.2, the spontaneous-spontaneous noise can be kept to a minimum by limiting the bandwidth, thus reducing the interactions of the photons at differing wavelengths. The OSNR can be approximated by [64]:

$$OSNR = 10\log_{10}\left(\frac{P_{si}}{4\Delta\lambda[G-1]n_{sp}N}\right), \qquad (3.3)$$

where P_{si} is the power of the signal and $\Delta\lambda$ is the bandwidth of the filter.

High gain in an EDFA can be achieved using an erbium-doped fibre with a high concentration of erbium ions. The use of dual pumping lasers will increase the gain and the noise. The use of a 980nm pumping laser has a lower noise figure, because it has a reduced spontaneous emission associated with an increased multilevel energy system compared to the energy level system for a 1480nm pumping laser.

Careful design of the EDFA will ensure the optimum length of erbium doped fibre is used; if this fibre is too long then the pump laser will not have the required power to excite enough electrons, for population inversion. This will cause the signal to experience attenuation as the failure of the pump laser to produce population inversion causes the erbium-doped fibre to become opaque in the 1550nm region. The pumps are connected to the erbium-doped fibre by Wavelength Division Multiplexers (WDM); Isolators (ISO) are generally used to remove any unwanted noise and wavelengths propagating in the opposing direction to that of the signal.

3.2.2 Raman Amplification

One aspect of Raman amplification is that it can be distributed over the entire length of the fibre: this is known as Distributed Raman Amplification (DRA). Unlike EDFA's, which provide lumped amplification over distances of roughly 10 metres, distributed amplification maintains the pulse energy, providing a more stable propagation through a 'transparency' of the fibre. The main draw back for Raman Amplification is the high pump powers needed to provide the gain to the system if the fibre spans are greater than 100km in length. These high powers can cause non-linearity in the pump laser propagation causing noise in the system to build up. The resulting gain can exceed 40dB [65].

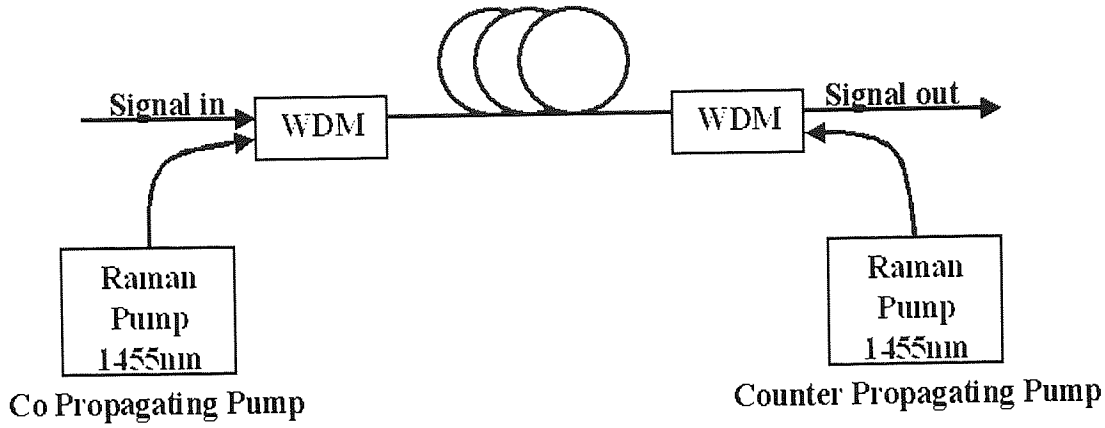

Figure 3.1 A typical Raman pump layout for co and counter pumping.

Figure 3.1 shows a typical Raman amplification scheme. The pump and the signal wavelengths are coupled into the fibre by means of a WDM. The method by which the pump energy is transferred to the signal is SRS (Section 2.3.9) and the pump laser can be either counter propagating or co propagating, as shown in Figure 3.1 [65].

To obtain amplification from a section of single mode fibre a signal must be propagated along the fibre with a pump laser, with a power normally greater than 0.2Watts.

Raman amplification of the signal occurs when the difference between the signal frequency and the pump laser frequency is within the Raman gain bandwidth. The gain, G_A, of a Raman Amplified system is given by [66]:

$$G_A = \exp\left(\frac{g_R P_0 L_{eff}}{A_{eff} K} - \alpha_S L\right), \qquad (3.4)$$

in linear units and

$$G_A = 4.34\left(\frac{g_R P_0 L_{eff}}{A_{eff} K} - \alpha_S L\right), \qquad (3.5)$$

in dB. Here g_R is the Raman gain coefficient, P_o the is the pump power, L_{eff} is the effective length, A_{eff} is the optical fibre effective area, a_S is the attenuation to the signal, L is the length of the fibre, and K the state of polarization of the pump laser. K equals 2 when the polarization is random over long distances in an optical fibre.

ASE is the dominant noise in a Raman fibre amplifier [67] as with the EDFA but not to the same magnitude.

A decrease in the size of the fibre core increases the Raman gain, since the gain is inversely proportional to the effective area of the particular fibre, as shown in equations 3.4 and 3.5. The diameter of Dispersion Compensating Fibre (DCF) is typically half that of Single Mode Fibre, therefore it has a smaller effective area, giving a significant increase in the gain for a given pump power. However too high a pump power into the DCF results in non-linear effects such as SPM (as discussed in Chapter 2) that can distort the optical signal leading to loss of data. The same effects occur in SMF but with much higher pump powers.

The amount of a particular type of dopant in the core of the fibre controls the amount of Raman gain. Standard fibre typically has 3% germanium in the core, which would give a gain of roughly $0.5W^{-1}km^{-1}$. However, if the germanium content in the core were increased to 18% then the gain would be increased to roughly $1.5W^{-1}km^{-1}$. Other types of dopant such as phosphate and fluorine in the fibre core can also increase the Raman gain [67].

The noise figure of a DRA system is close to the quantum efficiency limit, which is 3dB. The noise in a counter propagating Raman pumped system can be approximated in terms of number of photons, N_{noise}, and is described by:

$$N_{noise} \approx G_A \ln(G_A) \exp\left(-\frac{\alpha_S}{\alpha_P}\right), \quad (3.6)$$

where a_S is the optical attenuation of the signal and a_P is the optical attenuation of the pump laser in optical fibre.

The wide spectral bandwidth of the noise that builds up from DRA systems, due to the broad spectral amplification of Raman amplifiers, is such that photodiode shot noise can impair the signal. This can be overcome by means of a band pass filter placed just before the photodiode [65]. The power of the noise at the receiver is given as:

$$P_{noise} \approx h\upsilon_S \Delta F N_{noise}, \qquad (3.7)$$

where h is Plank's constant, ΔF is the bandwidth of the filter and υ_S is the frequency of the signal.

The noise figure at the receiver in an all Raman amplified system can be expressed as [66]:

$$NF = \frac{\ln(G)}{2\eta}, \qquad (3.8)$$

where G is the gain and η is the quantum efficiency of the photodiode and the division by two arises from the noise figure of Raman amplifiers at 3dB.

Fluctuations of the optical intensity at the output of a Raman amplifier may arise from temperature or spontaneous emission these fluctuations originate from the fibre laser within the Raman amplifier. These fluctuations are random and create a noise source called Relative Intensity Noise (RIN) [1].

For an amplified system (Raman plus key EDFAs), as used in the work described in this thesis, the combination of the detrimental effects of the noise from both amplifiers has to be taken into account. The noise contribution due to DRA is [68]:

$$OSNR_{DRA} = \frac{P_{Signal}}{\left(\rho_{ASE} B_0 + P_{DRB}\right)}, \qquad (3.9)$$

where B_0 is the optical bandwidth of the signal; ρ_{ASE} is the optical power density (W/nm) of the noise due to DRA, and P_{DRB} is the power of the distributed Raman backscattering (DRB) component, which can be assumed to be incoherent and to have a random polarization. The OSNR for a dual amplified transmission link, with contributions to the noise from the EDFA and the DRA, as described by equations 3.3 and 3.9 respectively, can be written as [68]:

$$OSNR = \left(OSNR_{DRA}^{-1} + OSNR_{EDFA}^{-1}\right)^{-1} . \quad (3.10)$$

Raman amplifiers have distinct advantages over EDFA's, such as a broader, flatter gain spectrum and a lower effective noise figure. Counter-propagated pumped distributed Raman amplification configurations are the most widely used as the noise from the laser pumps is effectively averaged over the fibre span that is amplified. This is in comparison the co-propagating distributed Raman amplification configuration, which is advantageous because of the lower signal power can be used, thus reducing optical non-linearity, but, because of the fast gain dynamics of the co-propagating regime this leads to a more effective RIN transfer leading to a reduction of the Q factor.

3.2.3 Transmission formats

Two commonly used transmission formats are non-return-to-zero (NRZ) and return-to-zero (RZ): other modulation formats include phase modulation, Phase Shift Keying (PSK) [69] and Differential Phase Shift Keying (DPSK) [70].

With NRZ a diode laser can be switched internally by modulating the applied bias, however, this leads to an enhanced (broader) optical spectrum that is a result of semiconductor dynamics [71]. To counteract this a constant wave source is used, which can then modulated externally by Electro-Optic (EO) or Electro-Absorption Modulators (EAM) to produce a NRZ output. The NRZ data format uses the entire bit slot (e.g. at 10Gbit/s the

bit slot is 100ps), with the off state defined by the 'one' position, and dispersion can cause the pulse to temporally spread into the neighbouring bit slot. In addition, the fact that the permanent state is 'on' increases non-linear effects that are detrimental to system performance.

The transmission format used in this thesis is RZ, so called because the pulse returns to the zero level before the end of the bit slot. A RZ pulse takes up less of the bit slot than a NRZ pulse and the RZ format is affected more by dispersion than the NRZ format. However, in the form of a soliton, the RZ format is more robust to pulse deformation caused by non-linearity with propagation distance. It is important when using the RZ format to ensure that the pulse peak power is not too high as this can lead to non-linear interactions.

The RZ format is characterized by the duty cycle, which is the ratio of the pulse duration to the bit period and the lower the ratio the better the system performance will be, e.g. a pulse duration of 5ps and a bit slot of 25ps, for a 40Gbit/s transmission system yields a duty cycle of 20%. However, the same pulse duration at 160Gbit/s gives a duty cycle of 80%, thus showing the need for much smaller pulse durations at higher data rates. The systems described in this chapter and thesis are generally concerned with RZ intensity modulation with no phase modulation.

3.2.4 Dispersion management

Pulse propagation that is stable under a high local dispersion is called Dispersion-Managed (DM) transmission system. Linear DM systems have a low power to negate any nonlinearity that may occur in the optical fibre, but enough optical power to maintain the requirements of the optical signal to noise ratio. The nonlinearity needs to be kept to a minimum in a linear DM system, as there is no passive means of reducing or compensating for it, therefore GVD is used to minimize the non-linear effect by dispersing the pulse quickly over the propagation system then recovering the pulse shape at the end of the span using a fibre whose GVD is opposite in sign to that of the first fibre. The main stipulation for this

propagation regime is that the average dispersion, ***D***, is low, and over the entire transmission link.

The nonlinearity in a DM system is unwanted, but a method of utilizing this nonlinearity is called the DM Soliton (DMS). In a DMS system pulse periodically breathes temporally between amplifier spacing causing a significant amount of chirp to build up, there is also considerable pulse broadening due to the large variations in local dispersion that can be compensated for periodically. This causes pulse-to-pulse interaction emanating from considerable overlap in the wings of the pulse, which induces a frequency shift from the phenomenon of cross phase modulation (discussed in Chapter 2). All this means that the DMS pulses are attracted to each other, which causes temporal jitter and inter-symbol interference (ISI): the overall effect is a reduction in the transmission distance. A useful property of this propagation regime is that it can reduce the growth of timing jitter and pulse distortion [72], [73] (timing jitter is discussed in Chapter 6) in DMS systems. A dispersion-managed soliton system that employs periodic dispersion compensation enhances the peak power of the pulse compared to that of a normal soliton, this is needed to balance the nonlinearity with the path average dispersion, and this can lead to a reduction in timing jitter [74]. One way to achieve dispersion compensation is to place a length of dispersion compensating fibre (DCF) before or after a length of single mode fibre (SMF).

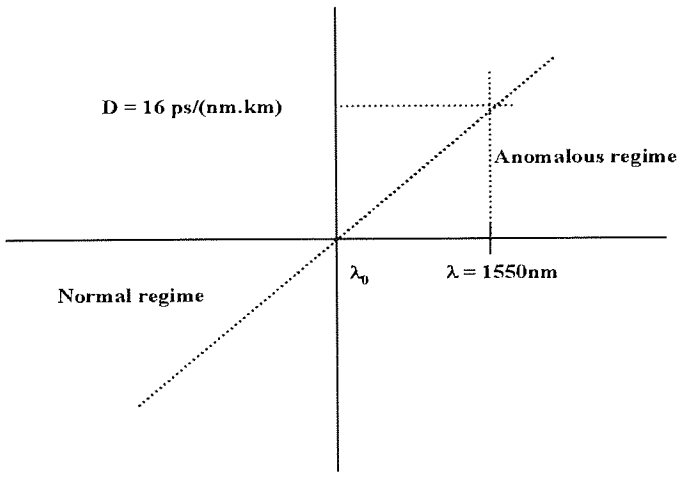

Figure 3.2 The typical dispersion for a single mode fibre with a λ_0 equal to 1300nm.

Figure 3.2 shows a plot of dispersion against wavelength, where λ_0 is the wavelength at which the dispersion is zero. At wavelengths less than λ_0, D is negative (normal regime) and at wavelengths greater than λ_0, D is positive (anomalous regime). As shown in this Figure, for standard single mode fibre, D = 16ps/(nm.km) at the operating wavelength of 1550nm, which is in the anomalous region.

For most systems employing a RZ modulation format at data rates of 40Gbit/s or greater the pulse duration is less than 7ps. For these short pulses dispersion management is a means of reducing the average Group Velocity Dispersion (GVD) to a minimum. However, for pulses with a duration less than 3ps the effect of third order dispersion can begin to have detrimental effect on pulse intensity; this can also be kept to a minimum by choosing a large value GVD for each section [74].

Good quality SMF has a dispersion value of ~16ps/(nm.km) at 1550nm, which gives a dispersion of 1120ps over a span of 70km. This amount of dispersion leads to considerable pulse broadening to the point where the pulse cannot be observed on an oscilloscope. If the power of the signal is high ISI can occur. SMF dispersion lies in the anomalous regime, which is positive and is shown in Figure 3.2. In DCF however, its dispersion lies in the normal regime, which is negative. For Instance, a length of DCF has a dispersion value of typically –80ps/(nm.km) at 1550nm and this can be cut to an appropriate length to compensate the SMF. Thus, 70km of SMF can be compensated by 14km of DCF.

Dispersion maps were employed in the work described in this thesis to optimize system performance. An example is shown in Figure 3.3. As can be seen there was a 77.8km length of SMF at 16.34ps/(nm.km) followed by a 15km length of DCF at –90ps/(nm.km). This was then followed by an 88.7km length of SMF with same dispersion value as above, compensated by a 15km length of DCF with a value of –91.66ps/(nm.km). The dotted line shows the average dispersion of the system, which is in the normal region.

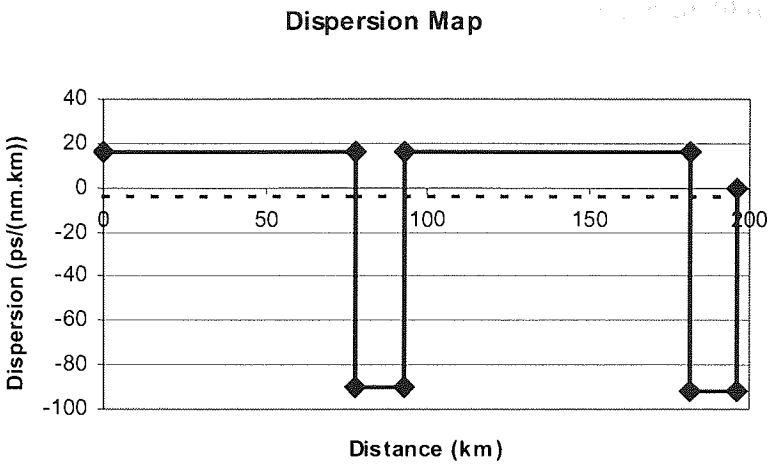

Figure 3.3 A typical dispersion map with the dashed line being the average dispersion in the normal regime.

The loss in DCF is higher than that of the SMF, where typical values are 0.5dB/km and 0.2dB/km respectively. In addition, there are coupling losses due to core diameter mismatch between the SMF and DCF, which have diameter core sizes of 10-μm and 6-μm, respectively.

Some systems use Dispersion Shifted Fibre (DSF) with low dispersion that are periodically alternated (anomalous/normal) to provide the dispersion compensation; these fibres typically will not suffer from a diameter core size mismatch if the correct specification of DSF is chosen. Raman and EDF amplification compensate the losses within the transmission system described in this thesis.

In the design of a dispersion-managed system one parameter that needs to be taken into consideration is the strength of the map, S, which is defined as [75]:

$$S = \left| \frac{(\beta_{2(1)} - \beta_{ave})l_1 \pm (\beta_{2(2)} - \beta_{ave})l_2}{\tau_{FWHM}^2} \right|, \quad (3.11)$$

where β_2 is the second order dispersion parameter, β_{ave} is the overall average dispersion in

the link (this can usually be neglected as $\beta_2 >> \beta_{ave}$); l is the length of fibre, and t_{FWHM} is the pulse duration at full width half maximum.

Map strengths between 0-10 provide the best performance as there is very little pulse spreading, so interactions are kept to a minimum, it is within this region where DMS systems are utilized. Map strengths of 10-100 give the worst performance as the pulse spreads and remains overlapped with adjacent pulses for long periods, which can lead to non-linear interactions and amplitude jitter [76].

Map strengths greater than 100 can provide a stable quasi-linear propagation regime i.e. to have a transmission system that exhibits linear propagation characteristics. To achieve a quasi-linear propagation regime the pulse needs to spread temporally rapidly, which occurs in a fibre that has a large value of chromatic dispersion. Once the pulse is fully dispersed it overlaps with many of the adjacent pulses and interacts nonlinearly with them by such means as intra channel four wave mixing and intra channel cross phase modulation. This non-linear interaction can be reduced if the optical power of the pulse is kept to a minimum for propagation but enough to overcome the level of noise so that the signal to noise ratio is not compromised, such as with a linear transmission system, so that once the pulse is fully dispersed the pulse-to-pulse non-liner interaction is weak.

The power of the signal at the inputs for the systems used in this work was kept low (–3dBm at 40Gbit/s and –9dBm at 10Gbit/s) to ensure a quasi-linear propagation [77] throughout the experiments. For high bit rate systems the limiting factor in optical transmission systems will be ISI [78], thus careful planning of the map strength is important.

If the pulse remains within its bit slot then ISI will remain at a low level. However, in DMS systems there is a strong breathing of the pulse, which leads to an increased pulse-to-pulse interaction, causing a build up of ISI induced timing jitter, which is directly linked to map strength. When the map strength is in the region 10-100, the ISI induced timing jitter is at its strongest.

ASE contributes to Gordon-Haus timing jitter [79] and is one of the major components of timing jitter is (this is discussed in detail in Chapter 6), Gordon-Haus timing jitter is proportional to the amount of dispersion in the system and to the cube of the length, making this type of timing jitter one of the limiting factors to most transmission systems. The use of distributed Raman amplification reduces the Gordon-Haus effect, as it has a lower ASE noise and this produces less of a soliton energy excursion [80]. The use of sliding filters [81], [82], and saturable absorbers reduces the Gordon-Haus effect by filtering out the ASE [83].

If a pulse is transform limited at the input then its optimum optical receiver position is the point in the fibre span where the pulse becomes transform limited again. The receiver position can then be altered to suit if the amount of chirp on the pulse is changed at the input. This can be an experimental advantage [84], as an amount of chirp can be added to the pulse before the input of the transmission span, which can negate any residual dispersion. This will then coincide with a recovered pulse shape at the end of the fibre span.

Pre and/or post-dispersion compensation [85] can be used as a method of optimising system performance. Active dispersion compensation is an automated system [86] that eliminates any excess dispersion without having to cut the fibre to the correct length. Active dispersion compensation is very useful for maintaining a low dispersion on a daily basis, since the transmission systems dispersion varies with temperature.

3.3 Transmission system performance

3.3.1 Bit-error rate

A signal will degrade when it is transmitted over optical fibre, where the extent of the degradation, depends on the system parameters. Signal degradation originates from amplifier noise, jitter, noise in the receiver and dispersion for example. These sources of degradation cause a loss of the 'bits' or 'ones' and these transpose into errors in the data

being transmitted. A count of errors is called the Bit Error Rate (BER), which is the ratio of all errors to the total number of bits: a BER Tester (BERT) performs this test. For a transmission system experiment, there is a limit to how many errors are acceptable. This limit is usually a BER of 10^{-9} in research, but in the commercial sector the standard is 10^{-12}, as market forces dictate a higher error threshold.

3.3.2 Burst measurement techniques

The measurement of the optical pulse duration, timing jitter, amplitude jitter, BER and Q-factor enable the performance of the optical transmission system to be assessed. The following sections deal with the measurement techniques used in this thesis given the equipment available.

Burst measurement is a technique that is specific to recirculating loops and requires careful timing. Measurement is taken on the last recirculation after N-loops of transmission propagation this is the required measurement window. In order to receive the incoming data the test equipment needs to be initiated, which is done using a delay generator. This technique is not required with point-to-point systems, as they do not have to repeatedly propagate down the same lengths of fibre. One of the most common pieces of test equipment used in the burst measurement technique is the BERT set, which over the measurement period divides the number of measured errors by the number of 'bits' counted [87] (as described in Section 3.3.1).

A good measurement technique is to plot the voltage vs BER, this shows how much noise is building up in the 'zero' level and the 'one' level and will provide a threshold voltage at which point the system or device becomes 'error free'. This measurement needs exactly the same optical input power for all tests.

Another measurement technique that can be used is to plot the input optical power vs BER. This demonstrates the minimum optical power level needed before it begins to degrade the system performance and errors become apparent on the BERT.

A quick way to ascertain the predicted BER is to use the Q-factor, which is measured by using the histogram setting on a Digital Sampling Oscilloscope (DSO). This is achieved by obtaining the 'ones' and 'zero' mean values and their standard deviations from the output on the DSO screen (the Q factor is originated from BER threshold measurement, where there is some Gaussian noise assumption applied: the results obtained are not prescient). The purpose of using Q factor is to accelerate error measurement procedure, which will take almost a week to reach 10^{-15}. The Q-factor is given by the following equation [88]:

$$Q = \frac{\mu_1 - \mu_0}{\sigma_1 + \sigma_0}, \qquad (3.12)$$

where μ is the mean value of the 'ones' and 'zero', with s being the standard deviation. The BER can then be calculated using the relation [89], which is an approximation valid for Q>8:

$$BER = \frac{1}{\sqrt{2\pi}} \frac{\exp\left(-Q^2/2\right)}{Q} \qquad (3.13)$$

In Table 3.1, there is a list of Q-factors and their respective BER's. For an error free propagation of 10^{-9}, a Q-factor of 6 is required.

The Q-factor provides useful information on how the system is performing: for example an OSNR of 16dB is generally required for a BER of 10^{-9}, but certain phenomenon such as Multi Path Interference (MPI) degrade the performance of the system, whist maintaining a high OSNR. However, a measurement of the Q-factor will determine that the pulse has undergone degradation due to MPI (discussed in Chapter 4).

Q	Q(dB)	BER
2	6.0	2.7E-02
3	9.5	1.5E-03
4	12.0	3.3E-05
5	14.0	3.0E-07
6	15.6	1.0E-09
7	16.9	1.3E-12
8	18.1	6.3E-16
9	19.1	1.1E-19
10	20.0	7.7E-24
11	20.8	1.9E-28
12	21.6	1.8E-33
13	22.3	6.2E-39
14	22.9	7.8E-45
15	23.5	3.7E-51

Table 3.1 The Q-factors with their respective BER's.

Another useful parameter to measure is the amplitude jitter, which can be done by using the histogram setting on the DSO, in much the same way as the Q-factor, and looking at the mean value of the 'ones'.

Timing jitter measurements can be taken on the DSO, again in the histogram mode by switching the window on the software. This allows the peak-to-peak and RMS timing jitter to be evaluated. However, the timing jitter measurement on the DSO has added jitter due to the clock recovery and the internal timing jitter on the DSO itself. Therefore, it is more accurate, especially over long distances, to use other methods such as the autocorrelator, to measure timing jitter (discussed in section 3.5). The autocorrelator that is used in transmission experiments where there are burst measurements taken, should not be internally gated, as this will cause the signal to be chopped. The gating should be externally driven and in these studies this was done by a third AOM connected to the same delay generator, which controls the burst measurement window. Ideally a slow sweeping autocorrelator should be used, with a long sweep range preferably over 100ps.

3.4Recirculating loop Set-up

3.4.1 Transmitter

The transmitter provides the optical signal containing the data to use in the transmission experiments. The recirculating loop used a mode-locked fibre-ring laser, a Pritel ultra-fast optical clock (UOC). The laser was pulsed at 9.953GHz with pulse durations of 3ps thus giving a duty cycle of 3% and the wavelength was also tuneable in the range of 1540 to 1560nm. The transmitter set-up: is shown in Figure 3.4 both electrical and optical connections are shown.

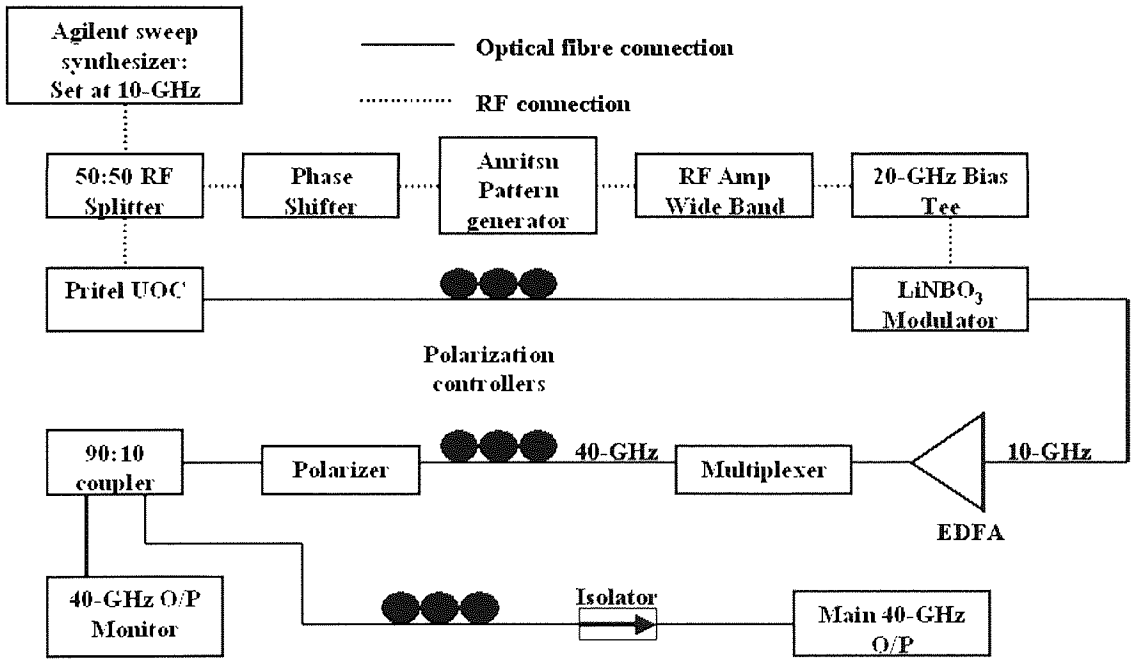

Figure 3.4 The transmitter set-up.

The Agilent synthesizer provided the 9.953GHz clock for the UOC and the Anritsu pattern generator provided the data. The timing jitter for the synthesizer was less than 50-fs

and the timing jitter exiting the UOC was ~100-fs. Typical wavelengths used were between 1550 to 1555nm region; this kept the path average dispersion to a minimum.

The UOC had a primary output power of 15dBm, which is too powerful for transmission experiments. The monitoring output was used for the main output and had a power of 4dBm. The other monitoring outputs went to an optical spectrum analyizer OSA and to a photodiode on a DSO to monitor the output when the UOC was locked in: this was observed on the DSO as a quasi-sine wave.

The UOC had two possible pulse durations 3 and 6ps. The limited resolution of the DSO meant that the only way to tell if the optical pulse was locked in to a pulse duration of 3ps was with the optical spectrum, which was much broader at 3ps than at 6ps. An example of the optical spectrum for a pulse duration at 3ps is given in Figure 3.5; this data was taken on an Optical Spectrum Analyser (OSA). As can be seen the optical spectrum has a bandwidth of 1.26nm and an optical signal to noise ratio (OSNR) of ~40dB at the output of the transmitter.

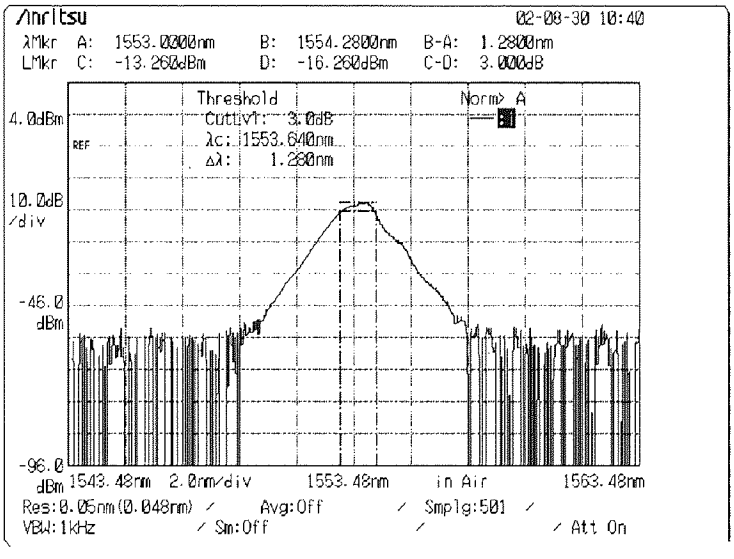

Figure 3.5 Optical spectrum of the 3ps pulse produced by the UOC.

The phase shifter (shown in Figure 3.4) was used to enable one bit of data exiting the pattern generator, to line up with the pulse produced by the UOC, thus giving a zone of optimization. The pattern produced by the Anritsu was a pseudorandom bit sequence (PRBS) and this had a length of 2^n-1, where n equals 7, 15, 23, 27 and 31, with n = 31 being the most like a data pattern in a real life transmission system.

The wide-band RF amplifier in Figure 3.4 had a gain of 1W (30dBm). The Sumitomo produced Lithium Niobate ($LiNBO_3$) modulator imposed the data pattern on to the UOC pulsed output. The polarization controllers (PC) before the modulator were required, due to the modulator being polarization sensitive. This meant the optimum setting needed to be found at every time the apparatus was setup, which can be done easily with a power meter or observing the peak power of the optical pulses on the DSO. The EDFA recovered the optical losses in the modulator and in the subsequent multiplexer and an ASE filter reduces the bandwidth of the noise. The set-up of the multiplexer shown in Figure 3.4 is given in more detail in Figure 3.6.

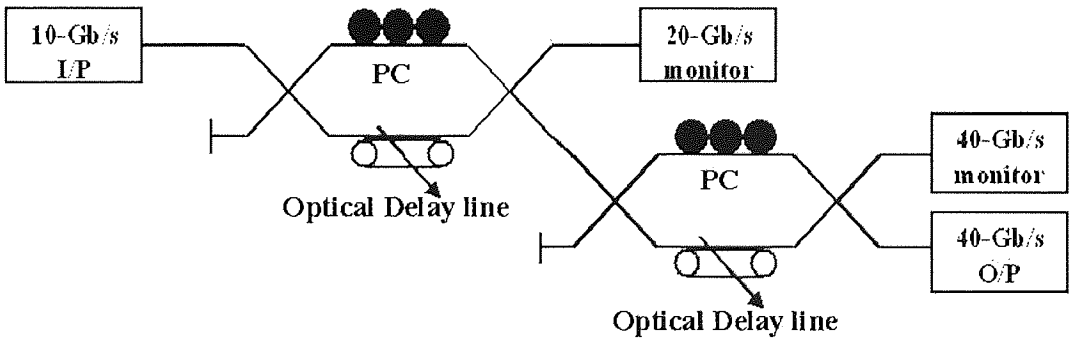

Figure 3.6 10 to 40Gbit/s multiplexer.

As shown in Figure 3.6, the optical signal was OTDM from 10 to 40Gbit/s. The pulse duration on leaving the multiplexer was ~4.0ps, which gave a duty cycle of 18% at 40Gbit/s. The multiplexer used in this experiment was affected by environmental changes

such as temperature, which meant that the output needed to be monitored throughout the experiment.

Particular care had to be taken in the setting of the system parameters and the optical pulse power to keep the output consistent on the DSO, as it was easy to have one channel with more optical power than the others: the optical powers are set by the polarization controllers. The spacing between bits is also important; this could drift with time. The optical delay lines removed the drift as shown in Figure 3.6, the optimum setting kept ISI to a minimum.

The polarizer and the last polarization controller shown in Figure 3.4 were used to obtain the best performance in the recirculating loop. The main output goes into the coupler used in the recirculating loop and the optical power entering the loop can be controlled by the EDFA before the multiplexer.

3.4.2 Receiver

The receiver provides the means of detecting the optical signal by converting it to a electrical format so that the data can be regenerated on the BERT. The layout for the receiver that was used in these studies is shown in Figure 3.7.

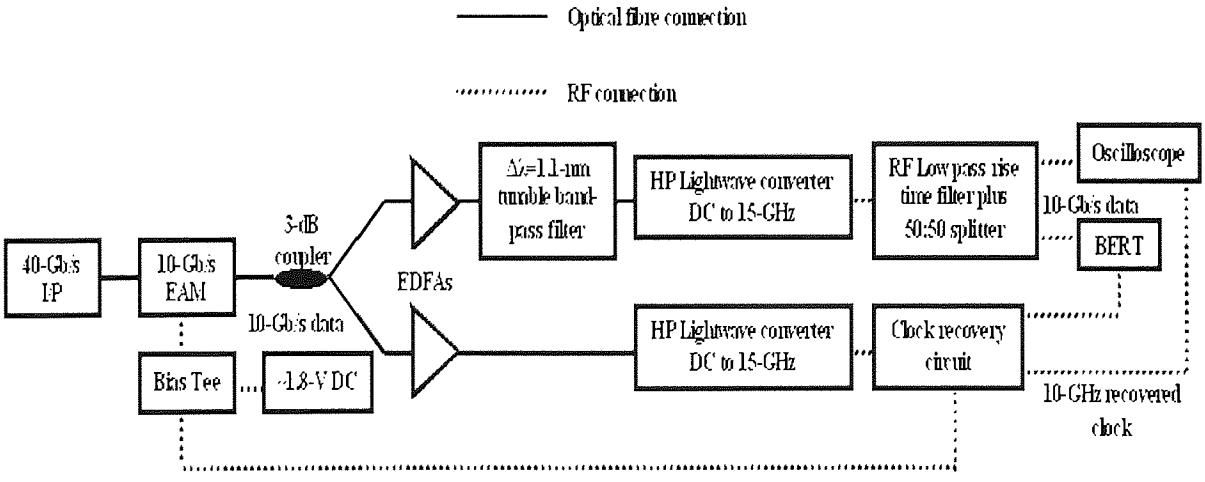

Figure 3.7 The demultiplexing and receiver setup from 40 to 10Gbit/s.

As shown on Figure 3.7 the 40Gbit/s optical signal was demultiplexed down to 10Gbit/s by the EAM. The DC bias for the EAM was ~-1.8V with an RF drive of 18dBm. After the EAM the signal was split 50/50 and passed through EDFAs.

After the EDFAs shown in Figure 3.7 (top), the data signal was then passed through a 1.1nm Band Pass Filter (BPF) to remove unwanted noise before going into the HP lightwave converter (photodiode). The electrical RF data signal was passed through a low-pass rise-time filter: this opened up the eye diagram on the DSO for better determination of voltage threshold on the BERT and it removed any unwanted high RF frequencies. The RF signal was then split 50:50 and connected to the BERT and the oscilloscope.

The clock recovery signal went directly into another HP lightwave converter (without a BPF). The converted clock signal was connected to the clock recovery circuit shown in Figure 3.7 (bottom). The unit that recovers the clock was a JDSU Q-Clock and is shown in Figure 3.8. The Q-Clock works by differentiating the spectral energy of the incoming RZ data stream at 9.953GHz and 10.664GHz. The clock can then be extracted at 9.953GHz using a narrow band resonance RF filter. The resultant clock was aligned with the use of variable phase shifters, as shown in Figure 3.8, to control the window on the EAM so that the channel that is required from the OTDM signal can be selected and demultiplexed.

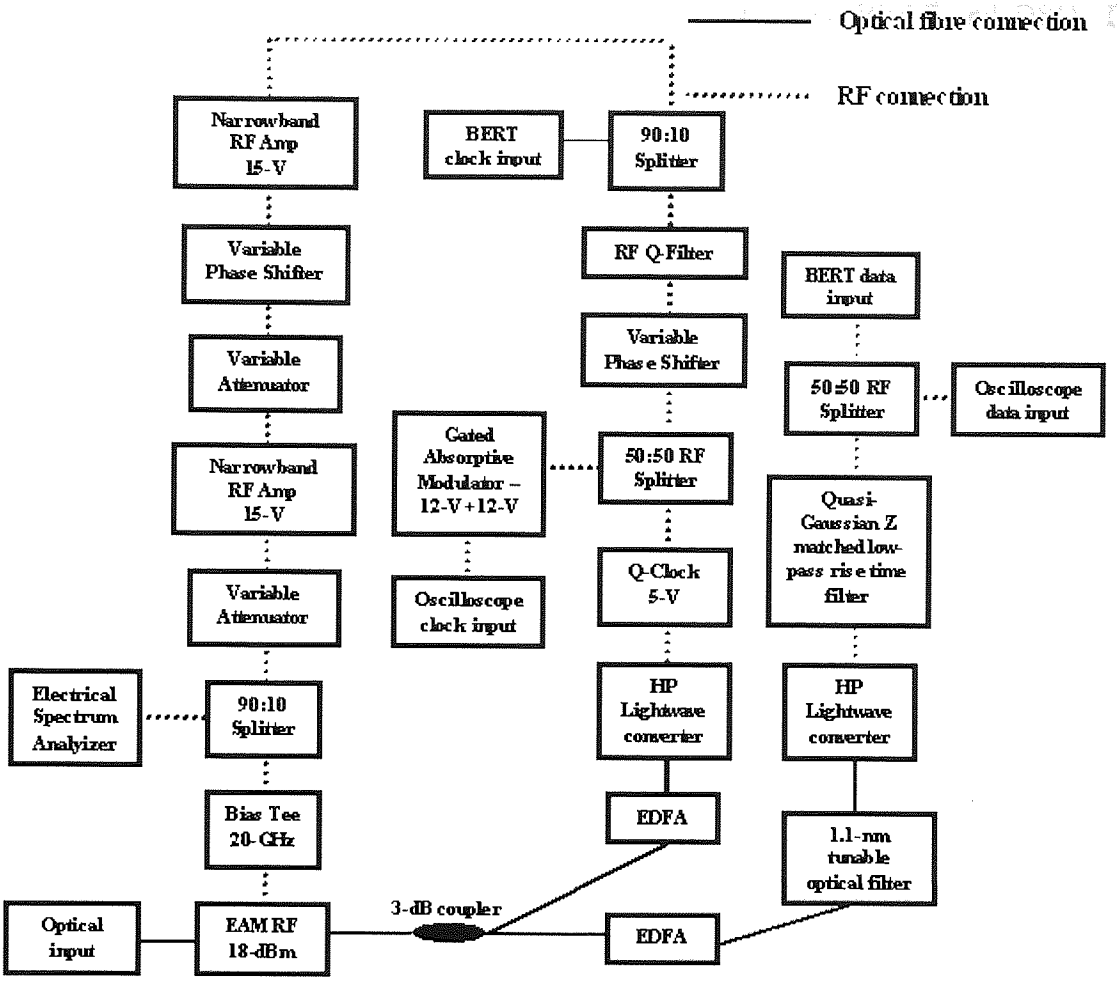

Figure 3.8 Clock recovery setup, shown in Figure 3.7.

The gated absorptive modulator shown in Figure 3.8 was connected to the delay generator and used to control the information going to the DSO, so that the DSO only sampled the data that was within the time allocated for the burst measurement.

The first narrow band RF amp had a low gain and recovered the losses from the preceding RF equipment. The narrow band RF amp between the variable attenuators was used to get the optimum RF power to the EAM. The electrical spectrum analyser (ESA) was used to monitor the clock output. The timing jitter of the recovered clock could be seen to increase after an increasing number of recirculations, by observing the OSNR of the 9.953GHz clock signal.

The recovered RF 9.953GHz clock was also connected to the BERT and DSO. The 10Gbit/s demultiplexed signal which was obtained without the rise-time RF filter is shown in Figure 3.9. The 10Gbit/s demultiplexed signal has a good clean eye with low amplitude jitter on the 'ones' and low noise on the 'zero'. The 40Gbit/s signal as shown in Figure 3.9 was obtained using a 32Gbit/s photodiode on one of the monitor outputs on the recirculating loop coupler (Section 3.4.3, Figure 3.11).

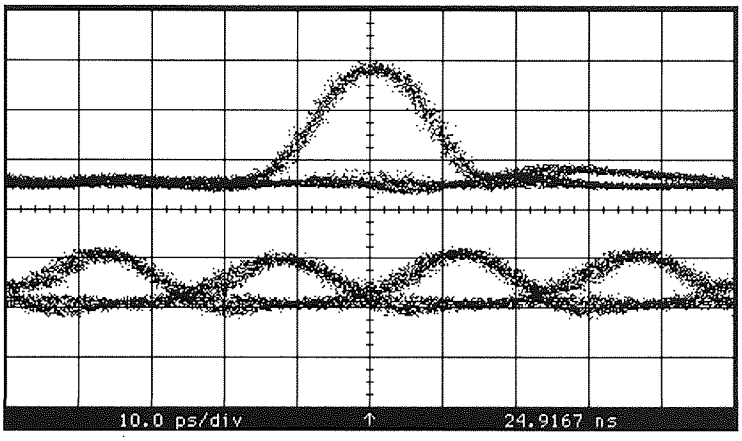

Figure 3.9 Eye diagrams for 10Gbit/s top, and 40Gbit/s bottom.

3.4.2.1 Receiver noise

When an optical signal is incident on a photodiode, the signal will have a certain amount of noise that has accumulated from the distributed and lumped amplification. In addition there will be noise added by the photodiode. The mean electrical signal to noise ratio (SNR) is defined as [24]:

$$SNR = 10\log_{10}\left[\left(\frac{P_{si}\lambda}{hc}\right)^2 \frac{1}{B\sigma^2}\right], \quad (3.14)$$

where B is the electrical bandwidth of the receiver and s is the noise variance. The noise variance that is associated with the photodiode is thermal noise, shot noise and beat noise between optical signals.

The contributions to the beat and shot noise are split into four categories, with signal shot noise being the most significant.

1. Signal-spontaneous beat noise is intensity variations with a broad bandwidth that occur from signal interference with the spontaneous noise, and cause current variations.
2. Spontaneous-spontaneous beat noise is intensity variations with broad bandwidth occurring from spontaneous noise interfering with spontaneous noise at a differing wavelength.
3. Signal shot noise is a constant noise signal that is produced by the mean of the signal power.
4. Spontaneous-shot noise is a spontaneous noise current that is produced by the mean of the spontaneous noise.

However, in a cascaded amplifier system the noise generated by the amplifiers is usually far greater than the noise variance generated by the receiver.

3.4.3 Recirculating loop arrangement

The recirculating loop has been used in soliton research [90] and transmission experiments [91] and a detailed description is given in [92]. The recirculating loop is an ideal platform for testing transmission systems as it allows optical fibre identical to that used in commercial systems to be tested and results that are acquired in computer simulations to be verified.

Generally, one or two spans of fibre with dispersion compensating fibre are coupled together with amplification to overcome the dispersion and loss in the system. The signal

can then be recirculated around the loop until the desired distance or BER floor (10^{-9}) is reached.

Once a recirculating loop is set up at the desired length, so that the path average dispersion is low, various propagation 'phenomena' can be observed: these include soliton interactions and four wave mixing. Components and devices may be tested to see how much they degrade/improve the system over many recirculations.

A schematic diagram of the recirculating loop is shown in Figure 3.10. The signal enters and passes through the first Acoustic Optical Modulator (AOM-1), which is controlled by the delay generator. AOM-1 controls the fill time of the loop, this should ideally be between one and a half to three times the propagation time of light in the fibre, to eliminate any excessive noise accumulation provided by the amplifiers when no signal is present. A fraction of the signal power is lost with each recirculation due to the loop coupler (shown in Figure 3.10).

An EDFA is used to compensate for the losses of the coupler and this was then followed by an ASE filter and a polarization controller (PC).

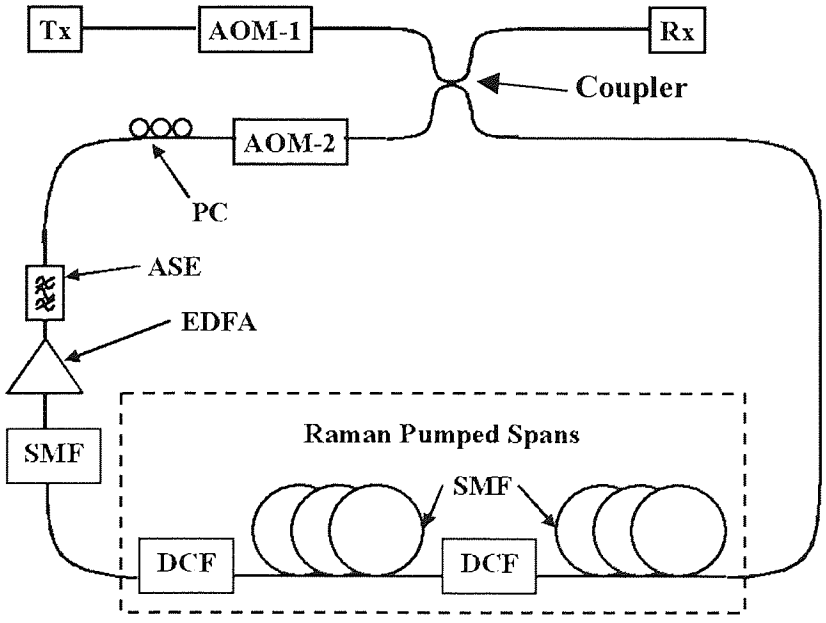

Figure 3.10 The core recirculating loop setup.

AOM's have a large optical extinction ratio (60 to 70dB on/off value), so leakage of the signal can be neglected: if the measurement timing is out this will lead to an AOM letting signal through, then a ghost signal may appear on the oscilloscope, which will add to the noise. The signal then passes through a 50:50 coupler: other ratios of couplers may be used, but the signal then has to be amplified either in the recirculating loop or before the receiver set-up.

The coupler arrangement [93] is shown in Figure 3.11, with the losses clearly indicated. It has one main output and two monitoring outputs.

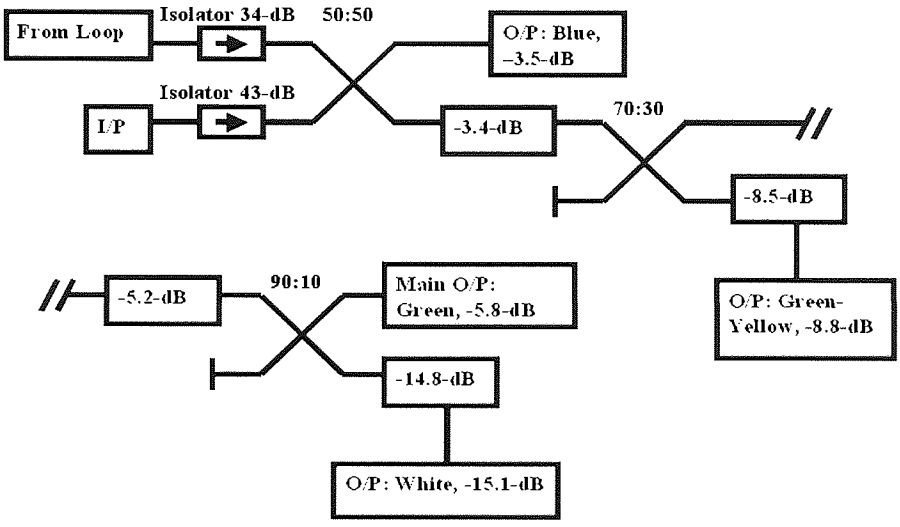

Figure 3.11 The coupler arrangement for the recirculating loop.

The white monitoring output shown in Figure 3.11 was coupled to a photodiode, which allowed the power within the loop to be observed on a 200-MHz oscilloscope. The recirculation loops are observed as steps on the oscilloscope with N-steps representing N-loops. The use of distributed amplification gives the steps a gentle curvature on the oscilloscope. If lumped amplifiers were used then the steps (loops) would have a sharp discontinuity. It is ideal to have the power on each of the N-loops the same, which can be achieved by matching up the steps to the same level.

The green-yellow monitoring output enables monitoring of the eye-diagram for the evaluation of the Q factor before it goes through the demultiplexer. The demultiplexer re-times the pulse thus reducing the timing jitter. It also reshapes the pulse in a similar way to synchronous modulation [94], and lead to re-timing of the signal. This output can also be attached to an OSA that can also be gated off the delay generator. As discussed in Section 3.5, the autocorrelator can be connected to this output monitor to observe pulse duration evolution and to make timing jitter measurements. The main output from the coupler goes to the receiver.

The delay generator setup is shown in Figure 3.12. The switching of the AOM's was controlled with electrical signals depicted as AB and –AB in Figure 3.12: AB was an analog signal and –AB was a digital signal. The Anritsu BERT had a low negative peak-to-peak voltage for the burst measurement control, therefore the 0 to 3V peak-to-peak voltage leaving the delay generator had to be converted to the lower negative voltage required 0 to –1V peak-to-peak. The electro absorptive modulator shown in Figure 3.12 was used to control the burst measurement on the DSO.

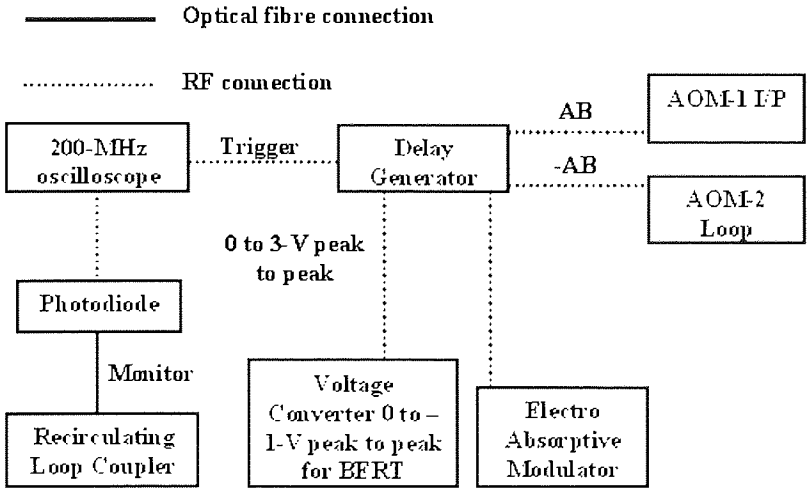

Figure 3.12 The delay generator setup.

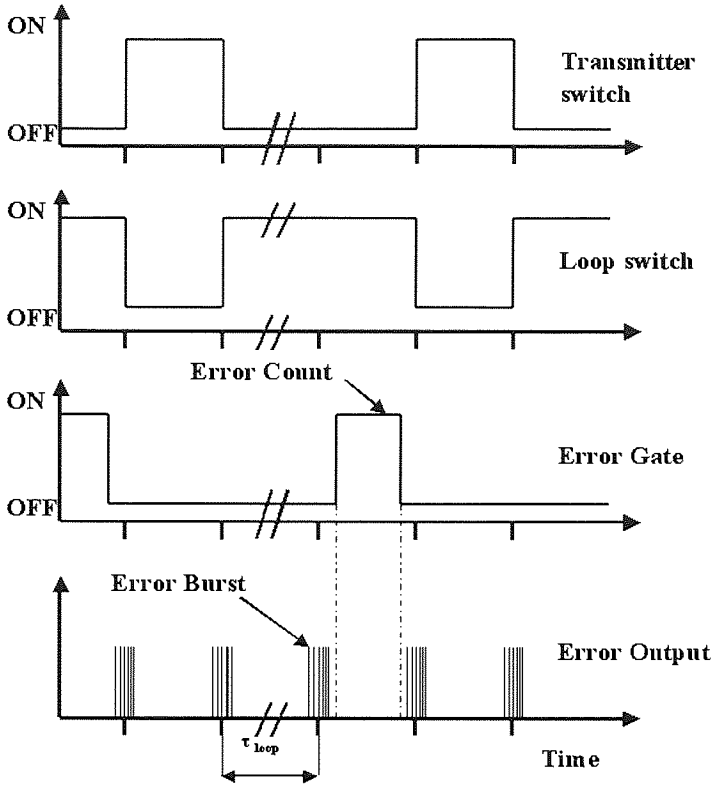

Figure 3.13 The electrical loop timing.

To allow switching to and from the recirculating loop (Figure 3.10), a switching time of ~68μs was allocated. Once the recirculating loop is full of data, AOM-1 closes and AOM-2 opens, AOM-2 allows the propagation of the signal. The timing for both of the AOMs was programmed into a delay generator. The loop timing controlled the fill time, recirculation time, measurement time and the reset time, and is shown in Figure 3.13.

The amount of time it takes a photon to travel around the loop is given by the loop round trip time:

$$\tau_{loop} = \frac{L_{span} n_{core}}{c}, \qquad (3.15)$$

where L_{span} is the total fibre length, n_{core} is the refractive index of the core, c is the speed of light in a vacuum, t_{loop} is indicated in Figure 3.13. The propagation time is given by:

$$T_{prop} = N\tau_{loop} + R_{time}, \qquad (3.16)$$

where N is the number of recirculations within the loop, and the resynchronization time for the BERT is given by R_{time}. The measurement time is governed by:

$$M_{time} = \tau_{loop} - R_{time} - S_{time}, \quad (3.17)$$

where S_{time} is the switching time of the AOM.

AOM-2 is controlled by the delay generator as discussed earlier, and this will stay open for the entire propagation time. The measurement time or burst measurement was smaller than one round trip as shown in Figure 3.13. Once it was set at the right time, it could be fine tuned using the BERT set to get the optimum position and to compensate for environmental changes during the experiment. There may be a need at the end of N-loops to have a small amount of time allocated for the resetting of the test equipment.

The fibre in the recirculating loop was Corning SMF-28, which was compensated for by the slope compensated dispersion compensated fibre (SC-DCF). In SMF β_3 is ~0.07ps^3/km. The Raman pumping configuration did not change between experimental set-ups, and the SMF and the SC-DCF were both backward pumped in relation to the signal. The two Raman pumps (IPG) were fibre lasers that provided up to 5W each. For the experiments in Chapter 4 these were split to the ratio of 70:30 (SMF:DCF). For the work described in Chapters 5 to 8 the pumps were split to the ratio of 50:50 (DCF:DCF) and 50:50 (SMF:SMF), so that the pump power going in to the DCF and the SMF could be controlled by independently.

Before any experimental measurements were carried out, reference optical pulse measurements were taken by setting the delay generator to allow the optical signal to pass straight through the coupler to the receiver; this can be called the back-to-back set-up. The reference optical pulse can then be used to obtain the Q factor, the BER and the

autocorrelation trace. All the settings in the transmitter are then generally optimized to produce the best propagation results. The reason an autocorrelator was used instead of a DSO for the pulse duration and jitter measurements was that the resolution on the DSO is only suitable for pulses with a duration greater than 14ps due to it's bandwidth and in this system the pulse duration was 3.5ps. The DSO adds 700-fs of timing jitter to the system, however, the autocorrelator requires no clock recovery, so, it provides a simpler, more accurate measurement of pulse duration and timing jitter.

3.5 Autocorrelation and measurements

To observe ultra-fast pulses with sub 14ps pulse durations, an alternative is needed to that of the DSO, as the bandwidth usually provided with the photodiode or the modules is not sufficient. There are DSOs that can measure pulse durations of less than 10ps to meet the need of a 40Gbit/s system but these can be costly. A streak camera could be used but these can have inadequate resolution [95]. There are also optical sampling oscilloscopes on the market that can resolve 1ps, but these are very expensive. The most cost effective way to resolve ultra-fast pulses down to 100-fs and less is to use an autocorrelator: a device that is based on the Michelson interferometer. The first autocorrelation measurement of optical pulse duration was performed by [96].

The autocorrelator is not ideal: if a pulse's intensity profile becomes complex then the intensity structure of the pulse tends to get lost. For noisy pulses with a complex intensity, such as those that have propagated over a long distance, this noise tends to be generated as a spike on the autocorrelator output: this process will be discussed in more detail in this Section and in Chapter 6. Certain information, such as phase, cannot be extracted using a standard autocorrelator as the autocorrelator averages over many events. However, for symmetric pulse's the autocorrelation measurement technique is useful for measuring pulse duration and timing jitter.

3.5.1 Autocorrelator set up

Within the autocorrelator, a pulse is manipulated in order to provide measurements on itself. The basic set-up of an autocorrelator is given in Figure 3.14: as shown, the pulse enters the autocorrelator and is split into two identical pulses, where one of the pulses undergoes a delay with respect to the other. The two pulses are then overlapped spatially in a second harmonic generation (SHG) crystal. The autocorrelation trace displays the SHG pulses energy (a product of the input pulses) versus delay.

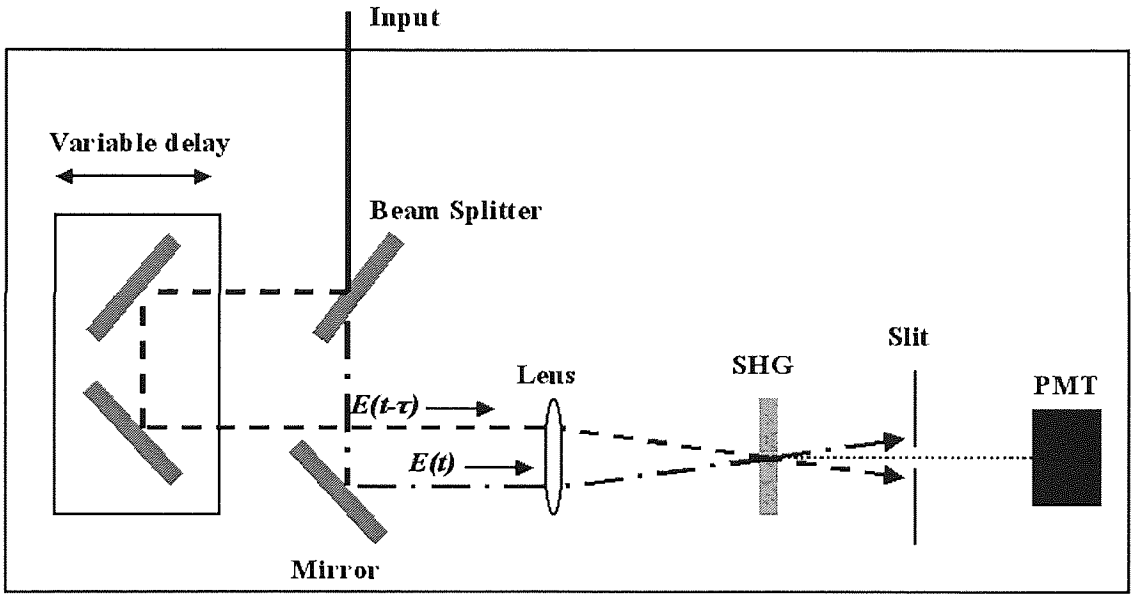

Figure 3.14 Basic set-up of an autocorrelator.

The SHG produces a signal at twice the frequency to the input signal with an electric field envelope, described by [97]:

$$E_{sig}^{SHG}(t,\tau) \propto E(t)E(t-\tau), \quad (3.18)$$

where ***E(t)*** is the electric field amplitude of the first pulse and ***E(t- t)*** is the electric field

amplitude of the second pulse. t is the delay imposed on the second pulse, with the condition that the delay t must be longer than the pulse duration. The pulses produced by the SHG have a maximum energy at $t = 0$. The intensity is also proportional to the product of the intensity of the two pulses:

$$I_{sig}^{SHG}(t,\tau) \propto I(t)I(t-\tau). \quad (3.19)$$

However, most detectors that are used in autocorrelators are to slow to resolve a single optical pulse so they measure the intensity correlation, $G(t)$, of many optical pulses [95]:

$$G(\tau) = \int_{-\infty}^{+\infty} I(t)I(t-\tau)dt, \quad (3.20)$$

A Photon Multiplying Tube (PMT) as shown in Figure 3.14, is used to measure the SHG pulses energy. By varying the delay, information about the initial pulses can be obtained by averaging out many optical pulses. The set-up of the autocorrelator is critical, as misaligned input beams or incorrect relative polarizations at the critical plane will lead to a loss of output of the mixed light beams within the SHG crystal.

For effective SHG to occur the momentum and energy from two photons at the fundamental wavelength must be transferred to a photon at the second harmonic. For this to happen the two wavelengths have to comprise an equal phase velocity. It is important that the phase velocities for both the ordinary and extraordinary wave in an appropriately chosen SHG crystal are matched (the latter cases are dependent on the polarization of the optical pulse see Figure 3.15), as is the optical axis alignment of the crystal to the propagating waves. Tilting of the crystal allows for changes in the wavelength and non-optimum cut crystal to be accounted for. Improvements in the cutting and polishing of commercially available crystals have simplified the alignment procedure [95].

This autocorrelator set-up with the polarizer at the input as shown in Figure 3.14 is known as Type 1 mixing. The two pulses within the autocorrelator travel with the same

polarization, but are displaced by mirrors and are focused onto the same plane within the crystal by a lens. All this leads to a non-collinear mixing to produce SHG in the crystal. This is shown more clearly in Figure 3.15.

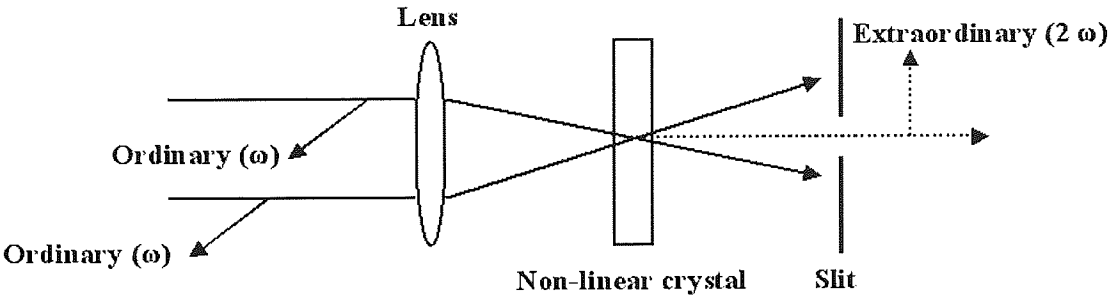

Figure 3.15 Details type 1 mixing: both inputs have the same ordinary polarization, after mixing in the crystal the second harmonic has a polarization at 90 degrees and in extraordinary.

Type 2 mixing occurs when the polarizations of the pulses are orthogonal to each other (ordinary and extraordinary), and the beams are not displaced by mirrors as in Type 1 mixing. Type 1 and Type 2 mixing are both dependent on which crystal is used and its quality of facet cut [95]. Both Type 1 and Type 2 mixing have a zero background noise autocorrelation: in Type 1 mixing this is due to the geometry of the setup, whilst in Type 2 mixing it arises from the orthogonal polarization. Type 2 mixing was not used in this research.

The autocorrelator used in this research was an Inrad 5-14-LD, the set-up of which is shown in Figure 3.14. A Femtochrome autocorrelator was also used for some back-to-back measurements, but as it was gated internally, it caused problems with measuring the pulse duration and timing jitter. This was due to the frequency of the internal gating, which was in direct conflict with the frequency of the gating for the recirculating loop and caused the

output to be chopped up on the oscilloscope. Therefore, an alternative solution was employed, which comprised a slow scanning autocorrelator as shown in Figure 3.16.

The inputted optical signal into the autocorrelator was 1550nm. The SHG crystal used in this set-up was Lithium Iodate ($LiIO_3$) and, as shown in Figure 3.16, could be swivelled to achieve the optimum angle to produce maximum SHG power from the crystal. The crystal could also be traversed parallel to the direction of propagation to coincide with the focused beams from the lens. The slits were used to eliminate the passage of the 1550nm signal that is residual after the crystal. The 1550nm filter was used to eliminate any unwanted signal.

The maximum scan range or variable delay that could be used was 180ps, but the most common setting used was 100ps, with a scan rate of 1 or 2ps/s. The translation stage controller performed this and this also controlled the gain of the photo-multiplier tube. The scan range of 100ps would capture the main pulse and the subsequent pulses for the use in cross correlation measurement.

The set-up of the autocorrelator was achieved using a helium neon laser, which lases in the visible part of the optical spectrum and enables the tuning of the geometry of the beams to be optimised more easily than using an infrared source. This is necessary as the optimal set up for a autocorrelation system can be difficult to achieve as the light beams have to be parallel and at the same height throughout the system. Once the light rays are geometrically correct then the visible source can be substituted for the infrared source, and the optimum angle for the SHG crystal found. The focal point of the lens should coincide with the middle of the crystal and tilting the crystal and observing the output of the PMT can find the maximum SHG. When this has been observed then the optimum focal point can be found by traversing the crystal parallel to the beams.

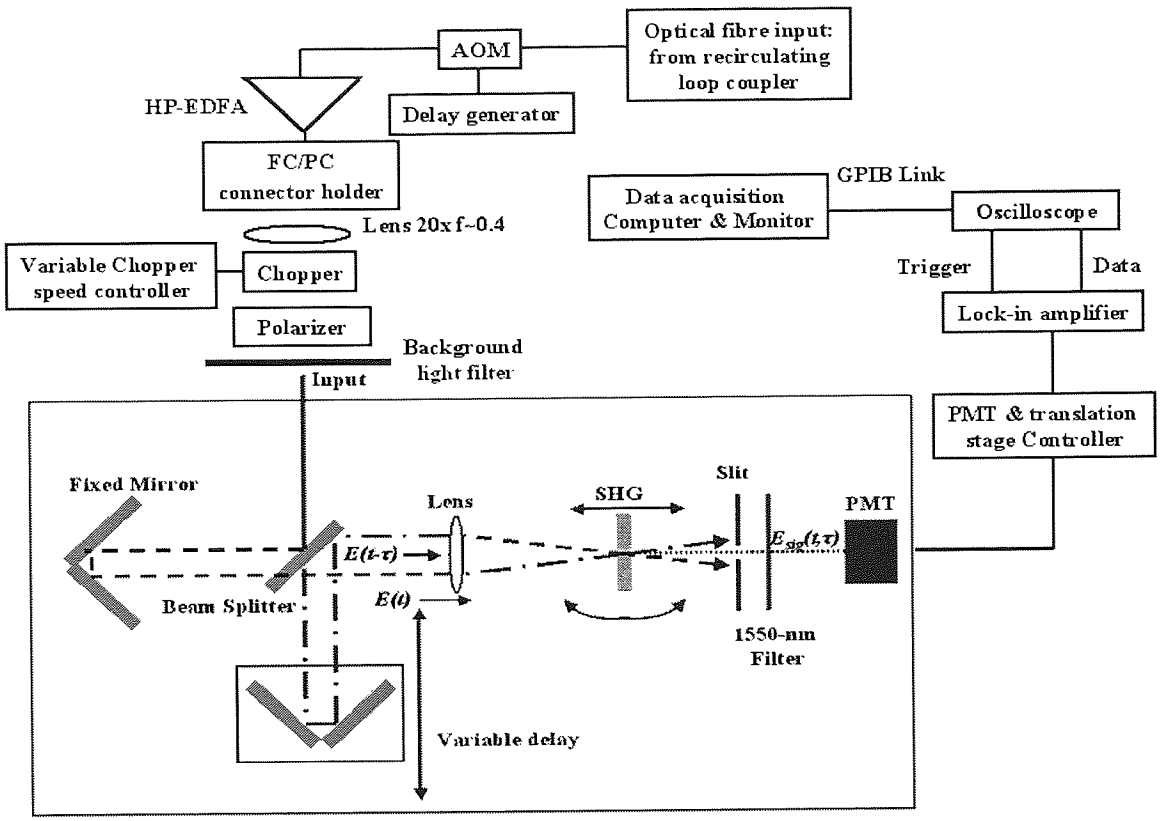

Figure 3.16 The experimental setup for the Autocorrelator used for pulse duration and timing jitter measurements.

At the input to the autocorrelator there is an iris and a background light filter. These are to protect the PMT, which is very sensitive to stray light that may enter the system. There was also polarizer at the input that could be adjusted to get the optimum polarization, which was also identified by observing the output power at the PMT. Generally, once the maximum output of the SHG is obtained then the rest of the components can be fine-tuned to achieve the optimum performance.

As shown in figure 3.16, a high power EDFA provided the gain to cover the losses incurred by the system and the power needed for SHG. A tuneable optical filter was used after the EDFA to remove any unwanted ASE. The signal coming from the recirculating loop passed through a third AOM, which was connected to the delay generator, thus synchronizing the autocorrelator with the measure time at the end of N-loops.

An optical chopper, whose speed could be varied, was used in conjunction with a low frequency lock-in amplifier; this gave narrow band amplification of the signal at the frequency set by the chopper, which was usually around 1-kHz. This frequency was chosen because it can be easily differentiated in the lock-in amplifier from the gating of the recirculating loop. The lock-in amplifier was used to reduce the received electronic background noise. The lock-in amplifier then triggered the oscilloscope, which displayed the temporal pulse shape, ***G(t)***. ***G(t)*** is an averaged pulse shape that exits the PMT, whereas ***I(t)*** is the pulse shape exiting the SHG. Therefore, knowledge of the input pulse is needed and any transformations of the pulse within the system, to be able to assume the exiting pulse shape. A computer was linked to the oscilloscope to capture and save the data points.

3.5.2 Pulse duration measurements

To recover the ***I(t)*** from ***G(t)*** in equation 3.20, it is assumed the ***G(t)*** at $t=0$ is symmetric and therefore ***I(t)*** is also symmetric about its maximum intensity. There can be a whole range possible pulse shapes [95], but it can be assumed that the pulse shape is either Gaussian, $sech^2$, Lorentzian or an one-sided exponential. Table 3.2 shows the conversion factors by which to relate the FWHM of the autocorrelation function (***G(t)***) with the FWHM of the input pulse, from which the pulse duration can be calculated. Explicitly, the FWHM of ***I(t)*** is equal to the FWHM of ***G(t)*** multiplied by 1/k.

Assumed pulse shape, *G(t)*	**Time bandwidth product, dv/dt**	**Conversion factor, dt/dt = 1/k**
Square	0.886	1
Gaussian	0.441	0.707
$Sech^2$	0.315	0.648
Lorentzian	0.221	0.500
Single sided exponential	0.110	0.500

Table 3.2 The correction values for autocorrelation traces with differing pulse shapes.

3.5.3 Noise and Timing jitter measurements using the cross-correlation method

If there is modulated noise present in the pulse then this will show up as a spike on the autocorrelator trace. The noise bandwidth or the temporal coherence range of the noisy signal would determine the width of the spike, and this noise will effect the contrast ratio. This spike will sit on the top of the pulse waveform and get progressively larger with increasing noise as the pulse is propagated over many kilometres. This is shown in Figure 3.17, which shows the autocorrelation trace for 40Gbit/s propagation.

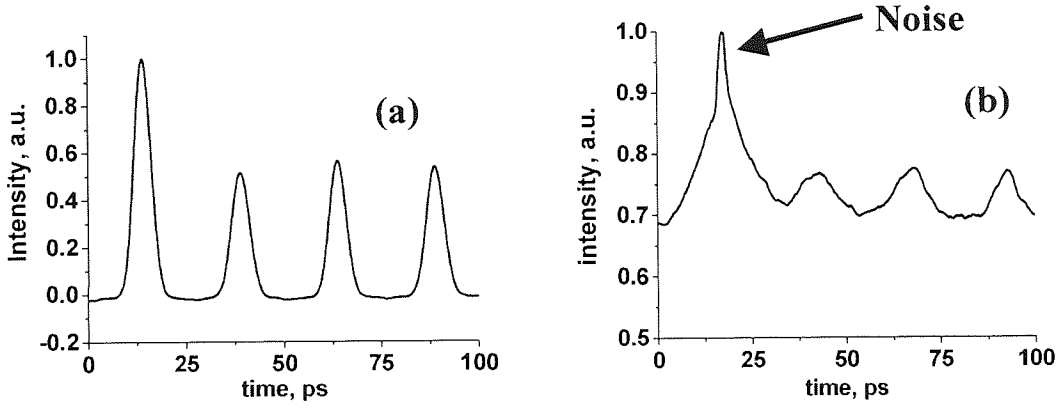

Figure 3.17 Plots of G(t): (a) autocorrelation trace back-to-back, (b) autocorrelation trace after considerable propagation with noise spike.

As can be seen in (a) on Figure 3.17 (discussed in more detail in chapter 6, in relation to the timing jitter) the contrast ratio is around 3:1 and the pulses for 40Gbit/s has a clean Gaussian shape. However, comparing with (b), the contrast ratio has reduced to 3:2, and there is a clear modulated ASE spike on the main peak, this in accordance with previous studies [98].

The reason the secondary pulses are at half the intensity is partly due to the PRBS, where the subsequent pulses have a 50% probability that they will be a 'one' or a 'zero', this results in an average of half the power and half as many pulses contribute secondary

pulse as to the main pulse. Another reason is that the timing jitter causes the intensity to spread to the sides of the pulses, and the timing jitter in the system increases as the propagation distance increases. This will also cause the intensity of the secondary pulses to fall below the 0.5 intensity mark.

The cross-correlation technique to determine the timing jitter of a propagated pulse was used by [99], and to look at the jitter in DM autosoliton system by [100], [101], [102]. The theory of the cross correlation technique and the mechanisms of timing jitter will be discussed in more detail in chapter 6.

To obtain the timing jitter from the resulting trace, as shown in Figure 3.17, the average FWHM of the secondary pulses are taken. There are three secondary pulses for 40Gbit/s propagation as the scan range of the autocorrelator is 100ps and the pulses are 25ps apart. The FWHM of the main pulse is then subtracted from the average FWHM of the secondary pulses to obtain the timing jitter. The calculation used depends on the Probability Density Function (PDF) of the timing jitter, which in most cases can be approximated, to be Gaussian.

3.6 Summary

In this chapter the details of the optical transmission systems and the measurement techniques used in the work described in this thesis have been outlined such as the recirculating loop, modulation format and transmission system performance. Included was a discussion of the problems associated with setting up the recirculating loop and dispersion management.

Transmitter and receiver set-ups were described and a short discussion on EDFAs was presented. Measurement techniques for optical pulses were described, and a detailed account of autocorrelator theory and set-up was given. Pulse classification and duration measurements were discussed, as was the measurement of timing jitter, which is discussed in more detail in Chapter 6.

Chapter 4 Evaluation of Dispersion managed, Raman amplified transmission systems.

4.1 Introduction

In this chapter, Section 4.2 is concerned with Raman amplification when applied to optical transmission systems. The theories behind the detrimental effects that occur to the optical signal when Raman amplification is used are discussed in Section 4.2. The experimental setup of the recirculating loop used in this chapter is described in Section 4.3. The results that were collated during the all-Raman pumped transmission at 40Gbit/s in standard single mode fibre over 1600km are shown and discussed in Section 4.4. Finally the chapter is summarized in Section 4.5.

4.2 Raman Amplification

Most long haul optical fibre networks installed to date use standard single mode fibre (SMF). Upgrading these systems to higher bit-rates such as 40Gbit/s and above represents a very attractive proposition.

Earlier studies have shown that advanced dispersion management and all-Raman amplification are likely to be the key elements in such an upgrade [103], [104], [105], [106], [107], [108]. Multi-path interference (MPI) caused by the double Rayleigh back scattering (DRBS) of the signal proves to be one of the major obstacles when implementing the high-power Raman amplification required in the systems with amplifier spacing of the order of 100km and above [107], [108], [109]. Studies on the cross-sectional area of the fibre and its affects on signal degradation due to MPI have been reported [110]. There has also been research into Raman effects with differing fibre types, and their effect on the propagation of wavelength division multiplexed systems [111].

In this chapter, the impact of span configuration on DRBS in a single-channel 40Gbit/s is reported. An all-Raman amplified standard SMF transmission system with the mid-range amplifier spacing of 80-90km is discussed. Four different span configurations are compared experimentally. A transmission distance of 1666km (1973km including Dispersion Compensating Fibre (DCF)) in SMF is observed.

4.2.1 Double Rayleigh backscattering and Multi Path Interference

As the gain on a Raman amplifier is increased, this not only increases the signal power but also the number of scattering events. These scattering events are often referred as the Rayleigh backscattered signal [112], [113]. The Rayleigh backscattered signal does not decay, but goes on to produce more Rayleigh backscatter, thus interfering with the signal at the receiver. This phenomenon is called Double Rayleigh Backscattering (DRBS) and it has been stated that this may be the limiting factor to Raman amplification [114], [115], [116], [117]. The main problem caused by MPI is that it's optical spectrum is the same as the signal and therefore special techniques need to be used when evaluating system performance.

Along several kilometres of fibre, numerous Rayleigh scattering events will take place. The amount of DRBS noise will steadily increase as the gain is increased and be mixed incoherently with the signal at the receiver. Each scattering event will result in an interfering noise signal with a different phase, such that, the resultant DRBS noise represents a delayed version of the original signal with random phases at each frequency component [115], [116].

Since the signal and the spectra of the DRBS coincide, the DRBS MPI impairments are not highlighted in Optical signal to Noise Ratio (OSNR) measurements. For this, a carefully designed Q factor measurement technique is needed to quantify how MPI degrades the system. The Q factor is a good determinant of whether a Return to Zero (RZ) transmission system has suffered degradation, it is calculated using the oscilloscope from the ratio of

background noise 'zeros' to signal level 'ones'. The degradation to the system caused by MPI can be viewed as a penalty to the Q factor, which can be expressed in decibels [117]:

$$\Delta Q[dB] = 5\log\left(1 + Q_{REF}^2 \frac{MPI}{k}\right), \qquad (4.1)$$

where Q_{REF} is the input signal Q factor. The mean DRBS noise to mean signal power gives the ratio of MPI. This is determined by k (the ratio of peak to RMS power of the pulse) in equation 4.1, the value of k is affected by the narrow band filter, and is calculated by taking the ratio of peak to average optical power after the filter, in the case of a RZ data signal k is also dependent on the pulse duration. In these studies a filter with a bandwidth of 1.1nm is used before the receiver, this is slightly narrower than the bandwidth of the pulse generated by the laser. Therefore, this optical filter removes a much of the noise in the wings of the pulse. The use of the 1.1nm filter was determined experimentally as it provided the best system performance.

The eye diagram given in Figure 4.1, shows a pulse with a peak electrical power of 215mV and a RMS value (including the offset voltage of 81mV) of 74mV. These voltages give a k value of ~3, this is in accordance with previous studies [117], which state that a RZ pulse should have a k value between 3 and 4.

The type of data format can also influence the amount of MPI in a system. For example it has been suggested that Q penalty (dB) for RZ has a greater immunity to MPI than Non Return to Zero (NRZ) by 1.5 to 2dB [117].

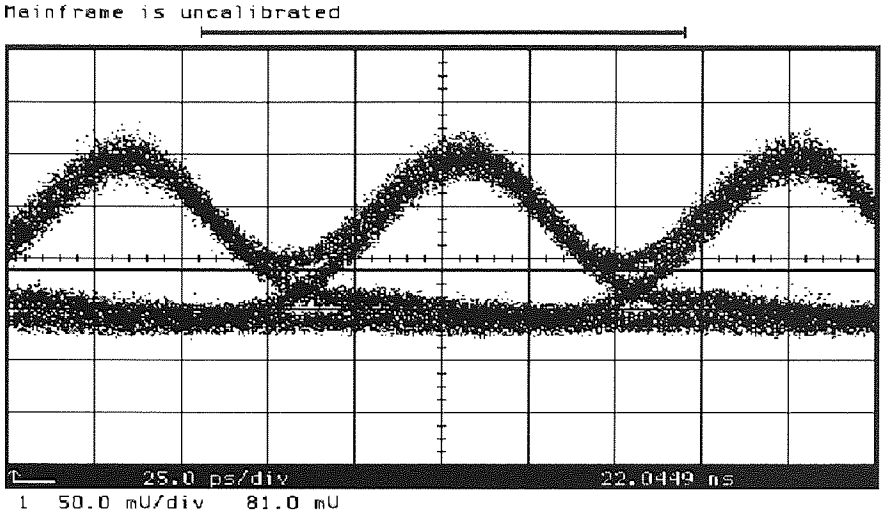

Figure 4.1 The electrical eye diagram that determines the k value in equation 4.1, the thick black line denotes the RMS electrical power level.

Counter propagation pumping increases the amount of MPI in the system but this can be reduced significantly by bi-directional pumping [114]. This method works by splitting the gain between the co and counter pumped amplifiers, MPI is then minimized due to the lower gains involved. This suggests that a counter-pumped amplifier with a high gain will suffer from DRBS and that Raman amplification would be far better suited to a distributed amplification scheme than a high gain lumped amplification unit.

4.3 Experimental set-up

Transmission experiments were conducted in a recirculating loop as shown in figure 4.2 and set-up experimentally similar to that described in Chapter 3, but with differing fibre lengths. In the transmitter, a tuneable mode-locked fibre laser (PriTel) generated 3.5ps pulses with a repetition rate of 10GHz. The pulses were modulated at 10Gbit/s with a 2^{31}-1 pseudorandom bit sequence and optically multiplexed to 40Gbit/s. All the pulses in the transmitter output were polarised identically. On the receiver side, the transmitted 40Gbit/s

data stream was optically demultiplexed to 10Gbit/s using an electro-absorption modulator [104]. Transmission performance was evaluated by measuring the bit error rate averaged over the four 10Gbit/s channels. Average signal power launched into the loop was in the range –3 to –1.4dBm, with the low powers used non-linearity could be kept to a minimum and the system could be said to be operating in the quasi-linear regime. The EDFA (Marconi) within the transmission loop had a noise figure of 5-6dB, whereas the Raman amplifiers (IPG) had a noise figure of 3-4dB.

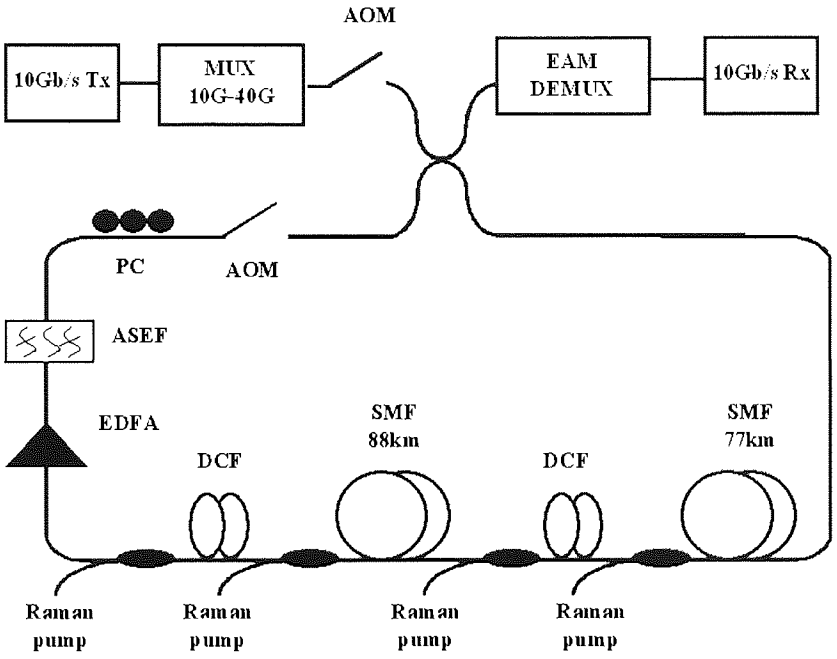

Figure 4.2. Experimental set-up, the EDFA within the loop had a NF~5-6dB, the max gain of the 77km SMF plus DCF was 37.3dB with a total NF~9.5dB. For the 88km of SMF plus DCF the max gain was 43dB with a NF~13dB.

The fibre span in the loop consisted of a dispersion over-compensated section and a dispersion under-compensated section, each including a length of SMF (Corning SMF-28) and a slope compensated dispersion compensating fibre module (SC-DCF), OFS DK80 with an effective area of 20-μm^2.

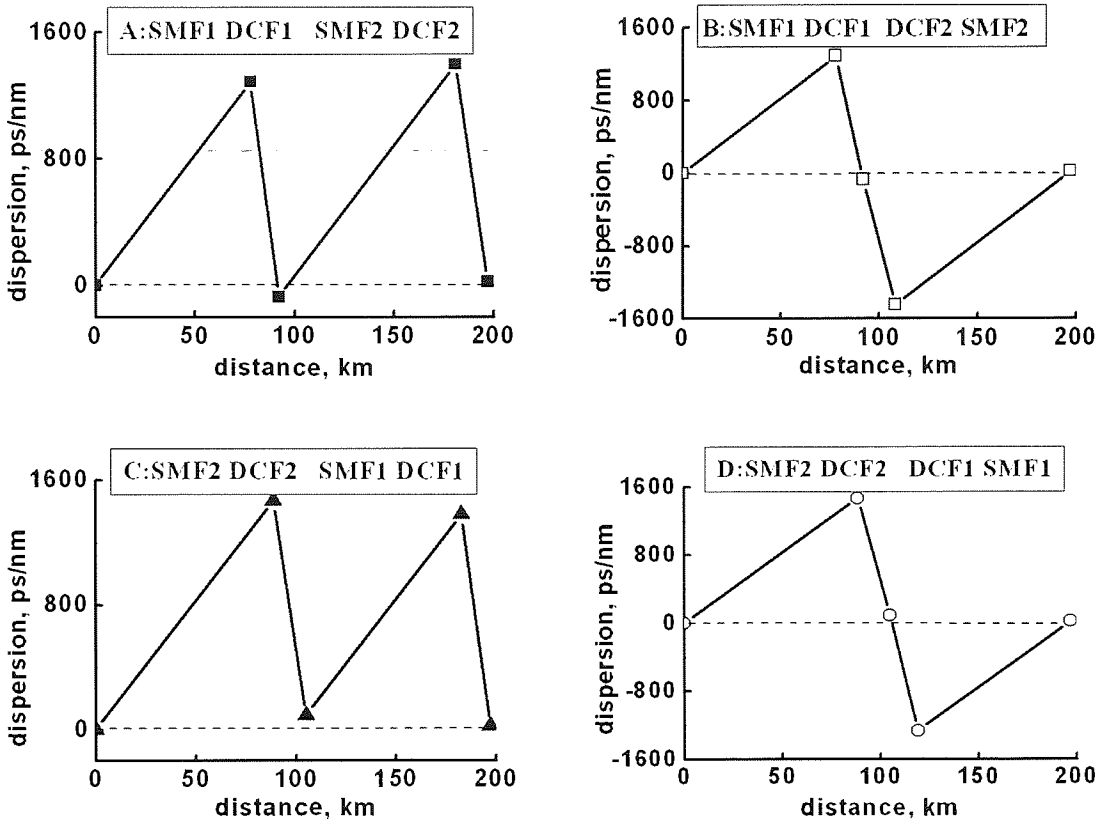

Figure 4.3 Dispersion maps of four types of fibre span configurations. Fibre connection sequences are given in each plot.

The SMF1 and DCF1 in the dispersion over-compensated section 1 had lengths of 77.88km and 14.14km, with the dispersion of 16.54ps/(nm·km) and -96.11ps/(nm·km) respectively. The SMF2 and DCF2 in the dispersion under-compensated section 2 were 88.76km-long and 16.33km long, with the dispersion of 16.54ps/(nm·km) and -84.2ps/(nm·km) respectively. The four different dispersion maps are shown in Figure 4.3. The important fibre characteristics of the two SMF section and the two DCF sections, are given in Table 4.1.

The differing SMF lengths and DCF placements were then studied experimentally by altering the sequences of the two sections of SMF and changing positions of SMF and DCF in each section. The accumulated dispersion over the two spans was 2726.23ps/(nm.km)

and the residual dispersion was 7.76ps/(nm.km). The average dispersion of the fibre over the total span was 0.04ps/(nm.km).

Two Raman pumps operating at a wavelength of 1455nm provided the amplification on each section. In each section, the pump power was split between the SMF and the DCF with a ratio 70:30. Hence, the SMFs and DCFs were pumped individually and acted as four distributed Raman amplifiers with a counter-propagating pump. Figure 4.4 shows a typical Raman amplification scheme. Isolators in Raman wavelength multiplexers (WDM) were used to eliminate the effects of any lumped reflections.

	Length, km	Loss, dB/km, @1550nm	Total Loss, dB @1550nm	Loss, dB/km @1455nm	Dispersion, ps/(nm·km) @1550nm	Dispersion slope ps/(nm²·km) @1550nm
SMF #1	77.88	0.209	17.49	0.247	16.54	0.06
SMF #2	88.76	0.201	20.55	0.279	16.54	0.06
DCF #1	14.14	0.520	11.66	0.81	-96.11	-0.0568
DCF #2	16.33	0.477	12.12	0.87	-84.2	-0.0574

Table 4.1 The fibre characteristics used in this chapter.

Gain in the two sections reaches an estimated value of 0.54dBkm^{-1} for the SMF and 0.87dBkm^{-1} for the DCF. This arises from the fact that the SMF has a lower Raman gain coefficient than that of the DCF. Specifically the gain coefficients are 0.27W^{-1}km^{-1} and the latter is 1.454W^{-1}km^{-1}, respectively.

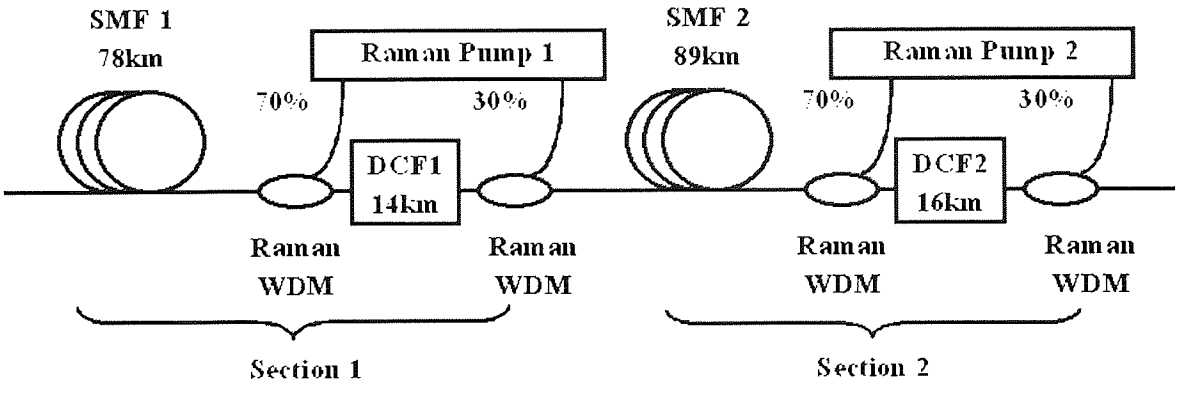

Figure 4.4 Typical amplifier configuration (dispersion map A).

4.4 Results and discussion

A plot of the Raman gain versus pump power for the individual SMF and DCF fibres is shown in Figure 4.5(a). Also shown is the gain saturation in DCF #2, which is in accordance with previous findings [118] for identical fibre length, pump power and core size. A plot of the OSNR versus pump power is given in Figure 4.5(b) for the individual fibres.

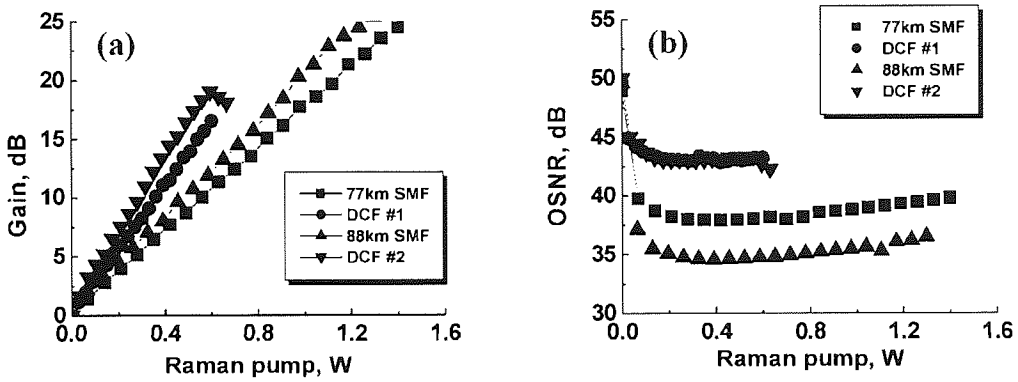

Figure 4.5 Raman gain for the individual fibres (a) and the OSNR for differing pump values (b).

Total optical loss in each section was ~16dB. To compensate for that loss, the Raman pump power was in the range of 1.2-1.3W per section. At this high power level, the DRBS becomes significant and MPI causes degradation of the Q factor of the received signal. At the same time, the optical signal-to-noise ratio (OSNR) remains high since the spectra of the DRBS and the signal coincide [108]. Therefore, the presence of DRBS can be detected by independent measurement of the Q factor and the OSNR. In the experiments, these measurements were carried out simultaneously whilst the Raman pump power was varied.

During the measurements, the power of Raman pump 1 (Figure 4.5) was kept at a constant level of 1.3W, whilst the power of pump 2 was varied in range 1.1-1.9W. As a

result, gain of the signal in the dispersion overcompensated section (section 1) was constant and equal to 30dB. Gain of the signal in section 2 varied (as the power of the Raman pump was increased or decreased) and this was then combined with the gain in the SMF in section 2. The gain to the signal was (15dB to 25dB) in the SMF and the gain to the DCF in section 2 was (11dB to 18dB).

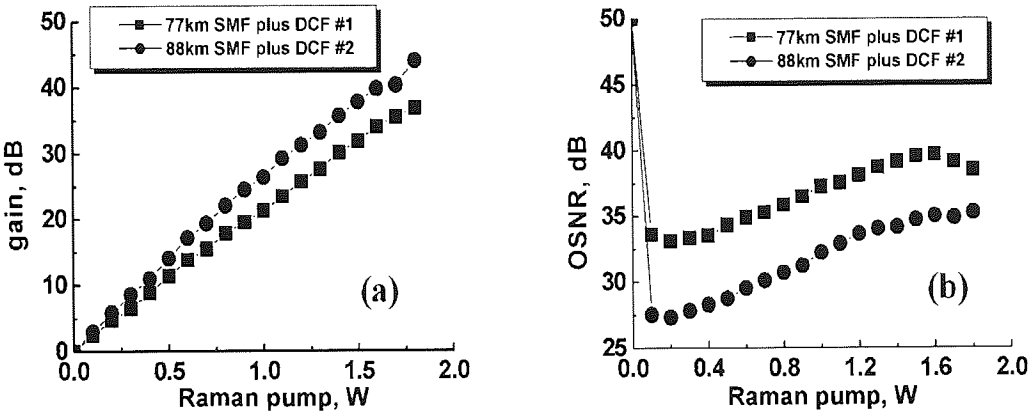

Figure 4.6 Gain Vs pump power for SMF and DCF (a) and OSNR Vs pump power (b).

In Figure 4.6(a), the gain in both the SMF and the DCF for both cases can be observed to increase linearly with pump power. The OSNR versus pump power in Figure 4.6(b), shows that an increase in fibre length of 11km produces a penalty in the OSNR of ~5dB. The OSNR can be seen to increase with pump power, before it reaches a peak and starts to reduce, this effect is more noticeable in the 77km SMF plus DCF #1 case. The reduction in OSNR is due to excessive ASE noise building up in the fibre link, and non-linear interactions from the higher signal power, primarily in the DCF. There is no observed saturation of the Raman gain as the input signal is -1.0dBm, which is low enough not to cause saturation within this length of fibre.

Figures 4.7(a) and (b) show the ONSR and the Q factor of received signals after six round-trips in the loop (approximately 1000km of SMF) as a function of the pump power. The Q factor was measured using a digital sampling oscilloscope. In the absence of MPI, OSNR and Q should have similar trend. It can be seen from Figure 4.8(a) that the OSNR constantly increases with the pump power, whilst the Q factors first increase with pump power and then decrease after reaching the peak.

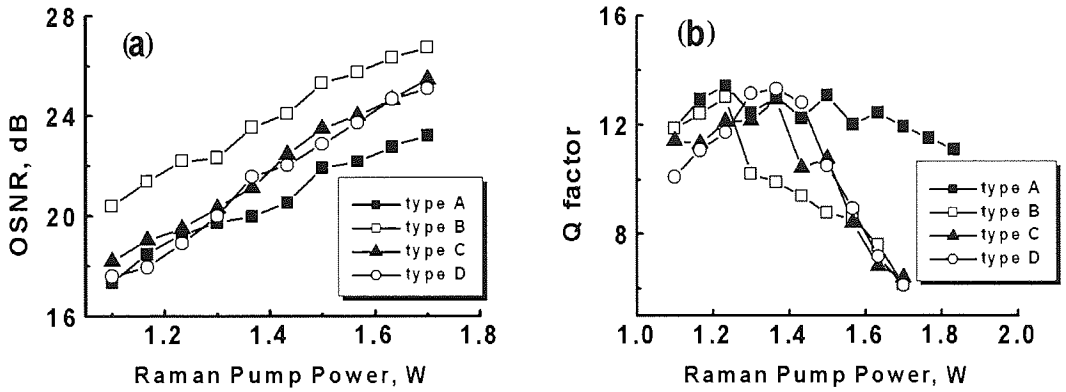

Figure 4.7 Pump power effect on output OSNR (a) and Q factor (b) after total 1200km of propagation.

It is estimated that the average power of the signal arriving to the DCF2 (Figure 4.3(b)) never exceeded 0dBm. The signal propagated in DCF2 is in quasi-linear regime, i.e. no significant degradation, caused by non-linear self-interaction of the signal occurred. Therefore, the observed rollover of the Q factor is attributed to strong DRBS at pump levels above 1.3W.

The increasing noise floor of the background MPI versus the Q penalty in dB is shown in Figure 4.8(a), and this was calculated using equation 4.1. The reference Q factor was taken back-to-back and is the best obtainable Q factor for this system. The delta Q factor for the specific type of map used was calculated by comparing the Q factor obtained over the

map type with the reference Q factor. The MPI could then be calculated with both of the Q factors obtained. The MPI value was then compared by increasing the Raman pump power.

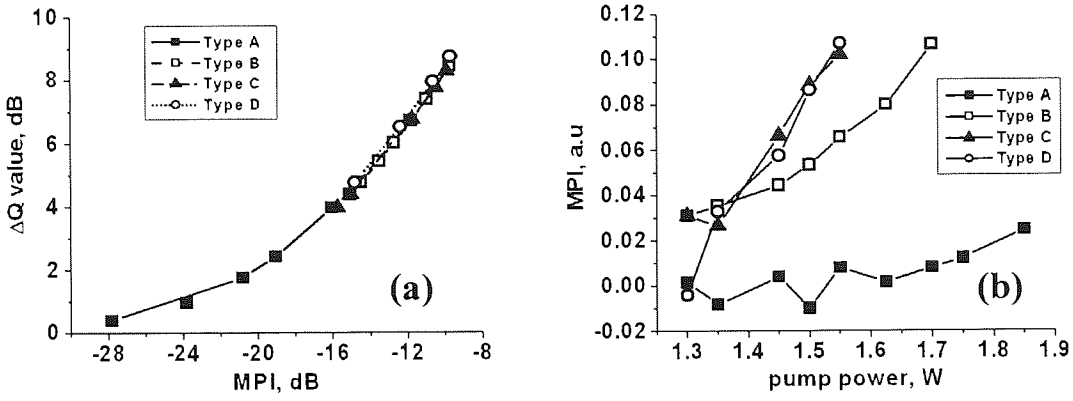

Figure 4.8 (a) Increasing level of MPI noise Vs the Q penalty, and (b) rising MPI level in linear units Vs the pump power.

The experimental results show a good correlation to the numerical results given in [117]. As can be seen the result for type A over this range of pump power produces the lowest value of MPI with all the other types of dispersion maps producing a higher MPI noise floor. As can be seen for map type A the change in Q factor is small which can be directly correlated to a low MPI value. All of the other maps have a large change in Q factor that leads to a higher MPI value. Figure 4.8(b) shows the normalized MPI value increase versus the Raman pump power for all four maps, and this shows that type A dispersion map has the optimum performance, with the MPI building up at a much-reduced rate. This result shows the direct link between the Q factor and the MPI value, and the use of the Q factor to determine any system degradation that OSNR values alone would miss.

In the earlier studies, it was found that the Q factor degradation due to DRBS is strongly dependent on the dispersion management in a dispersion map comprising positive dispersion fibre and negative dispersion fibre (PDF/NDF map) [107], [108], [109]. In line

with these results, there was observed a strong dependence on the dispersion map configuration in an SMF-based system. It was found that the most robust type of map configuration against DRBS was type A, where the dispersion over-compensated span was followed by dispersion under-compensated span as shown in Figure 4.3(a) along with the other types of map configuration.

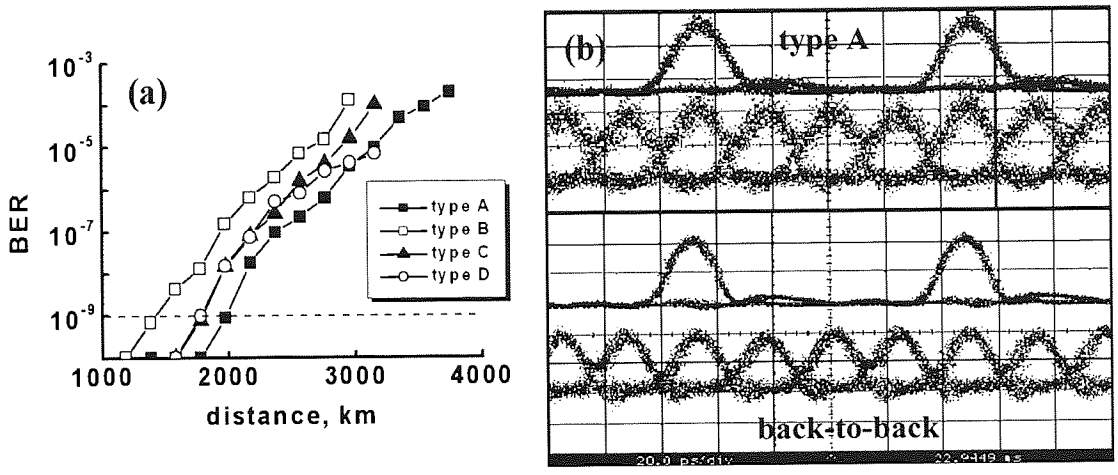

Figure 4.9 Comparison of BER performance of a single channel 40Gbit/s data stream in the four system configurations (a) and an example of the eye diagram (b) back-to-back bottom and type A top after 1970km total propagation (10Gbit/s demultiplexed eye above for each case).

The transmission performance of the four types of map used can be compared in Figure 4.9(a). The Raman pump levels were adjusted for each map in order to minimize the output error rate. The optimal pump power was in range 1.2-1.5W per section. As was expected given the previous measurements, the configuration type A showed the longest error free ($BER<10^{-9}$) transmission over 10 round-trips in the recirculating loop, corresponding to the transmission distance of 1666km in SMF (1970km including SMF and DCF).

The eye diagrams in Figure 4.9(b) shows; the 40Gbit/s and demultiplexed 10Gbit/s signal back-to-back in the bottom eye diagram; the 40Gbit/s and demultiplexed 10Gbit/s

signal after 1600km in the top eye diagram. As can be observed there is a small amount of added dispersion in the 40Gbit/s signal after 1600km, when compared to the back-to-back case. The retiming of the pulse can also be seen in both cases for the 10Gbit/s signals, with reduced timing jitter when compared with pulses in the 40Gbit/s data stream. This figure is the 'raw' transmission distance achieved without forward-error correction. It is estimated that a FEC scheme similar to that used in [106] could extend the transmission limit to 3000km if applied in the system presented in this chapter.

4.5 Summary

The results obtained in this chapter indicate that system degradation caused by DRBS can be minimized by optimization of the amplification regime. This yields a significant improvement, delivering system performance similar to the theoretically limited one. A further optimization of the dispersion map also gave improved results to a standard fibre transmission system. An error free propagation over 1666km of standard fibre has been achieved. The results demonstrated here show a possible route for upgrading the installed standard fibre networks.

Chapter 5 Signal propagation in dispersion managed systems guided by non-linear optical loop mirrors

5.1 Introduction

In this chapter, the main topic is the improvements in signal propagation that can be obtained by inserting a Non-linear Optical Loop Mirror (NOLM) into a transmission system.

In Section 5.2, the theories of the NOLM, effects of concatenation and DM autosoliton propagation are discussed. The improvements in propagation by the addition of a NOLM to a transmission system at 10Gbit/s and 40Gbit/s are also shown in this section. Signal propagation at 80Gbit/s requires the use of a different NOLM: this is discussed and experimental results are presented in section 5.3. Finally in section 5.4 the chapter is summarized.

5.2 Background theory

In this section the background theory of the Non-linear Optical Loop Mirror (NOLM) and its abilities to suppress background noise are discussed. The NOLM's application in a transmission system and the observed propagation regime that arises from concatenated loop mirrors is discussed.

On the fundamental level, degradation of the transmission performance of a soliton system is mainly caused by pulse-to-pulse interaction and an accumulation of spontaneous emission noise. These detrimental effects can be suppressed to some extent by an optimization of the dispersion map and improvements to other aspects of the transmission system, such as transmission format and amplification scheme. A more radical improvement can be achieved by signal regeneration. Even partial regeneration, including

reshaping and re-amplification of the signal (2R-regeneration) affects the system performance significantly.

One way to provide 2R regeneration is to employ a non-linear optical element acting as a saturable intensity filter. Non-linear optical loop mirror and semiconductor saturable absorber are two well known non-linear intensity filtering techniques [120], [121]. Data transmission over transoceanic distance in a low-strength dispersion map using saturable absorbers has been reported recently [120]. However, the NOLM has never been implemented in long-haul data transmission, in spite of receiving a considerable research attention over the last decade.

Recent theoretical studies have suggested that in-line NOLMs can provide stable pulse propagation in a dispersion managed fibre system [121], [122], [123]. Specifically, not only does the NOLM act as a 2R regenerator, but also a new DM autosoliton propagation regime is supported by a NOLM guided system that does not exist in an equivalent DM-system. The main advantage in using a NOLM instead of a Non-Linear Amplifying Loop Mirror (NALM) is that the NOLM is a completely passive device. Therefore, it does not introduce additional amplified spontaneous noise that is inevitably present in the NALM output.

There exists a considerable difference between the NOLM guided DM autosoliton and the filter-guided DM soliton. A filter is a linear element; hence the DM soliton's existence requires the propagation through the fibre to be essentially non-linear. On contrary, NOLM is a non-linear switch, and DM autosolitons can exist in the system even if the propagation in fibre is linear (or quasi-linear, as in our experiment). This stable wave (the ideal information carrier) is reproducible at the output of each section, and has its characteristics set by the system parameters only and not by the input and system parameters as with DMS systems.

Autosolitons can be described, as an asymptotically stable solitary wave in non-conservative media, when, in addition to the equilibrium condition between non-linearity and dispersion, there exists a balance between amplification, frequency-dependent damping and non-linear dissipation [124].

5.2.1 The Non-linear Optical Loop Mirror (NOLM)

The non-linear optical loop mirror originally proposed by [125], and this was experimentally demonstrated by [126] and [127]. The NOLM incorporates the Sagnac interferometer, and consists of a four port bi-directional coupler, where port one is the input port. Port three and four are connected together with a length of optical fibre (preferably with a high non-linear coefficient), and port two is the output.

A schematic diagram of the NOLM is shown in Figure 5.1. The operation of the NOLM in this work required an asymmetry to exist between the arms (that is between E_3 and E_4). There are numerous ways to construct the NOLM, such as using different coupling ratios [125], or by placing an attenuator after the coupler to create an asymmetry [128] (these were the methods used in this work). A gain element can also be used in the NOLM to achieve asymmetry [129], whilst differing the dispersion between the arms can have the same effect [130].

One of the most important features of the NOLM is that it can reshape a pulse, suppress the noise and dispersive wave radiation [128], even if the input pulses are non-soliton. Differing parts of the pulses see differing transmissivity, because of intensity modulation, which leads to a partial transmission and pulse break up. The NOLM can increase the pulse duration of inputted non-soliton pulses as a result of the dispersion added by the NOLM, pulse shaping, added spectral chirp and loss [131].

The pulse duration increase can be minimized with proper optimization in the construction the NOLM. If the input pulses are solitons they can be viewed as particle like, but there will be some pulse reshaping. This will be limited if the coupler is highly asymmetric thus keeping the optical power in one arm of the NOLM well below the soliton threshold. The pulse in this arm will see substantial broadening and dispersive wave radiation.

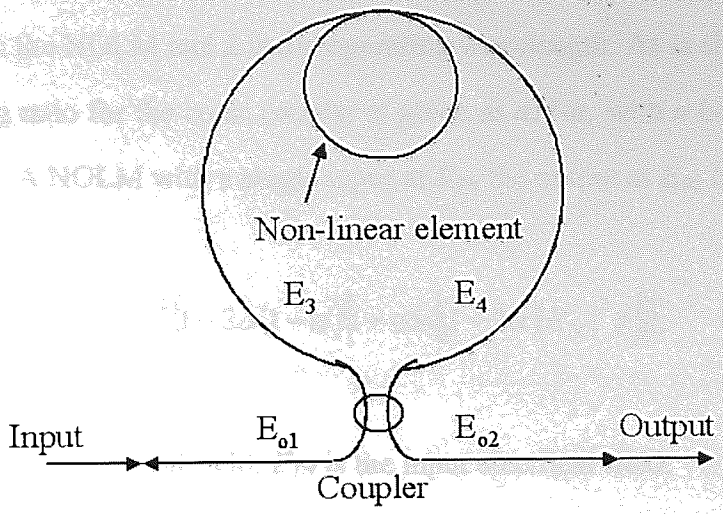

Figure 5.1 Schematic of the NOLM.

As shown in Figure 5.1, the propagating signal enters the NOLM, where it is split into two identical signals by a 50:50 ratio coupler. The two signals are then sent in counter-propagating directions to each other. On exiting the NOLM the two signals either constructively or destructively interfere with each other thus producing an interferometer. Altering the phase of one of the signals can control the interference and increasing the intensity of the optical field within the NOLM can control the phase. If a coupler with a 70:30 ratio is used, a greater magnitude phase shift will occur to the signal.

If the two counter-propagating signals have different intensities, this leads to a differential Kerr-effect-induced (non-linear) phase shift. As the input optical power is increased the signal is reflected back down port one until a $\Delta\pi$ phase shift is reached, at which point the signal is transmitted through port two.

The phase shift due to SPM, F, in the loop mirror is given as [125]:

$$\Phi = \frac{2\pi n_2 |E|^2 L}{\lambda}, \qquad (5.1)$$

where E^2 is the inputted optical power, n_2 is the non-linearity coefficient, L is the length of

optical fibre within the NOLM and λ is the operating wavelength. As is shown in figure 5.1, the power coupling ratio for the cross coupler is given as ***a:1-a***, with ***a*** being the amount of split optical power. A NOLM with a single input at E_{IN} the output at E_{02} is given as [125]:

$$|E_{02}|^2 = |E_{IN}|^2 \left(1 - 2\alpha(1-\alpha)\left\{1 + \cos\left[(1-2\alpha)|E_{IN}|^2 \phi\right]\right\}\right), \qquad (5.2)$$

where E_{02} is the output electrical field, E_{IN} is the input electrical field.

If the coupler's ratio is unbalanced this then switches the NOLM to a transmittance mode where the signals appear at the output port, where the transmissivity, T, is given as [121]:

$$T = \frac{P_{OUT}}{P_{IN}} = \left\{1 - 2\alpha(1-\alpha)\left[1 + \cos\left(\Phi + \frac{\pi P_{IN}}{P_{SWITCH}}\right)\right]\right\}, \qquad (5.3)$$

Here F is the bias, P_{IN} is the input power and P_{SWITCH} is the switching power and is given as:

$$P_{SWITCH} = \frac{\lambda A_{eff}}{2\pi n_2 L(1-2\alpha)}. \qquad (5.4)$$

where A_{eff} is the effective area of the fibre.

The NOLM is sensitive to polarization, and in the construction of the NOLM used in this work there were two polarization controllers within the loop mirror and one just before it. The number of polarization controllers could be reduced if birefringent fibre was used instead of DSF. The bias, F, in the experiments is set to zero or p, as the polarization in the NOLM is set by the polarization controllers [132].

If a NOLM has a low contrast (switching ability) then the output signal may be of no better quality than the input signal. This would then be pointless as an optical regenerator.

The transmission characteristics are dependent on the type of input. For instance, in the Continuous Wave (CW) case there is 100% transmission with a p phase shift. This result is similar for a soliton input as phase in solitons is time independent and is characteristic for the whole pulse duration. For these two cases the transmission peaks are shifted, with respect to the input optical power. For an input that is not CW or a soliton then the 100% transmission is not reached, therefore the contrast is reduced and the peaks are shifted, which requires more input power to achieve the switching point maxima.

5.2.2 Concatenated non-linear loop mirrors

The concatenation of NOLMs in a transmission link, was first proposed by [121], and was used to help provide stability to soliton propagation by intensity filtering and pulse amplitude control. The use of NOLM instead of other types of saturable absorber was simply a case of response time; the NOLM has an ultrafast response time in the sub-picosecond region. The work presented in [122] provides an insight to autosoliton transmission in standard fibre. If asymmetric couplers are used, then the fraction of background noise rejected by the NOLM will increase, with increasing asymmetry. Gain in the amplifiers needs to be slightly more than the loss in the system to overcome the fraction of the pulse power that was rejected by the NOLM; this was overcome in later sections by the use of an attenuator after the NOLM.

It is important to operate the NOLM just past the peak of the switching curve [121]. By operating past the switching peak, a negative feedback mechanism is set up where if the pulse power increases the transmissivity decreases and vice versa. This enables the pulse to keep at a steady state, while still eliminating the background wave radiation.

Timing jitter as discussed in Chapter 3, can be a considerable problem in a soliton transmission system, due to the Gordon-Haus effect. This effect can be reduced with the use of saturable absorber's noise suppression abilities. However, if an amplifier is to be used before the NOLM, then depending on the bandwidth of the amplifier a certain amount of

detuning can occur, caused by bifurcation. This can lead to an excessive amount of timing jitter. This can be overcome by placing a bandwidth-limiting filter between the amplifier and the NOLM.

The bifurcation effect is also marginalized by the soliton self-frequency shift [133], this was observed by [134], and is the downshifting of the optical carrier frequency through stimulated Raman scattering in the fibre. Placing an optical band-pass filter with a sufficiently narrow bandwidth after the amplifier can suppress this phenomenon [135], if the filter is offset by the equal but opposite amount to that seen by the soliton in Raman frequency shift.

The magnitude of the pulse is controlled by the bandwidth of the filter, however there will be more gain needed to overcome the losses incurred by the filter that leads to a building up of dispersive waves and noise at the carrier that are deleterious to the soliton. Dispersive waves or radiative background is always formed by solitons in optical fibre, and it originates from amplifier noise or from the mismatch between a soliton and a linear pulse.

The NOLM on the next round trip will then remove the unwanted noise radiation and ASE build up from the fibre span by intensity filtering [128].

5.2.3 DM autosoliton propagation

DM autosoliton [124] propagation in fibre has been proposed by [122], [136] and experimentally demonstrated by [137]. Autosolitons are dynamically stable solitary waves [136], these stable waves are the ideal information carrier, and DM autosolitons have their characteristics set by the system parameters, unlike standard soliton or DM soliton propagation as discussed in chapter 3, which is set by the input pulses as well as the system parameters.

The impetus behind DM autosoliton propagation is the need to keep the standard fibre maps that exists in the field. DM autosoliton propagation has to be shown to work on sections of SMF fibre between 80 to 100km in length with high dispersion (strong in map

strength), that have been routinely laid by telecommunication providers. DM soliton propagation cannot exist in these strong dispersion maps, often called the quasi-linear regime.

A fundamental feature of the DM autosoliton is that it can be set-up in a system independent of the input pulse parameters. The critical points are that the pulse duration and energy are restored at the end of each transmission link. The NOLM provides the non-linearity needed for DM autosoliton propagation unlike the DM soliton, which requires the energy of the pulse in the fibre to provide the non-linearity. To ensure that the optical power is restored to the initial level at the end of each cycle an attenuator was placed after the NOLM to provide quasi-linear propagation through the fibre span, this is the distinction between the DM soliton and the DM autosoliton transmission regime.

Before DM autosoliton propagation exists, there is a period of change; the autosoliton and other solitary waves, such as chirped Gaussian pulses are all perturbations of the initial pulse. As the pulses are propagating through the fibre, the solitary waves then disperse and go to form dispersive wave radiation, which get filtered out by the NOLM leaving the autosoliton. The DM autosoliton experiences no dispersive spreading at the output of each successive fibre span (undergoes significant dispersive spreading within the fibre span) and thus keeps its profile, more importantly any distortions to the DM autosoliton profile do not destroy the DM autosoliton, and it is maintained as dynamically stable solitary wave. This is the difference between DM autosoliton and a DM chirped pulse [136].

5.3 Experimental observation of autosoliton propagation in a dispersion-managed system guided by non-linear optical loop mirrors at 10 and 40Gbit/s

Ultra-long haul data transmission at high speeds over transoceanic distances represents a substantial technical challenge and usually requires the optical transmission system to support stable optical carrier propagation. The so-called fundamental soliton [138] and Dispersion Managed (DM) soliton [139] have been proved able to propagate over

transoceanic distances without distortion. These techniques provide in principle a solution to the problem of transmission at bit-rates up to 40Gbit/s. Speeds of 40Gbit/s and above require additional efforts, such as a carefully designed dispersion map constructed of a special dispersion-shifted fibre [140].

In these fibre links, the dispersion map strength, (a fibre link parameter that is proportional to the local dispersion variation and the map period and inversely proportional to the square of the pulse width [141]) is relatively small. However, more than 90 percent of the installed fibre to date is standard single mode fibre. Typically, the dispersion map strength in a standard-fibre system is in the range of 25 to 300, depending on the duration of propagating pulses and assuming the amplifier spacing is in the range of 80 to 100km. In such strong dispersion maps, neither the conventional soliton nor the DM soliton techniques can provide the stable carrier propagation over long distances [142]. As a result, the physically limited (i.e. measured without forward error correction (FEC)), error-free transmission distance at 40Gbit/s in standard fibre typically does not exceed 2000km [138] unless active regeneration techniques and/or FEC are employed.

5.3.1 Experimental Set-up

The experimental set-up is shown in Figure 5.2. The carrier signal was provided by a mode-locked fibre ring laser (Ultrafast Optical Clock, Pritel, Inc), operating at a central wavelength of 1553.5nm. The laser produced pulses of 3.5ps in duration at the repetition rate of 10GHz. The signal was encoded using a pseudorandom bit pattern with the bit word length of 2^{31}-1 by means of a $LiNbO_3$ modulator. This 10Gbit/s encoded signal was optically multiplexed to 40Gbit/s.

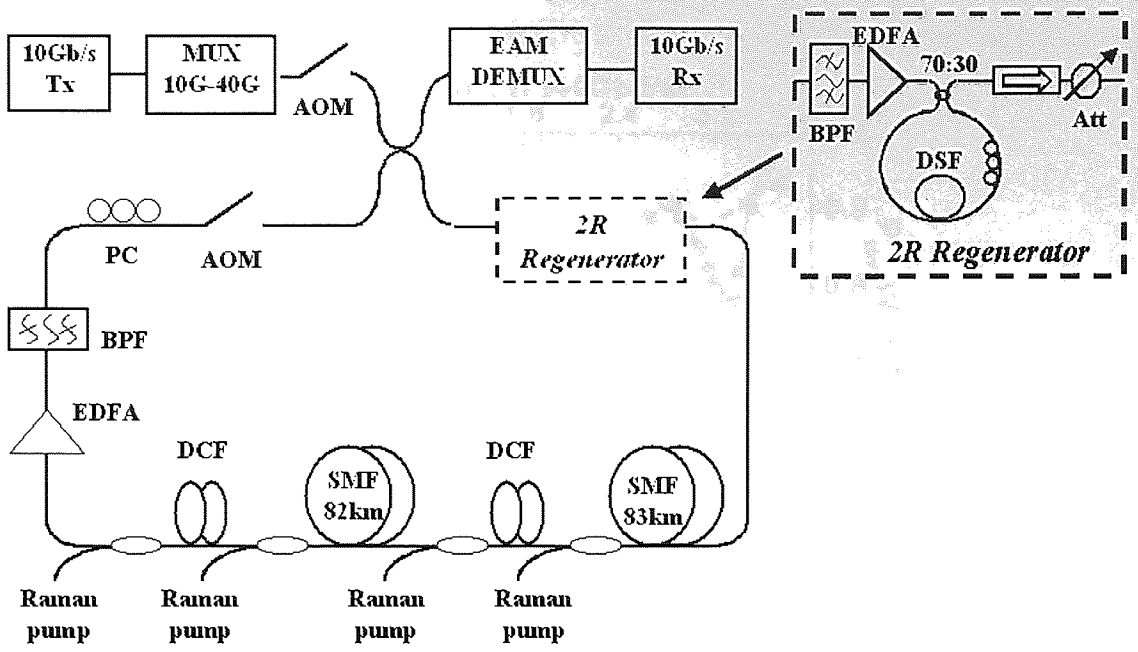

Figure 5.2 Experimental set-up of the transmission system used for DM autosoliton propagation.

The re-circulating loop comprised two spans of standard single mode fibre, 82km and 83km long, and two slope-compensating fibre dispersion compensators. Average dispersion in the system was set to be slightly anomalous, approximately +0.003ps/(nm.km) at the operating wavelength. The corresponding dispersion map strength is 280, which means the pulse is highly dispersed and unlikely to suffer degradation from intra-channel non-linearity due to the low peak power. An Electro-Absorption Modulator (EAM) was used in the receiver to demultiplex the signal from 40Gbit/s to 10Gbit/s.

The average signal power coupled into the recirculating loop was –9dBm at the data speed of 10Gbit/s and –3dBm at 40Gbit/s. The system was Raman amplified with the gain provided by Raman pump waves counter-propagating with the signal. A separate pump was used for each standard fibre and for each dispersion compensator. The Raman pump wavelength was 1455nm.

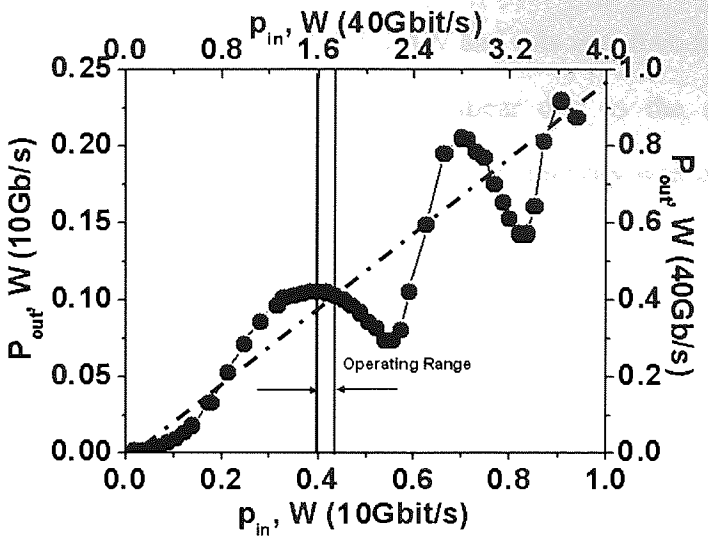

Figure 5.3 The NOLM switching curve, with the different powers for differing data rates, with the operational range of average optical power needed.

The operation of the generic DM system as described above was compared with that of an equivalent NOLM-guided system. For this purpose a NOLM was added to the system also added was a high power EDFA amplifier (1 Watt) to boost the power to the level required by the NOLM, as shown in Figure 5.3. In addition, an attenuator was placed after the NOLM in order to balance the power in the system. The NOLM switching curve given in Figure 5.3, as observed a 100% transmission is not reached as discussed in section 5.2.1. In this case it is ~25%, and the contrast is reduced to ~40%, this is due to a 70:30 coupler being used (if a high data rate is used it can be comparable to that of the CW scenario).

The NOLM used in this experiment comprised an asymmetric fibre coupler with splitting ratio of 70:30 and 2.3km of TrueWave fibre with an anomalous dispersion of +2.8ps/(nm.km) at 1550nm. The non-linearity coefficient, n_2 of the DSF was $1.6.10^{-20}$-m/W. The NOLM was placed at the beginning of the recirculating loop. An EDFA at the NOLM input was used to boost the signal to appropriate power level. In all measurements, the system was optimized in order to maximize the error-free (BER 10^{-9}) transmission distance

for a given configuration. Maximum transitivity of the NOLM operating at 40Gbit/s was reached with an input average power level of 1.3-1.4W and this is shown in Figure 5.3.

The propagation in our experiment was quasi-linear due to the special efforts to maintain the average power at low level. Considerable non-linearity was present only in the NOLM itself. The transmission format was Return-to-Zero, and the propagating pulses were considerably chirped virtually at any point in the re-circulating loop except for the region near the loop input/output.

5.3.2 Experimental Results

The signal dynamics were investigated in the above system at data rates of 10Gbit/s and 40Gbit/s. At both speeds, performance of the generic system was compared with that of the NOLM guided system. The effect of the NOLM was immediately evident from the Bit Error Rate (BER) measurements. At the data transmission speed of 10Gbit/s, the error-free transmission distance increased from 4,300km in the generic system to 11,000km in the NOLM-guided system, as shown in Figure 5.4(a). At the speed of 40Gbit/s, the similar increase was from 1,000km to over 4,000km (Figure 5.4(b)).

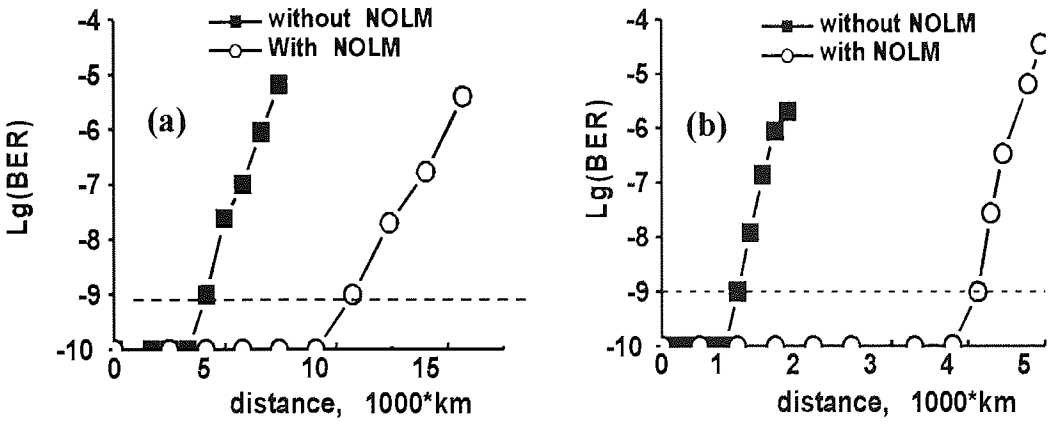

Figure 5.4 Transmission performance at 10Gbit/s (a) and that at 40Gbits/s (b). Closed squares and open circles correspond to the generic system, and to the NOLM-guided system, respectively.

The eye-diagrams for the 10Gbit/s signal are shown in Figure 5.5; in Figure 5.5(a) the generic system is shown with a substantial amount of amplitude jitter, and ASE noise on the zero. The NOLM guided system can be observed in Figure 5.5(b) where the amplitude jitter has been reduced along with the ASE. The NOLM suppresses the background wave radiation and, because of the NOLM's operation beyond the first switching peak, the negative feedback allows for a suppression of the 'ones'.

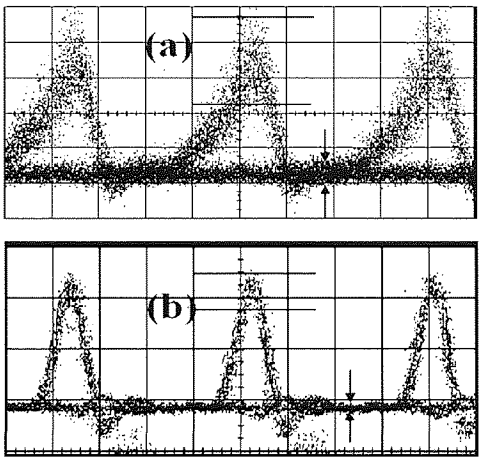

Figure 5.5 10Gbit/s eye diagrams at 4000km in the generic system (a) and at 11000km in the NOLM guided system (b).

In order to study the NOLM-guided system in more detail, the signal evolution in the spectral and temporal domains was monitored at 10Gbit/s. The stroboscopic evolution of the auto soliton pulse is shown in Figure 5.6, the evolution of the pulse can be seen to remain stable beyond 17,000km, both spectrally (Figure 5.6(a)) and temporally (Figure 5.6(b)).

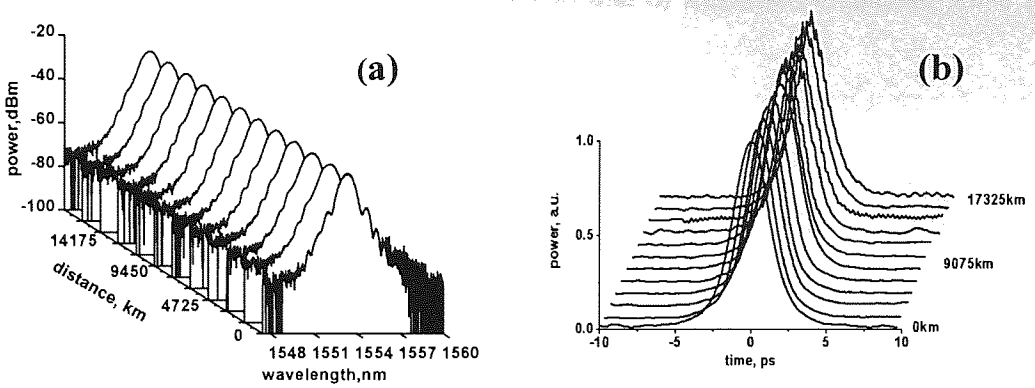

Figure 5.6. Spectral (a) and temporal (b) autosoliton evolution at 10Gbit/s in a NOLM guide system.

Evolution of the 40Gbit/s signal spectra in the generic and in the NOLM-guided systems is presented in Figure 5.7, where the OSA resolution is 0.05nm. In the generic system with a $\Delta\lambda$ of 1.1nm at 3dB, the signal spectrum experiences changes during the entire time of propagation, as shown in Figure 5.7(a). The signal gradually accumulates Amplified Spontaneous emission (ASE), this accumulation produces a narrow peak in the final spectrum, shown by the solid line in Figure 5.7(a). Multiple passes cause gradual narrowing of the ASE spectrum through the band pass filters.

In the NOLM-guided system, the spectrum evolves in a very different manner (Figure 5.7(b)). The spectral profile, $\Delta\lambda$ of 0.95nm, which is well approximated by the sech^2 shape, was formed during the initial stage of propagation over several hundred kilometres. The spectrum does not change within the error- free propagation distance and remains remarkably stable well beyond this distance, up to 10,000km and more. Figure 5.7(a), in the generic system the observed signal bandwidth gets progressively narrower, whereas in the NOLM guided system, shown in Figure 5.7(b), there was an initial reduction then a stabilization of the signal. This initial reduction originates from the intensity filtering of the NOLM, where there was a portion of the bandwidth switched due to intensity and the rest of the spectra rejected. The DM autosoliton regime is then set up and the pulse turns particle

like in nature and performs in a different manner to that of a chirped Gaussian pulse in the NOLM.

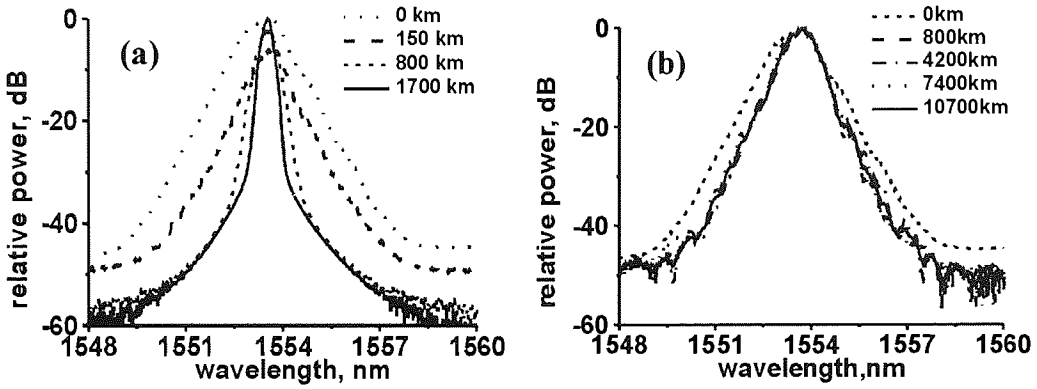

Figure 5.7 Spectral evolution of the 40Gbit/s signal in the generic system (a) and in the NOLM-guided system (b).

Evolution of the temporal profile was characterized by using a gated, background-free autocorrelator. Autocorrelation traces measured at several points in the generic system are shown in Figure 5.8(a), and those taken in the NOLM-guided system are shown in Figure 5.8(b). The pulse duration and shape were monitored as the signal propagated in the system. Each autocorrelation trace included a main peak and several additional peaks arising from the cross-correlation between adjacent pulses. These additional peaks are broader than the main peak because of the timing jitter. The timing jitter was evaluated by using a procedure similar to that as described in [143] and is discussed in further detail in Chapter 6.

As can be seen in Figure 5.8(a) the noise build up in the generic system shows up as a spike on the main peak, this is not evident on the NOLM guided system, where the pulse has kept its shape up to 10000km Figure 5.8(b). The background increase in the generic system Figure 5.8(a) is due to non-linear intra-pulse interaction and dispersive broadening. Whereas in the NOLM guided system (Figure 5.8(b)) the pulse shaping properties of the NOLM coupled with the DM autosoliton propagation regime maintain the pulse profile.

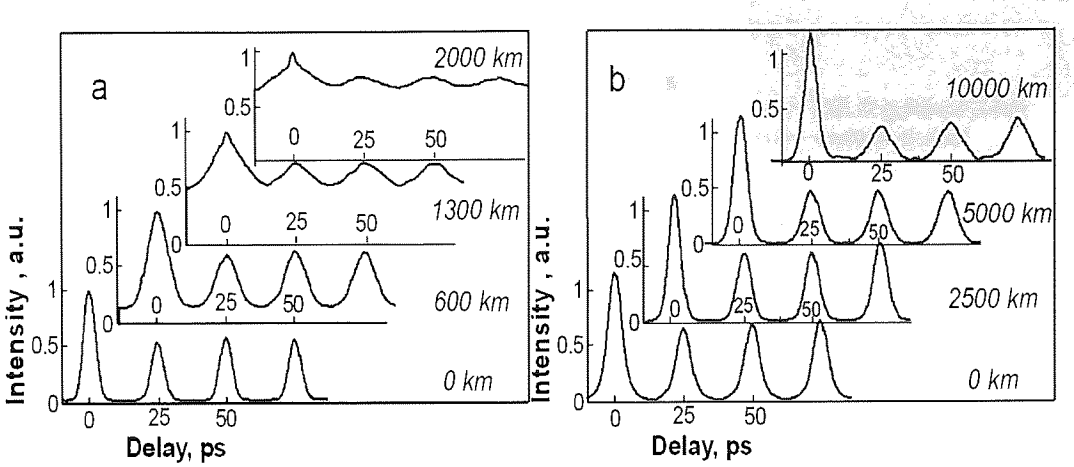

Figure 5.8 Autocorrelation traces showing the 40Gbit/s signal evolution in the generic system (a) and in the NOLM-guided system (b).

In the 40Gbit/s generic system, the pulse duration gradually increased due to non-zero average dispersion and reached 12ps after 2,500km (Figure 5.9(a)). Although it was possible to balance the dispersion with a greater precision and therefore to minimize the pulse spreading, this configuration was found to show a reduced error-free transmission distance and we chose not to study it any further.

The NOLM-guided systems pulse duration remained stable within the accuracy of measurements and was measured as 3.6ps during transmission over more than 10,000km. Notably, the pulse spreading was virtually eliminated in the guided system in spite of the fact that the NOLM dispersion added to the average dispersion, making it greater than that in the generic system. The dispersive pulse broadening was compensated for by the self-phase modulation in the NOLM.

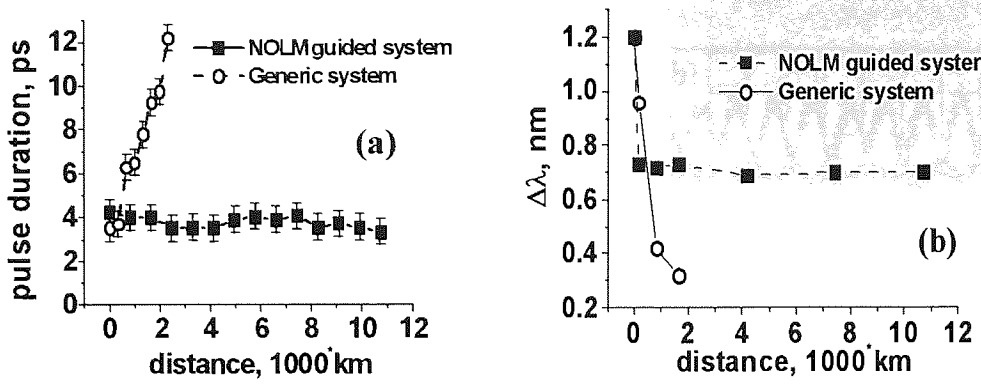

Figure 5.9 Dynamics of pulse duration measured in the generic system and in the NOLM guided system.

The transmission system was then optimized and further experiments carried out. Additional care was taken with the OTDM, to ensure the 'bits' were exactly in the centre of the time slot and the pulse-to-pulse power was the same from pulse to pulse (~6fJ peak power). The power in the recirculating loop was optimized to just under –2dBm, however this still ensured a quasi-linear propagation regime. The results of this optimization can be seen in Figure 5.10(a), where the transmission distance has increased to 5,800km, with a total transmission distance including the DCF of 7000km. The eye diagrams for the back-to-back signal are shown in Figure 5.10(b), the difference in the pulse to pulse optical power was 10%, where an improvement still could be made on the pulse-to-pulse peak power and the eye diagram after 5800km is given in Figure 5.10(c).

The 40Gbit/s eye diagrams at various stages of propagation are given in Figure 5.11 (top), with the 10Gbit/s demultiplexed eye diagram on the bottom of each individual picture. A good clear eye can be observed at all distances up to 7500km, which indicates that with further optimization there could be further gains in transmission distance.

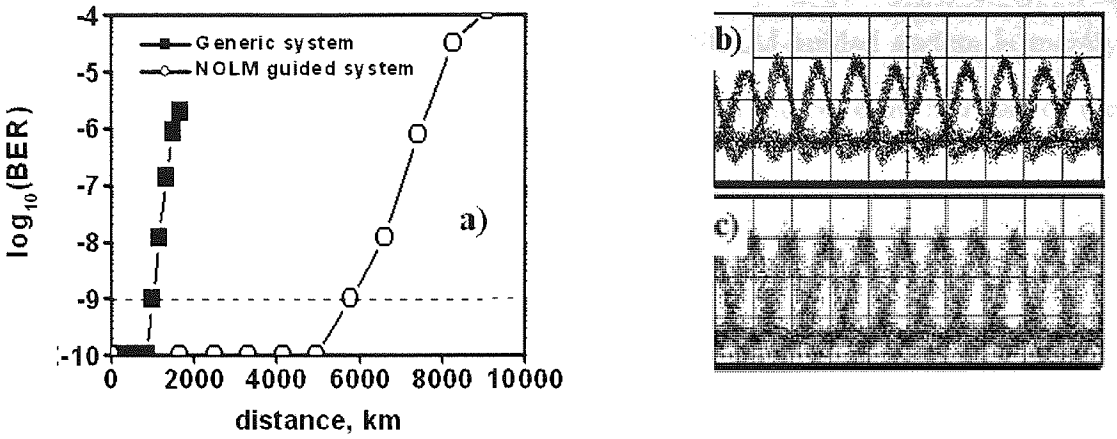

Figure 5.10 (a) BER performance of de-multiplexed 10Gbit/s data versus propagation distance. Eye diagrams of 40Gbit/s data stream, (b) back to back, and (c) propagation over 5,800km of SMF using 2R regenerators.

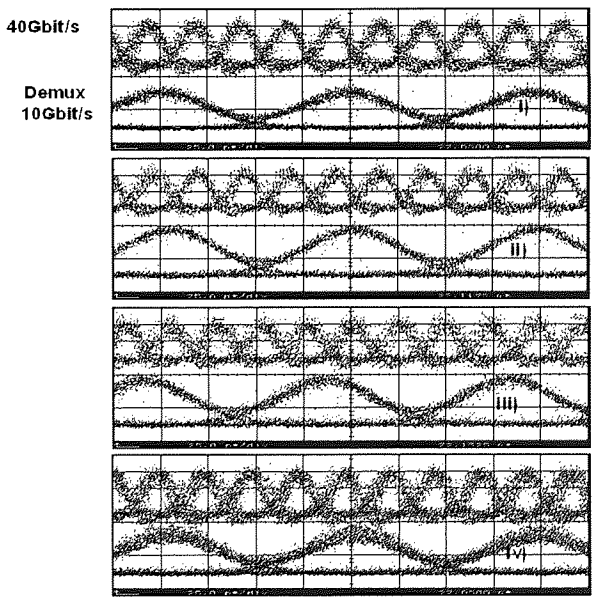

Figure 5.11 40Gbit/s eye diagrams at i) 2500km, ii) 4000km, iii) 6000km and iv) 7500km. With the respective demultiplexed 10Gbit/s signal below.

The results confirmed the existence of DM autosolitons in the NOLM-guided system, in line with the earlier theoretical results [122], [123]. There exists a propagation regime where the pulse duration, power and spectrum, measured at a certain point in the system,

remain stable over a virtually infinite distance. The NOLMs act as 2R-regenerators and the degradation of the data transmission performance in the NOLM-guided system is mainly due to the timing jitter increase. The measurements confirmed the constant increase of the timing jitter, shown in Chapter 6. In principle, it could be possible to optimize the dispersion map in order to reduce the accumulated timing jitter which represents a potential for further improvement of the demonstrated method.

5.4 DM autosoliton propagation at 80Gbit/s using concatenated non-linear loop switches in standard fibre

One of the ways in which optical data transmission is progressing is through the steady increase in bit rate per channel. As 40Gbit/s technologies mature, interest in even higher speeds increases. In particular, the feasibility of long-haul transmission at 80Gbit/s is of considerable interest.

To date, non-regenerated transmission at 80Gbit/s per channel has been limited at distances up to 200km in standard fibre [144] and up to 1,200km in dispersion-shifted fibre [145]. Long-haul type transmission has been also demonstrated (10,000km, dispersion shifted fibre) although at the cost of using relatively complex optical retiming [146].

2R regeneration is one possible way to improve the transmission at 80Gbit/s and to make it more practical whilst keeping the complexity of the system low compared to complete (3R) regeneration. In the previous section there was demonstrated data transmission at 40Gbit/s over 7,000km in standard fibre and DCF by 2R regeneration using in-line non-linear loop switches [147]. The key to this kind of transmission is the design of dispersion-managed system that supports switch-guided autosolitons [148].

In this section, switch-guided DM autosoliton propagation at 80Gbit/s was evaluated. Switch-guiding is using the NOLM at the optimum power point on the transmission curve to transmit the pulse and reject the noise. By comparing the dynamics of spectra and pulse duration, signal transmission in the dispersion-managed switch-guided system is directly compared with a generic dispersion managed system. The stable DM autosoliton propagation over distances in excess of 3,000km was observed in the switch-guided system.

5.4.1 Experimental set-up

The experimental set-up is shown in Figure 5.12, and is similar to that of our earlier experiments carried out at 40Gbit/s [147]. Measurements were taken in a re-circulating

loop. A mode locked fibre laser (Ultrafast Optical Clock, Pritel Inc) generated a 10GHz pulse train with the pulse duration of 3.5ps. A 2^{31}-1 pseudorandom bit pattern was imposed on the carrier signal by a $LiNbO_3$ modulator. The signal was then optically multiplexed to 80Gbit/s.

The generic recirculating loop consists of 165km of Single Mode Fibre (Corning SMF-28) split into two spans of equal length, and two slope compensated dispersion compensating modules, resulting in an average dispersion of +0.003ps/(nm.km). The map strength for the system was approximately 280. The average power at 80Gbit/s in the recirculating loop was kept at ~1dBm during the experiment to maintain a quasi-linear propagation regime.

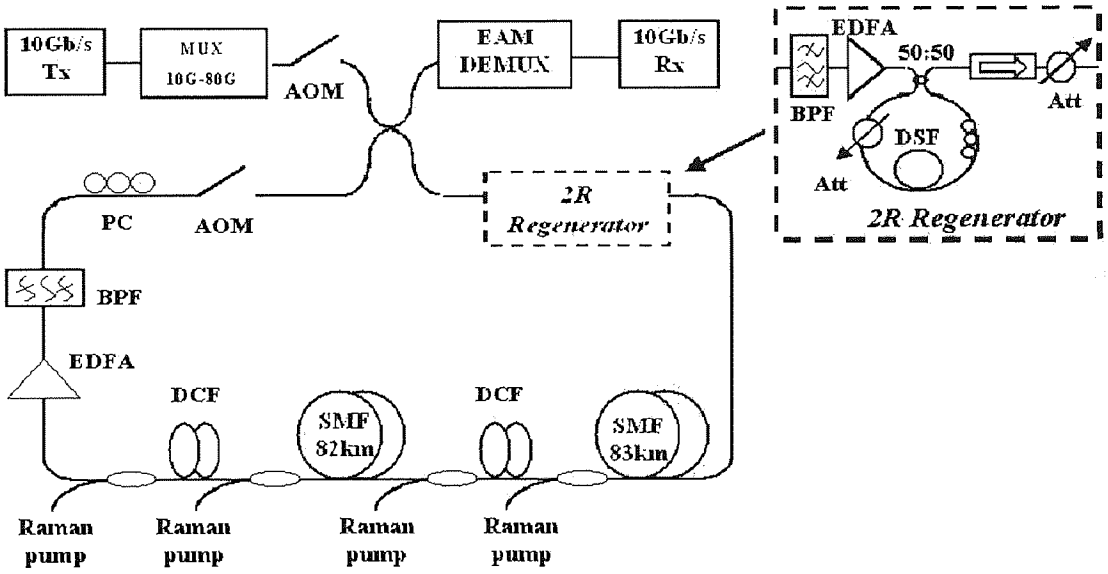

Figure 5.12 Experimental set-up.

Non-linear switching was provided by an in-line non-linear optical loop mirror (NOLM). The NOLM comprised a symmetric (50:50) fibre coupler and 2.3km of TrueWave fibre (DSF in Figure 5.12) with an anomalous dispersion of +2.8ps/(nm.km). Asymmetry was provided by a variable attenuator placed inside the NOLM near one of the ports. Polarisation controllers inside the NOLM compensated for the fibre birefringence.

Polarisation and attenuation inside the NOLM were adjusted to minimize the transmitted noise. An auxiliary attenuator at the NOLM output was used to maintain the appropriate average power in the system. By using a gated output, spectra and background-free autocorrelation traces were taken at a given number of round-trips around the re-circulating loop.

5.4.2 Experimental results and discussion

In the experiment, the signal evolution in the NOLM-guided system was compared with that of the generic system. The generic system was formed by the removal the 2R regenerator unit (the loss across the NOLM was minimal as the power into the 2R unit was accounted for by the EDFA before and the attenuator after the NOLM)(see Figure 5.12) from the recirculating loop; the generic system was then subsequently optimised for maximal transmission distance.

The switching curve of the NOLM is shown in Figure 5.13. The Operating range of the NOLM was chosen to be slightly beyond the transmission maximum as discussed previously. Therefore, the non-linear effects of the NOLM were essential during pulse propagation in the NOLM-guided system. Transmission through the NOLM caused some elongation of the transmitted pulse from 3.8ps to 4.1ps. The spectral bandwidth at the NOLM output was 0.84nm corresponding to the time-bandwidth product of 0.43.

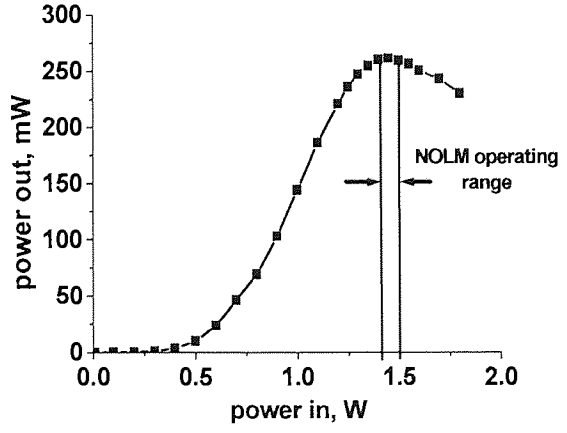

Figure 5.13 Switching curve of the 50:50 split NOLM with asymmetrical loss.

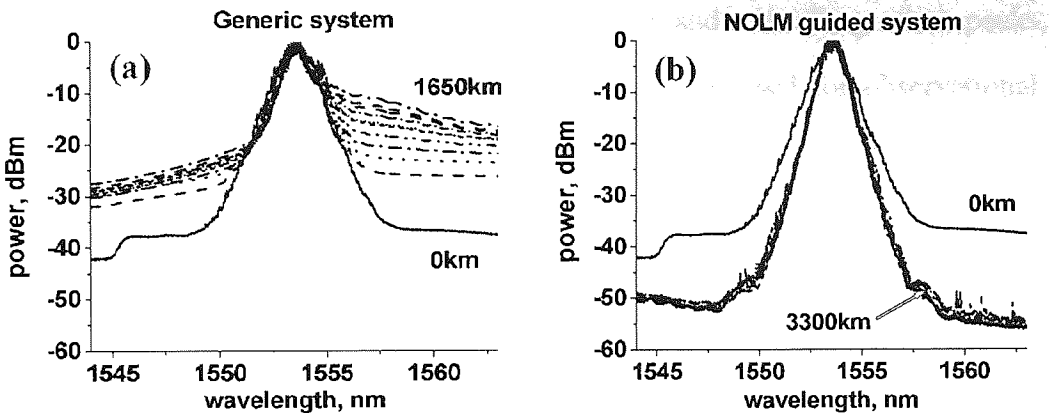

Figure 5.14 Spectral evolution in the generic system (a). Spectral evolution in the NOLM guided system (b).

Figure 5.14(a) and Figure 5.15(b) show the spectra measured in the generic (a) and in the NOLM-guided (b) systems. A gradual accumulation of the amplified spontaneous emission (ASE) was evident in the generic system, resulting in almost complete signal degradation at a distance of 1,600km. A shift of the central wavelength and a slight narrowing of the bandwidth were also visible. Contrary to the above, the signal spectrum in the NOLM-guided system forms a well-defined shape at the initial stage of propagation over several hundred km and subsequently maintains this stable shape over a distance of more than 3,000km (Figure 5.14(b)).

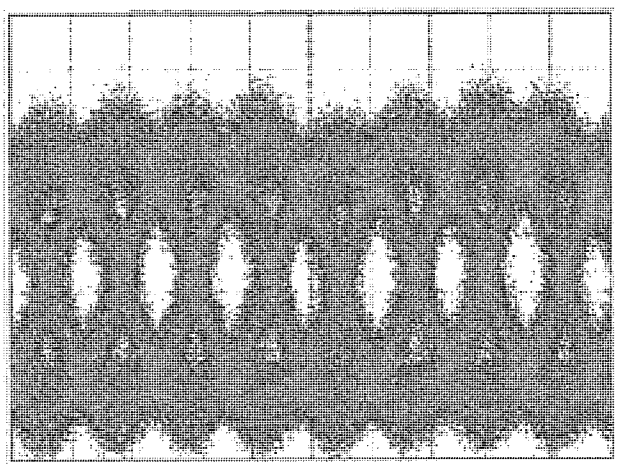

Figure 5.15 Eye of the 80Gbit/s signal back to back after the NOLM.

The 80Gbit/s eye diagram is shown in Figure 5.15, this was taken back-to-back with the NOLM in situ. There was a suppression of the noise level and a levelling of the peaks, but as the bandwidth of the detector is 32GHz, it could only be used for observational and setting up purposes. Care had to be taken to align all the pulses correctly within their allocated time slot.

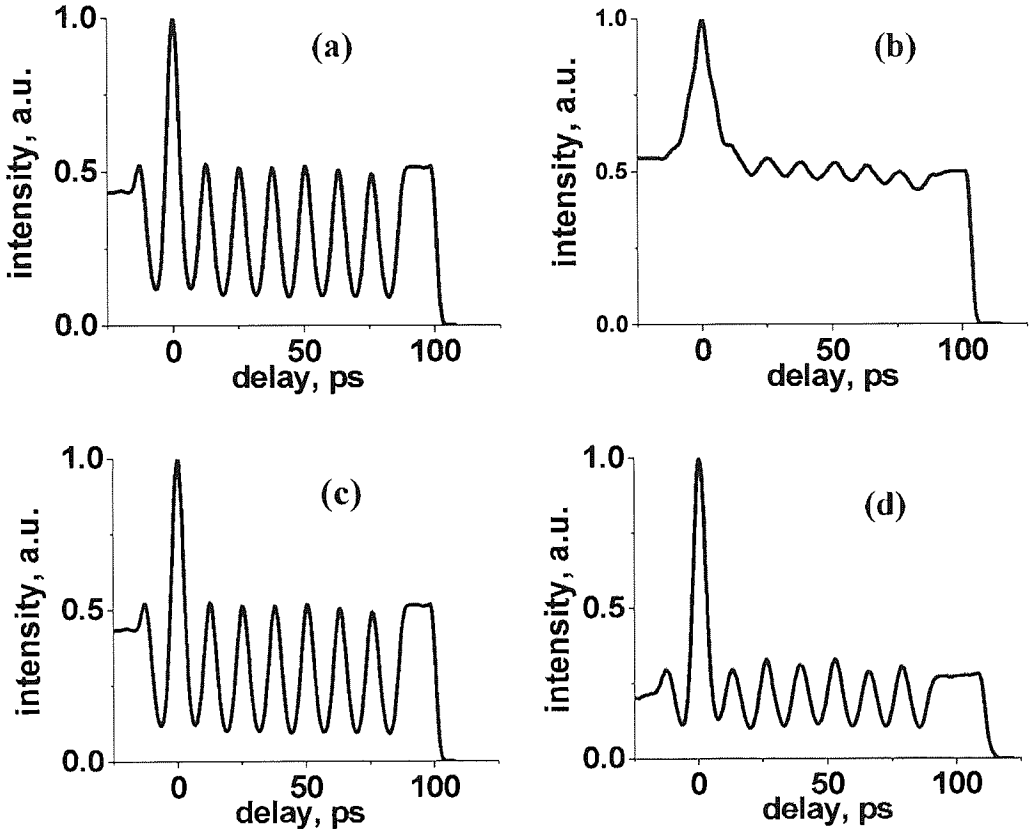

Figure 5.16 Autocorrelation traces measured: a) back to back; b) after 1000km in the generic system; c) immediately after NOLM during the first round-trip; d) after 3300km in the NOLM-guided system. Left parts of the traces are not shown.

For monitoring the temporal dynamics, autocorrelation traces were measured at regular intervals in the generic and in the NOLM-guided systems. Results of the autocorrelation measurements are shown in Figure 5.16. The considerable difference between the traces in

Figure 5.16(b) and Figure 5.16(d) was due to the gradual pulse broadening in the generic system as well as the growth of pedestal due to accumulated ASE. The peaks in Figure 5.16(d) are better resolved and have a greater contrast, indicating the pulse duration stabilization and noise suppression in the guided system. The plot of pulse duration is given in Figure 5.17, and it shows a significant difference between the generic and the switch-guided systems.

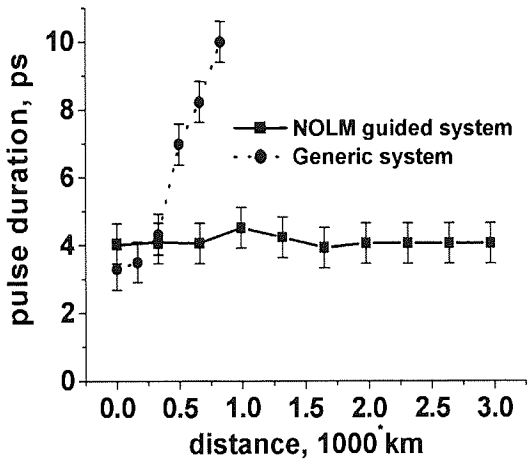

Figure 5.17 Evolution of pulse duration in the generic system (circles) and in the NOLM-guided system (squares).

In the generic system, the pulses broaden because of non-zero average dispersion. The dispersion non-zero value was chosen in order to optimize the transmission performance of the generic system. In the guided system, the pulse duration stabilizes at 4ps and remains unchanged up to 3,000km and beyond, after which the jitter makes the autocorrelation traces difficult to measure. The timing jitter was taken using a method similar to [149] and this is discussed in detail in Chapter 6.

The spectral and temporal measurements above indicate the existence of a stable propagation regime in the NOLM-guided system. This regime is characterized by a fixed pulsed duration and a constant spectral profile and was similar to the DM autosoliton propagation [146],[147]. Any increases to the ASE and intra-pulse interaction were

efficiently suppressed by the NOLMs. However, ISI will probably be the dominant mechanism responsible for signal deterioration in this system as shown in previous studies [140].

5.5 Summary

In section 5.3, autosoliton propagation in a dispersion managed transmission system controlled by in-line NOLMs has been experimentally demonstrated. The in-line NOLM provides stabilization of the signal in the spectral and temporal domains as well as the ASE suppression.

The temporal stabilization was shown by the obtained autocorrelation traces and the comparison between the regenerated system and the generic system. This demonstrated the increasing pulse duration in the generic system from the onset whereas in the regenerated system the pulse duration remained constant up to 10,000km. This was also confirmed spectrally, where the spectrum for the regenerated system remained unchanged with increasing propagation distance.

Improvement of the error-free propagation distance from 4,300km to 11,000km at a speed of 10Gbit/s and from 1000km to 4,000km at a speed of 40Gbit/s has been achieved. In later experiments the 40Gbit/s result was improved to 5800km, with still possible scope for improvement.

In section 5.4, autosoliton propagation of an 80Gbit/s data stream in a dispersion-managed system with a strong dispersion map has been demonstrated by in-line 2R regeneration in non-linear loop switches. Stable pulse propagation over 3,000km has been observed by comparing the pulse duration measured on an autocorrelator of the regenerated system with that of a generic system.

This resulted in a constant pulse duration under propagation in the regenerated system up to a distance of 3,300km, whereas in the generic system there is a rapid increase in the pulse duration. A spectral comparison was also made between the generic and regenerated

transmission systems, which showed there was no change spectrally in the regenerated system. A reduction of ASE (as confirmed by the OSNR) to minimal levels has been achieved by in-line non-linear switching.

Chapter 6 Timing Jitter in an regenerated dispersion managed transmission system

6.1 Introduction

This chapter is concerned with the aspects of timing jitter and its effect on optical pulse propagation. Timing jitter was evaluated at data rates from 10Gbit/s to 80Gbit/s. In section 6.2 the different mechanisms that lead to an increased timing jitter are dealt with theoretically. Section 6.4 deals with the experimental set-up of the transmission systems. In section 6.5 the results are given and discussed. Finally the chapter is summarized in section 6.6.

6.2 Theory

There have been a number of experimental studies looking into the effects of timing jitter in DMS and soliton systems such as [150], [151], [152]. The following sections deal with the types of timing jitter that occur in a standard transmission system and a non-linearly guided system.

6.2.1 Gordon-Haus effect

J. P. Gordon and H. A. Haus proposed in 1986 that a transmission system's limitation would be noise added to the system by amplifiers. In particular, the noise that is generated at the same frequency as that of the carrier pulse, this noise, which itself is fluctuating randomly, would create random frequency shifts within the optical pulse, due to Group Velocity Dispersion (GVD). These frequency shifts lead to differing travel times of individual optical pulses within the transmission system, causing shifts in time of the pulse at the receiver, this phenomenon is known as Gordon-Haus timing jitter.

Calculation of the variance of the timing jitter due to the Gordon-Haus effect, can be done by understanding that after each optical amplifier in a transmission span there are random perturbations in the timing of the pulse caused by the random noise. Therefore, in a transmission system, the number of amplifiers with their individual carrier frequency shifts can be summed together. This leads to a overall temporal growth of the timing jitter that is non-linear with distance to the cubic power.

The random timing jitter induced by the Gordon-Haus effect in a strongly dispersion managed soliton transmission system is given by the equation 6.1 [153], where the path average dispersion and energy enhancement factor E_0 are taken into account:

$$\left\langle \sigma_N^2 \right\rangle = 0.0174 \frac{N^2 D^2 \lambda^3 L^3 \eta_{sp} h \Gamma}{c \tau_{FWHM}^2 E_0}, \quad (6.1)$$

where D is the dispersion (path average dispersion), λ is the operating wavelength, t_{FWHM} is the pulse duration, N is the number of amplifiers per span, h is planks constant, η_{sp} is the spontaneous emission coefficient of the amplifier and G is the power lost per km by the signal in the fibre.

The G-H timing jitter occurring in the transmission system used in this work was caused by distributed Raman amplification. The loss between amplifiers is given as G = $\exp(GL_{AMP})$, where L_{AMP} is the spacing between the amplifiers and G is the gain of the amplifiers. However, as the loss between amplifiers is small and G can be approximated by: $G = GL_{AMP}+1$.

The study of reducing the Gordon Haus induced timing jitter, has been numerically shown to offer a reduction in timing jitter in a distributed Raman amplified system [154]. A similar effect is seen for hybrid amplification [155], when compared to lumped amplification alone. This is also the case for dispersion management [150], [156], in particularly when a strong dispersion map [153], post compensation [157], soliton transmission control [158], and the sliding-frequency guiding filter [159], [160] are used.

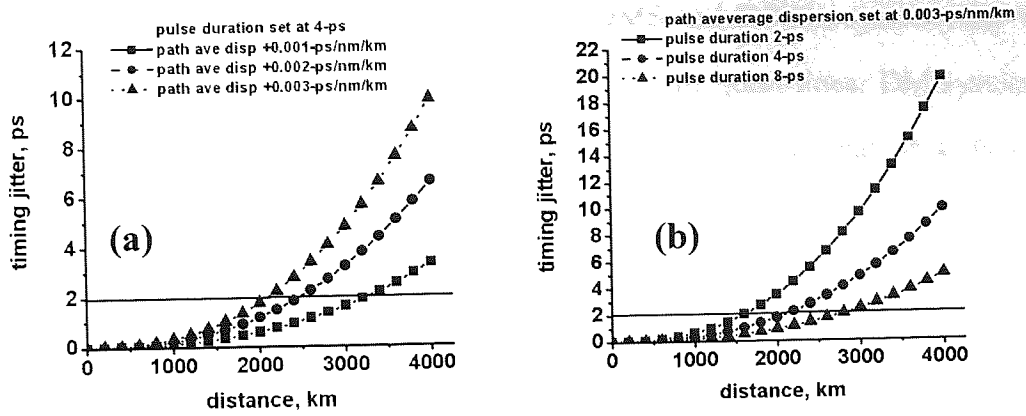

Figure 6.1 The Gordon-Haus jitter for the generic system used in this thesis, with (a) variations in path average dispersion and (b) variations of input pulses duration.

The theoretical values of the Gordon-Haus timing jitter are given in the graphs of shown in Figure 6.1. These plots show varying amounts of path average dispersion at the operating wavelength (a), and differing pulse durations (b). For a generic system with a path average dispersion of 0.003ps/nm/km at the operating wavelength, and a pulse duration of 4ps, an allowable timing jitter of 2ps at 40Gbit/s is reached after 2100km. The spontaneous emission coefficient used was 1.13 (acceptable for a Raman amplifier), and the energy of the pulse was 6.24fJ (peak power of 1.56-mW).

6.2.2 Intra channel non-linearity

One of the most common ways to increase the throughput of optical transmission system is to increase the bit-rate. However, this leads to the pulses being in a closer proximity to each other, which leads to the power in the wings of the pulse altering the refractive index seen by the following pulse. The estimation of the impact of intra-channel non-linearity it is useful to distinguish between soliton, DMS and quasi-linear systems.

The main difference between quasi-linear DM, DMS and Soliton systems lies in the interaction between dispersion and non-linear effects. For the quasi-linear DM system case the transmission behaviour of the optical pulse in the fibre is like that of a dispersion dominant linear system with Gaussian pulse shape profile, due to the fully dispersion compensated nature of the transmission system. The non-linear effects play a detrimental role in propagation of a quasi-linear optical pulse to alter the properties of the optical signal. For a soliton or a DMS propagation regime the nonlinearity is utilized so that a stationary propagation solution can be obtained due to the balance between dispersion and non-linear effects.

The high values of local dispersion coupled with short pulse durations give large map strengths beyond the regime where the stationary DM soliton exists. Strong pulse-to-pulse interactions occur if the map strength S is greater than 10 [161], leading to a break down of the DMS propagation regime. If the map strength is over 100, therefore if the initial pulse peak power is low and a pulse duration is selected so that pulse-to-pulse interactions are of quasi-linear nature and the net dispersion close to zero, then quasi-linear pulse shape is totally destroyed over the whole dispersion map length, recovering only at its end again, leading to minimal non-linear interaction. There have been studies that show that as long as the time spent at the point of maximum interaction is short then strong dispersion managed systems have low non-linear interaction [162] called quasi-linear DM systems.

In soliton and DMS systems, adjacent solitons are periodically attracted to each other, if they are of the same phase, or repelled, if they are of opposite phase [162]. This is known as soliton-soliton interaction, which in time introduces timing jitter and eventually leads to the collapse of the soliton, if the pulse-to-pulse temporal separation is too small. To minimize this effect the pulse duration needs to be reduced and pulse power increased, however, this will then lead to increases in other mechanisms of timing jitter such as the Gordon-Haus effect and acoustic jitter. To reduce these effects orthogonal polarization time division multiplexing can be used to bypass the pulse overlap problems [152].

Quasi-linear DM systems, lead to the pulse becoming highly dispersed in a short period of time, which leads to the dispersion length being much shorter than the non-linear length. The time induced dispersion and compression leads to a much altered power distribution that averages out the non-linear effects.

If the input power is too high then this leads to a significant build up of non-linear pulse-to-pulse interactions. These interactions lead to phenomenon, such as intra-channel Four Wave Mixing (FWM) and intra-channel Cross Phase Modulation (XPM), where these are both main mechanisms of pulse jitter and distortion. I-FWM can lead to the creation of ghost pulses that propagate and grow logarithmically with distance, and can be reduced by the square of the pulse separation. I-XPM induces timing jitter on adjacent pulse and visa versa through pulse peak power. I-FWM and I-XPM, become significant at data rates of 40Gbit/s and above, but with careful dispersion management, the intra-channel non-linear effects can be minimized. All the above effects lead to an overall problem called Inter Symbol Interference (ISI), which has been the major factor in limiting transmission distance in high data rate systems [163].

6.2.3 Electrostriction

Electrostriction, which is variations in refractive index along the fibre core, leads to acoustic timing jitter, which has been studied extensively, both theoretically [164] and experimentally [152]. Electrostrictive interaction is described as occurring when the distance between picosecond pulses is larger than their duration, and arises from an acoustic wave produced by electrostriction in the fibre core.

The acoustic waves propagate radially out of the core until a change of refractive is encountered, then a fraction of the wave energy is reflected back causing changes in the core refractive indices. The interaction lasts for the lifetime of the sound wave, which is in the nanosecond region. Subsequent pulses then see a difference in dispersions arising from the change in refractive index caused by the acoustic wave, leading to differing arrival times

at the receiver. The timing jitter, which is caused by electrostriction, is described in the following equation [152]:

$$\left\langle \sigma_{ac}^2 \right\rangle = \frac{46.7}{A_{eff}^{1.5}} \frac{D^4 L^4}{\tau_{FWHM}^2} \left(B - \frac{7}{A_{eff}^{0.5}} \right), \qquad (6.2)$$

The above equation, is arrived at by assuming a constant value of the coefficient for the intensity reflection of the sound (over the whole length of the optical fibre span), from the cladding-coating boundary (r = 0.25). The acoustic timing jitter is greatly reduced in a dispersion-managed system, where the path average dispersion is close to zero compared to that of a system with a uniform dispersion. Inserting the experimental values into equation 6.2, D = 0.003ps/nm/km, t = 4ps, A_{eff} = 80 μm^2 and B = 40Gbit/s at 10Mm gives 0.4-fs of timing jitter for the generic system, clearly this form of jitter can be neglected.

6.2.4 Polarization mode dispersion

Polarized Mode Dispersion (PMD) induced timing jitter unlike the previous forms of jitter discussed in this chapter is bit-rate and pulse duration independent. The case studied here is for 1st order PMD only and the higher orders are not discussed. PMD arises from discrepancies in the birefringence of the optical fibre along the length of propagation. PMD scales linearly with length and is expressed as units in ps/km$^{0.5}$. Although all optical fibre produced is affected by it, the fibres produced in the last few years generally have a PMD of 0.1ps/km$^{0.5}$, but older fibres can have values greater than 1ps/km$^{0.5}$.

Generally, older fibres are used in existing global transmission systems, therefore any up-grade in the data rate of the system requires the impact of PMD to be accessed, especially if the systems are to transmit in excess of 40Gbit/s per channel. The timing jitter attributed to PMD can be calculated using the following equation [165]:

$$\left\langle \sigma_{PMD}^2 \right\rangle = \frac{\pi \Gamma h \upsilon}{16 E_0} p^2 L^2, \quad (6.3)$$

where G, p, E_0 and L are taken, so that G = 0.043km^{-1}; p = 0.1ps/km$^{0.5}$; E_0 = 6.24-fJ and; L in the range 0 to 4000km.

Figure 6.2 shows the timing jitter calculated from equation 6.3. For the scenario were the optical fibre is new, as in the case for the fibre used in this thesis, then the accumulation of timing jitter due to PMD can be neglected for these distances in the generic system as the dominant jitter comes in the form of the Gordon Haus effect. However, if the fibre used were old, then the timing jitter accumulation would be split between the G-H effect and PMD.

For cases with long propagation distances, as with the previous chapter where 10Gbit/s is transmitted over 100Mm in a NOLM guided system, the majority of the timing jitter could only be attributed to PMD, as ISI and the G-H effect are negligible. This highlights the fact that there is considerable research into reducing the effects of PMD.

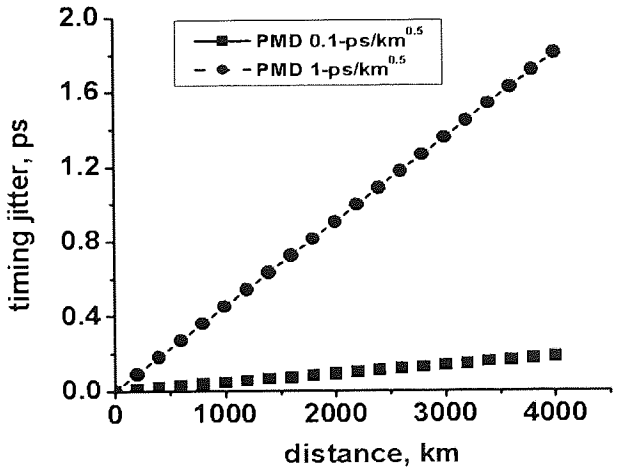

Figure 6.2 The accumulation of timing jitter attributed to PMD for 0.1ps/km$^{0.5}$ (squares) and 1ps/km$^{0.5}$ (circles), obtained using said values in equation 6.3.

From figure 6.2, the amount of timing jitter accumulated in the NOLM guided system that can be attributed to PMD at 8000km is 0.3ps, this can then be subtracted, from the overall timing jitter obtained in results. The remainder can be attributed to ISI in the higher data rates.

6.2.5 Timing jitter measurement using the cross correlation method

The setup of the autocorrelator used to obtain the data is described in Chapter 3. The Cross Correlation (XC) signal between adjacent pulses, at all of the data rates used in this thesis, was used to estimate the timing jitter [166]. For this purpose, autocorrelation traces were taken with the scanning range greater than the pulse-to-pulse period. As a result, each autocorrelation trace included a main peak and several additional peaks arising from the cross-correlation between adjacent pulses. These additional peaks are broader than the main peak because of the timing jitter. The expression used to calculate the timing jitter from the data received from the autocorrelator is given as:

$$\sigma \approx \frac{1}{4N}\sum_{k=1}^{N}\left(\frac{\Delta\tau_{kXC}^{2}-\Delta\tau_{AC}^{2}}{\ln(2)}\right)^{1/2}, \qquad (6.4)$$

where t_{AC} is the pulse duration of the main peak in the autocorrelation trace and t_{kXC} is the pulse duration of k-th sub-peak. A peak number k in the autocorrelation trace corresponds to the cross-correlated signal between pulses separated by k repetition periods. The measurements were averaged over the peaks thus improving the accuracy of the estimate.

The measured timing jitter in the XC method for a small distance is approximately equal to the temporal resolution, making the accuracy of the timing inversely proportional to the timing jitter itself [166]. To evaluate the temporal resolution, ΔR, which results from the relation below:

$$\Delta R \cong \Delta\tau_{XC} - \Delta\tau_{AC}, \qquad (6.5)$$

The expression for the smallest measurable timing jitter is shown as:

$$\sigma^2_{\min} = \frac{\Delta R \Delta\tau_{AC}}{(8\ln(2))}, \qquad (6.6)$$

where ΔR for this system was 160-fs, which gives the smallest measurable timing jitter as 317-fs.

6.3 Evolution of timing jitter in non-linearly-guided, dispersion managed transmission systems

The limiting factors of most optical transmission systems today are amplitude jitter and timing jitter. As data-rates reach 40Gbit/s and beyond, sensitivity intolerance to timing jitter on the bit error rate becomes more pronounced. The differing mechanisms that make up the timing jitter are Gordon-Haus effect [167], non-linearly induced Inter-Symbol Interference (ISI) [163], electrostriction [164] and timing jitter due to polarization mode dispersion (PMD) [165].

Numerous techniques have been employed in soliton systems to reduce timing jitter, such as sliding filters [168], and synchronous modulation [169]. One way to reduce the effects that cause timing jitter is to use a passive optical device such as a Non-linear Optical Loop Mirror (NOLM), where it was found that it reduced the jitter considerably in a 40Gbit/s system [170].

The NOLM acts in two ways, firstly by reducing the ASE noise that leads to the Gordon-Haus effect [171], and secondly because of the stable nature of the propagation regime there is a reduction of the ISI, which has been shown to be the limiting factor in dispersion managed soliton (DMS) systems [163].

In this chapter, the timing jitter results experimentally measured in a 2R regenerative NOLM guided system are discussed, and the results at 10, 20, 40, and 80Gbit/s are compared with the results from the generic system at the same data rates. The autocorrelation traces are taken at distances set by N recirculations of the transmission loop, and the timing jitter is then extracted using a cross-correlation technique (XC), similar to that used in [166].

6.4 Experimental set-up

The experimental set-up is shown in Figure 6.3. A 10Gbit/s pulse train with a pulse duration of 3.5ps at Full Width Half Maximum (FWHM) was produced by a commercially available mode-locked fibre ring laser (Ultrafast Optical Clock, Pri-Tel). The centre wavelength exiting the laser was 1553.6nm. The signal was then encoded with a 2^{31}-1 pseudorandom binary sequence (PRBS) using a Lithium Niobate ($LiNbO_3$) modulator. The signal was then passed through a Mach-Zender (MZ) optical multiplexer to achieve 20Gbit/s and passed through subsequent MZ multiplexers to achieve the higher data rates.

The re-circulating loop comprised of two spans of standard single mode fibre (SMF-28), 82km and 83km long, and two slope-compensating fibre dispersion compensators (DCF). Average dispersion in the system was set to be slightly anomalous, approximately +0.003ps/(nm.km) at the operating wavelength. The corresponding dispersion map strength is 280. Low values of path average dispersion give a reduction in timing jitter, by reducing the translation from frequency jitter to timing jitter.

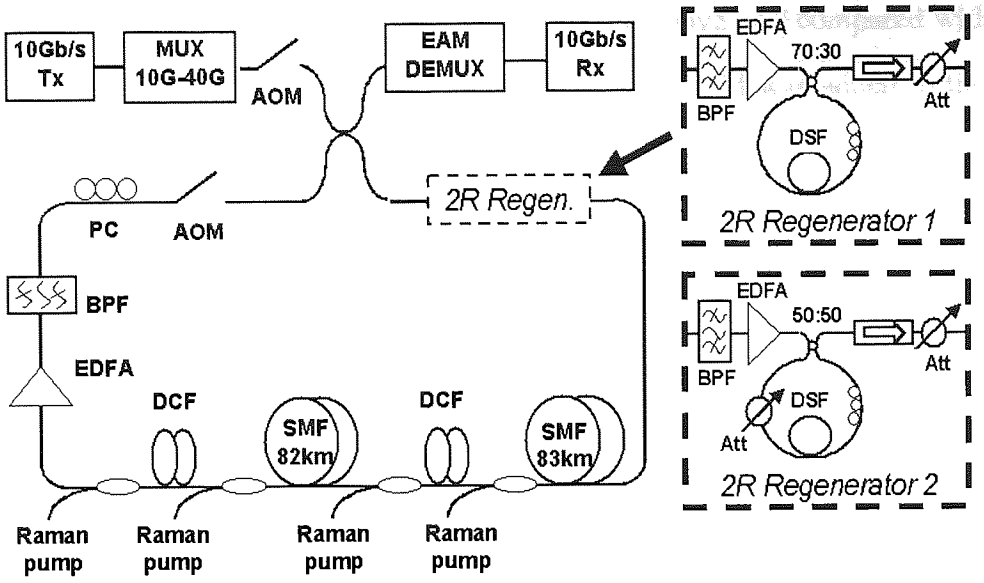

Figure 6.3 Experimental setup for the generic and the NOLM guided system. 2R regenerator 1 was used for data rates up to 40Gbit/s and 2R regenerator 2 was used for 80Gbit/s.

The average signal power coupled into the recirculating loop was -9dBm at the data speed of 10Gbit/s, –6dBm at 20Gbit/s, -3dBm at 40Gbit/s and 0dBm at 80Gbit/s to ensure a quasi-linear propagation regime for this particular system. The system was Raman amplified with the gain provided by Raman pump lasers counter-propagating with the signal. A separate pump was used for each standard fibre and for each dispersion compensator. The Raman pump wavelength was 1455nm. An Erbium Doped Fibre Amplifier (EDFA) was used in the recirculating loop to overcome the losses from an Acoustic Optical Modulator (AOM) and the recirculating loop coupler.

A commercially available Q-Clock (JDS) then recovered the clock. An electro-absorption modulator (EAM) was used at the receiver to demultiplex the signal from 40Gbit/s to 10Gbit/s and from 20Gbit/s to 10Gbit/s. The 80Gbit/s data was not demultiplexed.

The operation of the generic DM system as described above was compared with that of an equivalent NOLM-guided system. For this purpose, a NOLM was added to the system and a power amplifier to boost the power to the level required by the NOLM, as shown in Figure 6.4. In addition, an attenuator was placed after the NOLM in order to balance the power in the system back to quasi-linear regime.

Two NOLMs were used in this experiment. The first, which was used for the data rates 10, 20 and 40Gbit/s, comprised of an asymmetric fibre coupler with splitting ratio of 70:30 and 2.3km of TrueWave fibre (OFS) with an anomalous dispersion of +2.8ps/(nm.km) at 1550nm. The second NOLM was used at data rates of 80Gbit/s and it consisted of a 50:50 coupler with the asymmetry coming from an internal attenuator the non-linear element was 2.3km of TrueWave fibre (OFS) with an anomalous dispersion of +2.8ps/(nm.km) at 1550nm The two NOLMs were placed at the beginning of the recirculating loop. The transmission function was similar for the two NOLMs.

The method of measuring the timing jitter was to use a gated autocorrelator by means of an AOM linked to the recirculating loop controller. The autocorrelator was background free using the non-collinear output from the crystal. The scan range used was 163ps for the 10Gbit/s results and 102ps for the remaining data rates. The scan rate was set at either 1 or 2ps/s. An optical chopper and a lock-in amplifier were also used. The timing jitter was then extracted from the autocorrelation traces using a XC technique.

6.5 Results and discussion

Pulse duration measurements over all data rates in the generic and the NOLM guided system are shown in Figure 6.4. It can be seen in this figure that the pulse duration stabilizes into the DM autosoliton regime within a few hundred kilometres, which is in contrast to the generic system, which undergoes broadening from the onset.

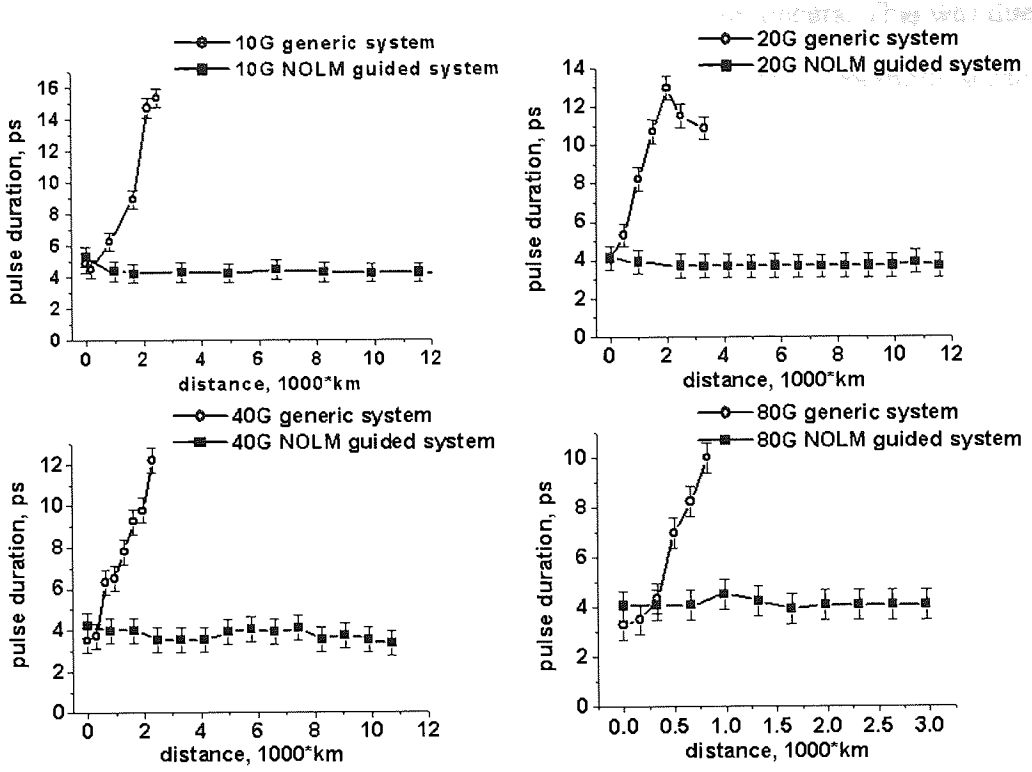

Figure 6.4 Pulse duration measurements as a function of distance, at data rates of 10, 20, 40, and 80Gbit/s. The stable pulse propagation at all the data rates in the NOLM guided system is shown (squares).

In Figure 6.5 the timing jitter measured by the XC method is shown for both the generic and NOLM guided system, along with the timing jitter measured on the DSO for both regimes. As one can see from Figure 6.5, the timing jitter increase in the generic system at 10Gbit/s is essentially non-linear and accelerates with distance, especially at the lower bit rate, when the jitter increase is considerably affected by the spontaneous noise accumulation. A theoretical plot in Figure 6.6, presents an estimate of the Gordon Haus timing jitter and shows reasonable agreement with the jitter dynamics measured in the generic system at 10Gbit/s.

When the results shown in Figure 6.5 are compared with the theoretical plots shown in Figure 6.1, there is a good match up to 2000km, when a timing jitter of 2ps is reached.

However, as the distance increases a discrepancy in timing jitter occurs. This was due to the system being strongly dispersion managed and any resemblance to a hyperbolic secant pulse shape is quickly lost in the generic system. In addition, as the filter and the AOM are at the end of each fibre span shown in Figure 6.3 (when the pulse shape is fully recovered), there could be a slight frequency offset by the AOM. This may affect propagation by causing a tail off in the G-H effect, similar to the sliding-frequency guiding filter effect [159], which would account for the lower values of timing jitter observed in Figure 6.5. It was also reported in [151] that the calculated timing jitter was two times the measured timing jitter.

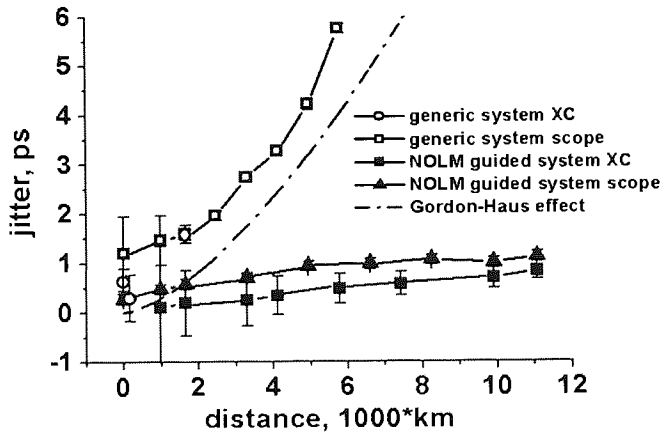

Figure 6.5 Timing jitter measurements as a function of distance at the data rate of 10Gbit/s. The large error for low values of timing jitter is because the error (using the XC method) is inversely proportional to the jitter value.

The difference in the timing jitter between the XC NOLM guided system (filled in squares) and the NOLM guided system on the DSO (triangles), was about 300-fs and is due to the amplitude jitter dependence of the DSO, compared with the amplitude jitter insensitivity of the XC method. The DSO converts amplitude jitter to timing jitter when using the eye diagram as the source [163]. This was one of the reasons the XC method was chosen over the DSO , another reason was that the XC method had a smaller resolvable

timing jitter than that of the DSO. It is for this reason that the first value of the NOLM guided system using the XC method (filled squares) in Figure 6.5 is not shown; it is below the resolvable limit.

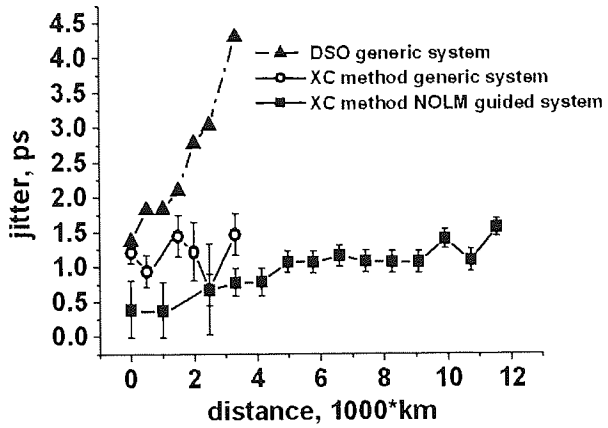

Figure 6.6 20Gbit/s jitter results using the DSO and the XC method.

The timing jitter for a 20Gbit/s data rate is shown in Figure 6.6. This figure shows that the jitter for the NOLM guided system is reduced to 1.5ps at 12Mm compared with that in the generic system, which is 4.3ps at 3.5Mm. Comparing the two results for 10 and 20Gbit/s; at 3.5Mm the measured timing jitter for the generic system was 2.8ps in the 20Gbit/s system, this gives a difference of the total timing jitter of 1.5ps to that of the 10Gbit/s system. Therefore, 1.35ps can be allocated to ISI and 150-fs to the optical demultiplexing process (shown up on the DSO). In the NOLM guided system the amount of timing jitter attributed to ISI is 0.45ps after a comparison between 10 and 20Gbit/s at 12Mm, assuming negligible affects from electrostriction.

For the generic system at 10 and 20Gbit/s, the XC method was not conclusive, but for the NOLM guided system it gives credible results, so one can ascertain that it was not directly due to the amount of delay between the pulses. This only leaves the noise build up within the frequency bandwidth of the optical pulse during the long scans of the

autocorrelator at lower data rates, as it was minimal in the NOLM guided system, but substantial in the generic system.

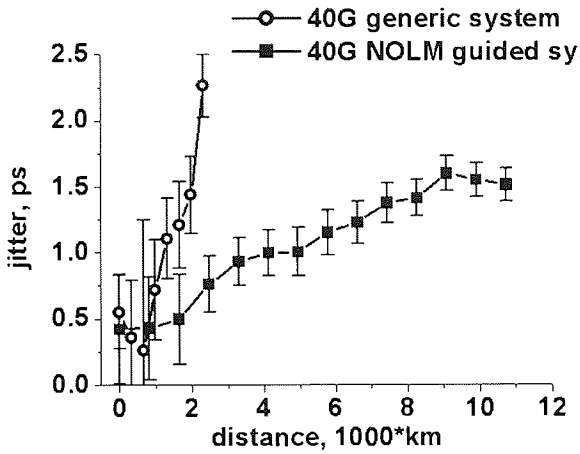

Figure 6.7 Timing jitter measurements as a function of distance, at the data rate of 40Gbit/s. The timing jitter results at this data rate for the generic system are more definite and show a rapid increase.

The timing jitter for the generic system at 40Gbit/s increased from approximately 0.5ps in the back-to-back signal to 2.1ps after 2.5Mm as shown in Figure 6.7. This result is in good agreement with the theoretical value shown in Figure 6.1, where 2ps of timing jitter is achieved after 2.1Mm of propagation. The jitter accumulated in the NOLM guided system after 10Mm is 1.5ps. The amount of timing jitter at a data rate of 40Gbit/s at 12Mm that can be attributed to ISI is 1.25ps, when compared to the NOLM guided system at 10Gbit/s.

Figure 6.8, shows the timing jitter for the generic 80Gbit/s system increases from less than 0.5ps in the back to back signal to 2ps at 0.5Mm, whereas the timing jitter accumulated in the 80Gbit/s NOLM guided system after 3Mm was 1.2ps. When the 80Gbit/s jitter is compared to the 10Gbit/s jitter, 1.25ps can be allocated to ISI after 3Mm, and ~5ps at 12Mm. At 80Gbit/s it was 4 times the amount than at 40Gbit/s, and double the amount of what would be expected if there were a linear increase. The reason for this is the amount of

overlap causes non-linear ISI in the higher data rates; this will lead to a non-linear increase in the rate of timing jitter from one bit rate to another, assuming the pulse maintains a Gaussian shape through propagation.

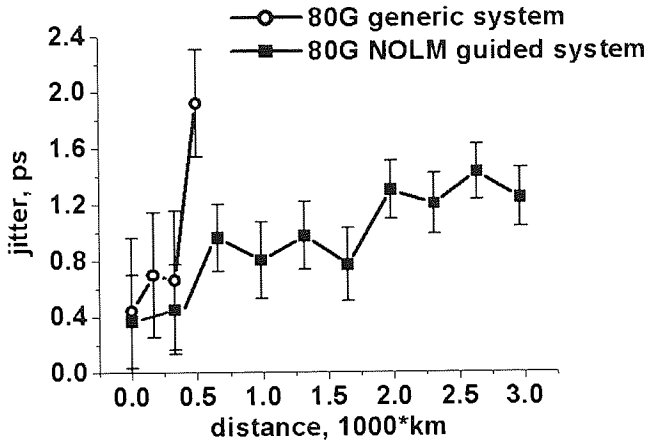

Figure 6.8 Timing jitter measurements as a function of distance, at the data rate of 80Gbit/s

The timing jitter increase rate, measured in femtoseconds per kilometre, is presented in Figure 6.9. In the guided system, the jitter increase rate was defined between the launch point and the end point of the link. In the generic system, the jitter increase rates for each bit-rate were defined separately at zero distance and at maximum transmission distance, in order to take into account the non-linear behaviour of the jitter increase. The height of each error bar in Figure 6.9 is defined by the difference between the timing jitter rate in the beginning and at the end of transmission.

The dramatic effect of non-linear guiding is evident from the data presented in Figure 6.9. At 10Gbit/s, the rate of increase is 0.5±0.3-fs/km in the generic system, which is reduced to 0.07±0.03-fs/km in the guided system. At 80Gbit/s, the timing jitter is reduced from 1.87±0.7-fs/km to 0.37±0.1-fs/km, respectively. The rate of timing jitter accumulation

for a system with a PMD value of 0.1ps/km$^{0.5}$, is 0.05-fs/km, this makes PMD the limiting factor for any ultra-long haul 10Gbit/s system using saturable absorbers. As for the remaining data-rates, a non-linear dependence of the timing jitter with bit rate that can be allocated to non-linearly induced ISI is evident.

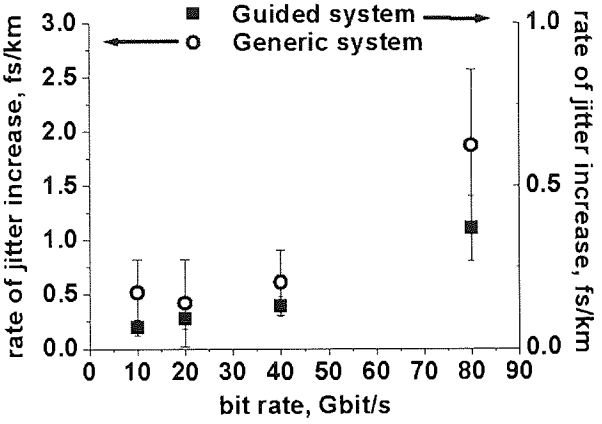

Figure 6.9 Rate of timing jitter accumulation in the generic and the NOLM guided system.

An example of PMD is given in Figure 6.10, which is one of the linear components of timing jitter. The 10Gbit/s NOLM guided system has a reduced Gordon-Haus effect and a weak ISI, so using a method described in [166], a theoretical plot was produced and compared with the data acquired from the autocorrelator for the 10Gbit/s NOLM guided system in section 5.3. As can be seen the theoretical PMD (the dispersion was set at 0.1ps/km$^{0.5}$) plot matches well with the 10Gbit/s data; the PMD within the recirculating loop may be slightly greater than 0.1ps/km$^{0.5}$ and the added affect from electrostriction may need considering along with the timing jitter added by the NOLM. However, most of the timing jitter in a NOLM guided 10Gbit/s system can probably be attributed to PMD. This alone will limit the propagation distance. Note that the timing jitter for the same system

(Section 7.3, Figure 7.4), but measured on the DSO gives substantially more timing jitter, this is due to the conversion of amplitude jitter to timing jitter.

As PMD is bit rate independent, approximately a quarter of the timing jitter at 40Gbit/s at 10Mm can be PMD. The NOLMs effect on the PMD could prove useful for future work along with the NOLMs effect on timing jitter compared with other 2R regenerator's effect on timing jitter.

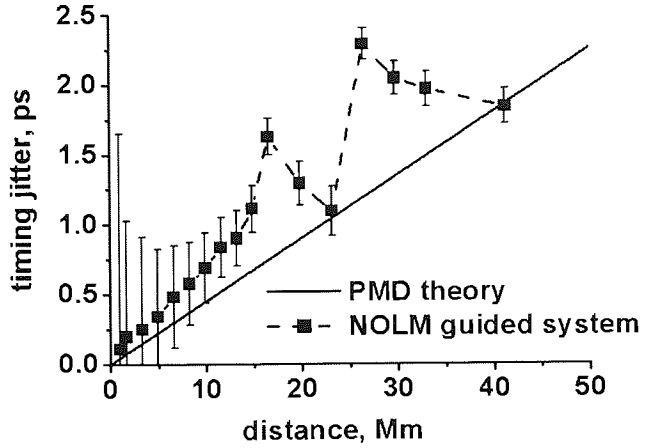

Figure 6.10 Timing jitter for the guided system at 10Gbit/s (squares), and theoretical PMD plot.

There are several factors contributing to the efficient suppression of jitter by NOLM. Firstly, the NOLM restores the pulse shape and suppresses the spontaneous emission and dispersive wave radiation. Secondly, non-linear switching in the NOLM compensates for the small residual dispersion in the system thus preventing the pulse broadening during propagation. Finally, the NOLM operates at a point of the switching curve where the amplitude fluctuations are efficiently reduced. Therefore, transposition of amplitude fluctuations into the timing jitter is also reduced.

6.6 Summary

The comparison of identical transmission system apart from the inclusion of a regenerator has been made and at all data rates there was a reduction of the inter-symbol interference, a result of the pulse-shape control in the NOLM guided system and the ASE suppression, which leads to a reduction of the Gordon-Haus effect in this system.

The timing jitter was obtained on an autocorrelator for both the generic system and the regenerated system and for all the individual data rates there was rapid increase in timimg jitter for the generic system, whereas in the NOLM-guided system the timing jitter was observed to increase at a reduced rate. Therefore, in the NOLM-guided system, the timing jitter for all the data rates steadily increased to 0.37-fs/km at 80Gbit/s, but the rate of increase was lower than that in the generic system, which reached 1.87-fs/km at 80Gbit/s.

The main limiting factor at lower data rates was a combination of timing jitter added by the NOLM and PMD and at higher data rates it was, ISI, which is in good agreement to the results given in [163].

Chapter 7 Signal propagation in dispersion managed systems guided by non-linear optical loop mirrors with filter control

7.1 Introduction

In this chapter the benefits of placing a band pass filter at the exit of the non-linear optical loop mirror are presented.

The theory of placing a Band Pass Filter (BPF) after the NOLM and thus further increasing the transmission distance, is discussed in Section 7.2. Experimental results are presented in Section 7.3 and 7.4 for 10Gbit/s and 20Gbit/s transmission systems respectively, where the transmission system for 20Gbit/s propagation included a demultiplexer. The Chapter is summarized in Section 7.4.

7.2 Background theory on a filter for soliton control

The use of a narrow band filter after an amplifier to reduce the amount of soliton self-frequency shift is well documented [135]. In addition, the use of a NOLM as an intensity filter [121] has been discussed. The research performed by [172] used WDM filters after the NOLM, where the results indicated the inclusion of a BPF did not expand the transmission distance, gave negative results, although this may have been due to the narrow bandwidth of the WDM. One of the conclusions of this research was to optimize the filter bandwidth to gain maximum propagation distance. The impact of the filter bandwidth on the system performance is investigated in the following sections.

Theoretical and experimental research on soliton squeezing [173], [174], [175] yields an insight into the effect of frequency shift of the soliton at the output of the NOLM. The band pass filter after the amplifier will remove some of the soliton self-frequency shift that builds up in the 'wings' of the pulse.

As the NOLM is asymmetrical, the low power arm carries the linear dispersive wave

radiation, and the other high power arm has the N = 1 soliton. Although the effects are not as great as reported in the research by [175] the pulse will undergo a small Raman induced frequency shift in that arm. This was found to be the limiting factor in [175]. All of the optical spectral measurements were taken at the coupler before the NOLM after each recirculation; therefore, the observable spectrum seen was comparable with earlier loops. The overall result is a DM autosoliton effect similar to sliding filter control in a soliton system, where the NOLM offsets the carrier frequency on each loop then the filter corrects this after the amplifier before the NOLM.

The pulses entering the NOLM have instabilities that arise from the high power introduced by the high power optical amplifier. This will cause differences in the amount of soliton self-frequency shift within the NOLM itself, and this will produce slight variations of the carrier frequency at the output. All this translates to different pulses traveling at different speeds around the recirculating loop, and frequency induced polarization instabilities with the addition of a secondary band pass filter, which is offset slightly in frequency, with a bandwidth wide enough to minimize reshaping of the autosoliton pulse. The instabilities are virtually eliminated; this should allow physically limited transmission at all data rates.

7.3 10Gbit/s transmission over 100Mm with a bit rate distance product of 1Tbit/sMm in standard fibre using 2R regeneration in an optical loop mirror

In principle, ultra-long-haul data transmission at a relatively low (by today's standards), bit rate of 10Gbit/s can be achieved without any regeneration [176], [177]. This requires a carefully designed dispersion map and appropriate power balance in order to support the Dispersion-Managed (DM) soliton propagation. The Gordon-Haus effect also imposes a fundamental limit on these systems. On the other hand, passive 2R regeneration can provide high-quality transmission using lower signal power and longer amplifier spacing. 2R

regeneration suppresses the accumulated spontaneous noise and thus reduces the Gordon-Haus jitter [178], [179].

Previously, data transmission at a bit rate of 10Gbit/s over a practically unlimited distance (one million kilometres) has only been reported in a 3R-regenerated system [180]. Compared to the 3R regeneration, all optical 2R regeneration is considerably more cost-effective, as it does not require a complex re-timing scheme and therefore it can be achieved in a simple, purely passive device, such as a saturable absorber [181], or a Non-Linear Optical loop mirror (NOLM) [182]. The NOLM has proved to be one of the most versatile all-optical switching devices for high speed all optical networks [183], [184]. The ultrafast nature of operation in the NOLM, the simplicity of the device and its multi-wavelength operability make it an ideal element for 2R regeneration in all optical networks [185], [186].

DM autosoliton propagation regime in a NOLM-guided transmission system has been shown in the work described in this thesis to dramatically improve the transmission quality and increase the transmission distance [187].

7.3.1 Experimental set-up

The experiments were carried out using a re-circulating loop configuration, as shown in Figure 7.1. The carrier signal was provided by a mode-locked fibre ring laser (Ultrafast Optical Clock, Pritel, Inc) operating at a central wavelength of 1553nm. The laser produced 3.5ps long pulses at a repetition rate of 10GHz. The signal was encoded using a pseudorandom bit pattern with the bit word length of 2^{31}-1 by means of a $LiNbO_3$ modulator.

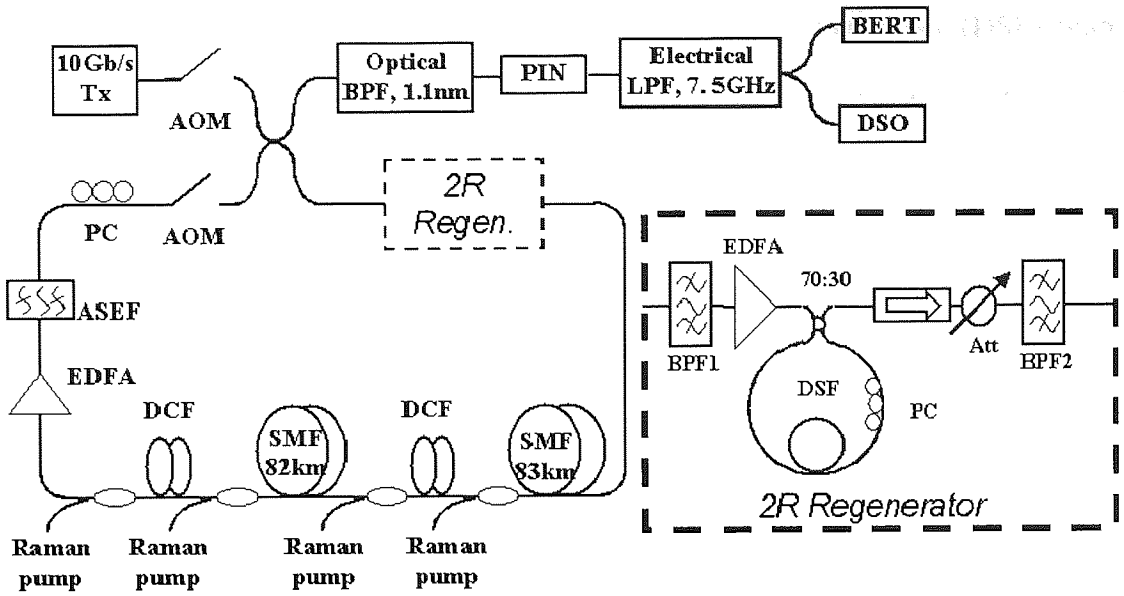

Figure 7.1 Experimental configuration, showing re-circulating loop (generic system) and design of the 2R-regeneration module (inset).

At the receiver input, an optical band pass filter with a Gaussian-shaped, 1.1nm-wide transmission window and an electrical quasi-Gaussian low pass filter with 3dB bandwidth of 7.5GHz were used.

The re-circulating loop comprised two spans of SMF, 82km and 83km long, and two slope-compensating fibre dispersion compensators. Total dispersion in the system was set to be slightly anomalous, approximately 0.6ps/nm at the operating wavelength. The corresponding dispersion map strength is 280. The system was all Raman amplified with the gain provided by Raman pump waves counter-propagating with the signal. The Raman pump wavelength was 1455nm. An auxiliary erbium-doped fibre amplifier was used to compensate for the signal losses induced by the acoustic-optical modulator (AOM) and the 3dB fibre coupler, forming the re-circulating loop. A high-pass Amplified Spontaneous Emission (ASE) filter was inserted after the amplifier in order to remove the ASE peak at 1530nm.

The NOLM used in the experiment comprised an asymmetric fiber coupler with

splitting ratio of 70:30 and a 2.3km length of Dispersion Shifted Fiber (DSF) with an anomalous dispersion of 2.8ps/(nm·km) at 1550nm. The NOLM was placed at the beginning of the re-circulating loop. A high-power EDFA at the NOLM input was used to boost the signal to appropriate power level. A band pass filter BPF1 with a Gaussian-shaped, 1.1nm-wide transmission window was placed before the high-power EDFA to reduce ASE noise arising from Raman amplifications. An attenuator placed after the NOLM was used to adjust the average power of the re-circulating signal in order to assure quasi-linear pulse propagation in the link. Finally, one more band pass filter BPF2 (Gaussian-shaped, 2.3nm-wide transmission window) was placed at the NOLM output (see Figure 7.1) to compensate for the spectral changes occurring in the NOLM. Addition of this last filter proved to be essential as it dramatically improved the transmission stability, in line with the earlier studies of filter-guided pulse propagation [178], [179].

7.3.2 Results and discussion

Initially, the transmission performance of the NOLM was characterized. Figure 7.2 shows the switching curve of the NOLM measured with a 10Gbit/s, pseudorandom data stream. Several transmission maxima appear in the plot, typical for the NOLMs of this type. The best regeneration performance was obtained when the input power was slightly above the first transmission maximum, as shown by shaded area in Figure 7.2(a). In this regime, the amplitude fluctuations of the input signal as well as the low-intensity spontaneous noise can be suppressed efficiently [183].

The transmission performance of a generic system was used as a reference. Removing the 2R regenerator from the recirculating loop formed the generic system. The generic system was subsequently optimized by adjustment of gain in all the amplifiers and by tuning the total dispersion in the system. The longest error-free transmission distance obtained in the optimized generic system was approximately 4Mm. The signal was considerably distorted at this point showing a noisy eye-diagram.

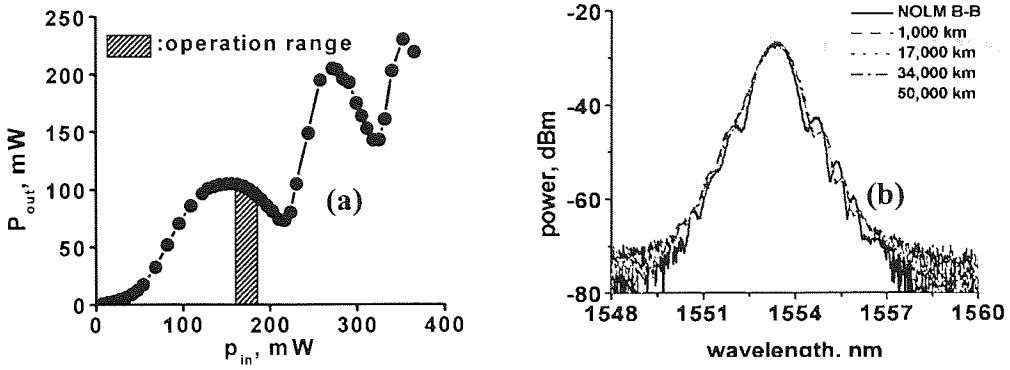

Figure 7.2 Measured switching curve of the NOLM. Shaded area shows the operation range used in the experiments.

At the next stage, the system was evaluated with the in-line 2R regenerator present. The system was optimized for the best transmission performance. Stable propagation of pulses with constant pulse width and unchanged spectrum was obtained, similarly to earlier results [187], as shown in Figure 7.2(b).

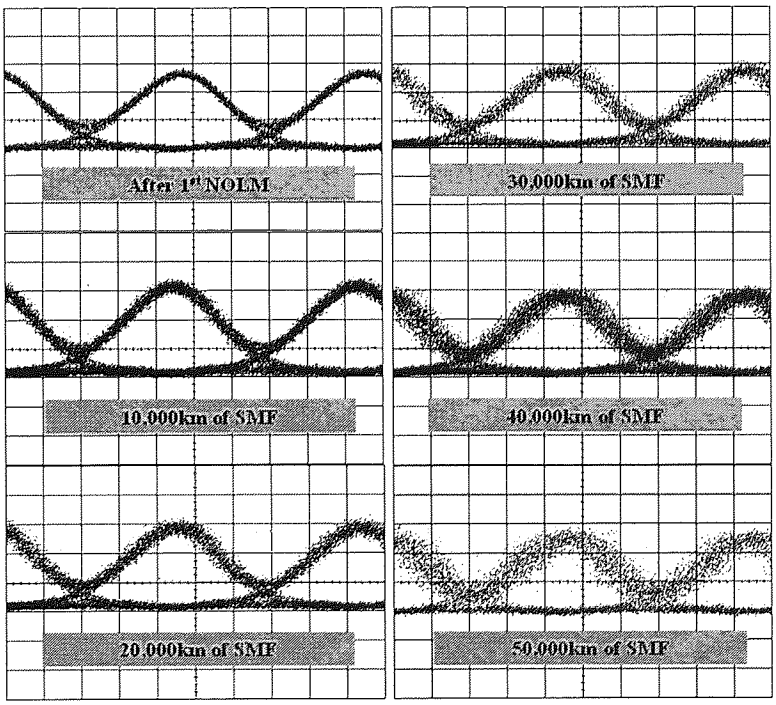

Figure 7.3 Eye diagrams measured back-to-back (top row) and after 50Mm (lower row) in the regenerated system.

Figure 7.3 shows the eye diagrams measured back-to-back and up to a distance of 50Mm, respectively. Clear, open eye with no signs of waveform distortion was observed up to 50Mm, indicating an excellent signal reshaping capability of the regenerator. Some degradations of the eye quality occurred at this point, and general deterioration of signal with distance, are due mainly to the timing jitter increase. The measured evolution of timing jitter is illustrated in Figure 7.4(a), which shows a practically linear increase at a rate of approximately 0.1ps/Mm.

The evolution of amplitude fluctuations is shown in Figure 7.4(b) as standard deviation of 'ones' and 'zero' rails in the eye diagrams measured at different distances by maintaining a constant received signal power. Suppression of background noise at "zero" level and a certain increase of amplitude fluctuations at 'one' level are evident in this plot. At the same time, the mean amplitude values of 'zero' remained virtually unchanged and that of 'ones' went down slowly, shown in Figure 7.3. This suggests that the amplitude jitter increase is due to the accumulation of timing jitter and not noise.

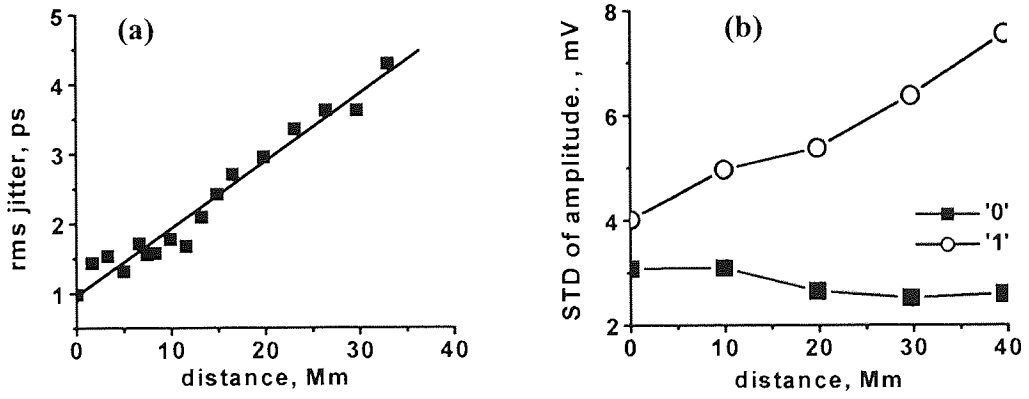

Figure 7.4 (a) Measured evolution of timing jitter with distance. (b) Standard deviation (STD) of amplitude for "ones" and " zeros" as a function of distance.

The measured Q-factor as a function of propagation distance is shown in Figure 7.5(a). The error-free data transmission was observed for 610 round-trips of re-circulating loop, corresponding to a distance in excess of 100Mm of standard fibre this gives a bit rate distance product of 1Tbit/sMm. No forward-error-correction was used at any time; therefore, the transmission distance was physically limited. In the final stages of transmission, timing jitter exceeded the pulse duration measured at the "chirp-free" point. At a distance of 100Mm, the measured timing jitter of the signal was as large as 10.5ps, thus severely distorting the eye diagram.

The corresponding BER for the NOLM with the BPF is shown in Figure 7.5(b). The error free propagation can be seen to be in excess of 100Mm, whilst in the NOLM guided system alone the maximum achievable error free distance is 27Mm.

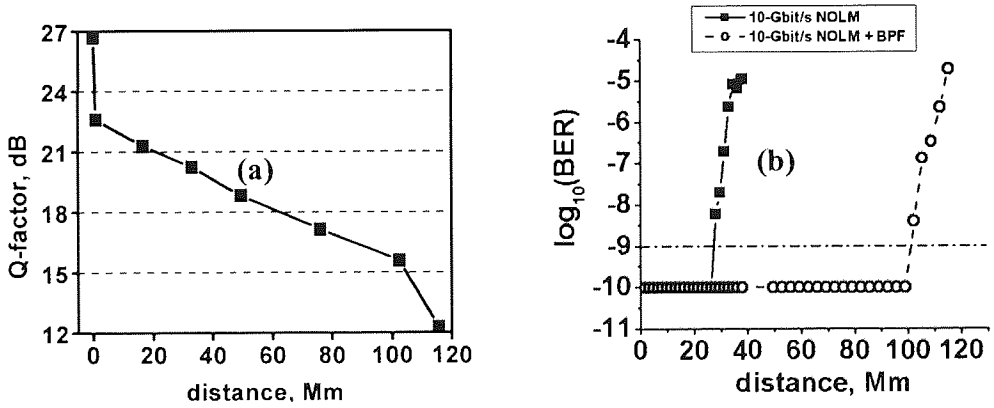

Figure 7.5 Experimental Q-factor evolution against transmission distance (a). BER for the NOLM with/without the BPF.

A corresponding simulated eye diagram is presented in Figure 7.6. However, strong filtering by an electrical low pass filter placed before the receiver was sufficient for signal recovery and dramatically improved the eye quality Figure 7.6 [188]. As a result, signal recovery was made possible after the transmission distances in range 50-100Mm.

The optimum average power of the re-circulating signal, measured immediately after the 2R regenerator, was approximately –6dBm, corresponding to a peak power of approximately 12-mW. Therefore, the pulse peak power was well below the level required for conventional soliton transmission, and propagation in the system was quasi-linear. The system possessed a strong dispersion map resulting in considerable pulse breathing. The regenerator essentially represented non-linearity of the system.

These results show that there is a virtually unlimited propagation distance, where the pulse duration, power and spectrum, measured at a certain point in the system, remain stable over a virtually infinite distance. The DM autosoliton propagation was unaffected by changes in the input pulse, and the NOLMs provide the non-linearity, with the transmission line being quasi-linear. In contrast the propagation regime for DM solitons was non-linear, and dependant on the input pulse.

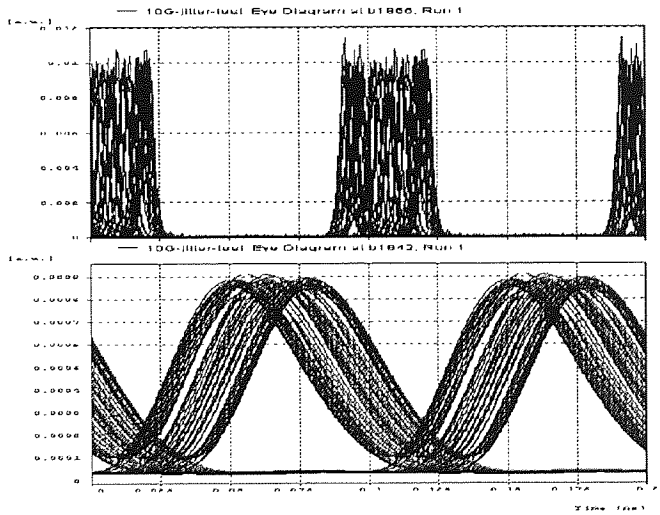

Figure 7.6 Simulated eye diagrams corresponding to the transmitted signal without (upper plot) and with (lower plot) the 7.5GHz Gaussian low-pass electrical filter [188].

7.4 20Gbit/s transmission over 20Mm giving a bit rate distance product of 400Gbit/s.Mm in standard fibre using 2R regeneration in an optical loop mirror

There is considerable interest in increasing the data rate in long haul and submarine optical transmission cables. 3R and 2R regeneration offer this upgrade-ability while maintaining the transoceanic distances required.

Gaussian RZ pulse propagation in DSF at 20Gbit/s is limited to 5,500km [189]. Soliton propagation at 20Gbit/s over 200km was first observed by [190]. The use of sliding frequency-guiding filters in soliton propagation has allowed the transmission distance to be extended to 19Mm [191] also using DS fibres.

An other means of extending the transmission distance is to use 3R regeneration, which has proven very successful, with 7,150km achieved with in-line phase synchronous modulation. This method also eliminated the need for dispersion management [192]. 150Mm has been achieved with an in-line electro-absorption modulator [193]. However, these methods can prove costly, as the clock has to be recovered, leading to expensive electronics. Also, all the above methods use DSF whilst field transmission systems mainly use SMF in strong dispersion maps.

Passive 2R regenerators are a less complex and cost efficient option when compared to the 3R regeneration. Passive semiconductor saturable absorbers have been shown to improve propagation at 20Gbit/s [194]. The NOLM has been experimentally proven to extend the propagation distance at data rates from 10 to 80Gbit/s [187], [195], and with the use of a band pass filter, this distance was extended to in excess of 100Mm [196].

In this section, the aim is to observe the propagation characteristics at 20Gbit/s to confirm the results achieved at 10Gbit/s.

7.4.1 Experimental set-up

The 20Gbit/s signal was taken at the 40Gbit/s multiplexer's 20Gbit/s monitor, and the

experimental set-up was the same as shown in Figure 7.1. The power in the recirculating loop was maintained at –4 to –3dBm, with 12mW peak power, which ensured a quasi-linear propagation regime. The EAM was inserted at the receiver to demultiplex the data from 20Gbit/s to 10Gbit/s. Other than that, the set-up was the same as described in Section 7.3, with a 2.3nm band pass filter placed after the NOLM and before the attenuator as shown in Figure 7.1. This was to compensate for the spectral changes occurring in the NOLM due to the soliton self frequency shift. The addition of this last filter has proved to be essential as it dramatically improved the transmission stability, in line with the earlier studies of filter-guided pulse propagation [178], [179].

The EAM in this experiment was impaired, due to age, giving a 3dB power penalty in the receiver sensitivity from earlier studies, to overcome this the optical power from the EDFA's before the clock and data recovery photodiodes had to be increased adding extra noise. The system was tested at 40Gbit/s but the transmission distance achieved was down by 50%. Even though the EAM reduces the overall propagation distance, it was still possible to investigate the effect of inserting the NOLM and BPF to the system.

7.4.2 Results and Discussion

The transmission performance of a generic system was used as a reference. Removing the 2R regenerator from the recirculating loop formed the generic system. The generic system was subsequently optimized by adjustment of gain in all the amplifiers and by tuning the total dispersion in the system. The longest error-free transmission distance obtained in the optimized generic system was approximately 2Mm. The signal was considerably distorted at this point showing a noisy eye-diagram.

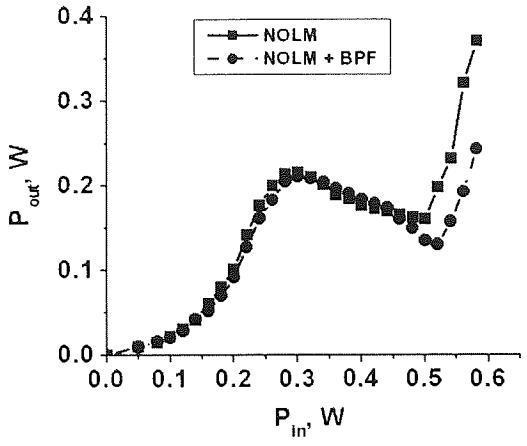

Figure 7.7 The switching curve for the NOLM at 20Gbit/s with and without the band pass filter.

The switching curve of the NOLM at 20Gbit/s is shown in Figure 7.7, the curve for filter can be observed to become more mesa-like, giving a slightly more added stability. The contrast for this NOLM is 60%. The spectral output after the NOLM is shown in Figure 7.8, the resolution of the OSA is 0.05nm. $\Delta\lambda$ for the NOLM was 0.95nm, and this was reduced to 0.87nm when the BPF was added. The filter can be observed to clip the wings of the pulse and give a reduction of noise on the blue and red-shifted wavelengths.

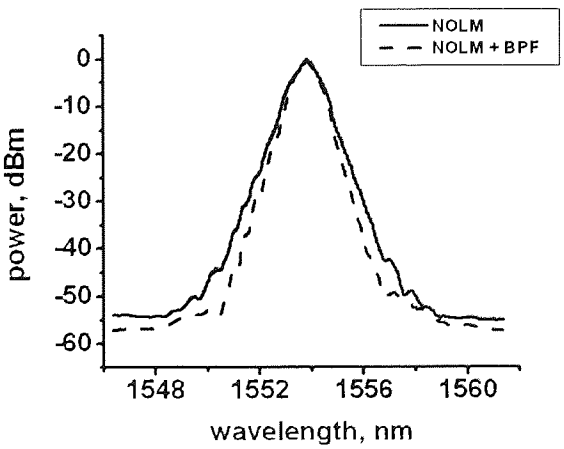

Figure 7.8 The spectrum exiting the NOLM with and without the band pass filter.

The pulse duration stabilization imposed by the DM autosoliton regime is illustrated in Figure 7.9(a) that is consistent with all the previous studies. The pulse duration for the generic system can be seen to increase from 4ps to 13ps at 2000km. The decrease in pulse duration after 2000km was attributed to the background level build up in the autocorrelator arising from increased background noise, which was associated with increasing the PMT gain. In contrast, the NOLM guided system starts at 4ps then reaches a steady state of 3.5ps, which continues up to 12Mm. In Figure 7.9(b), the temporal pulse shape can be observed before and after the NOLM, and is compared to a soliton fit. The wings in the pulse exiting the NOLM have been increased along with the pulse duration, giving it a comparable temporal shape to that of a soliton.

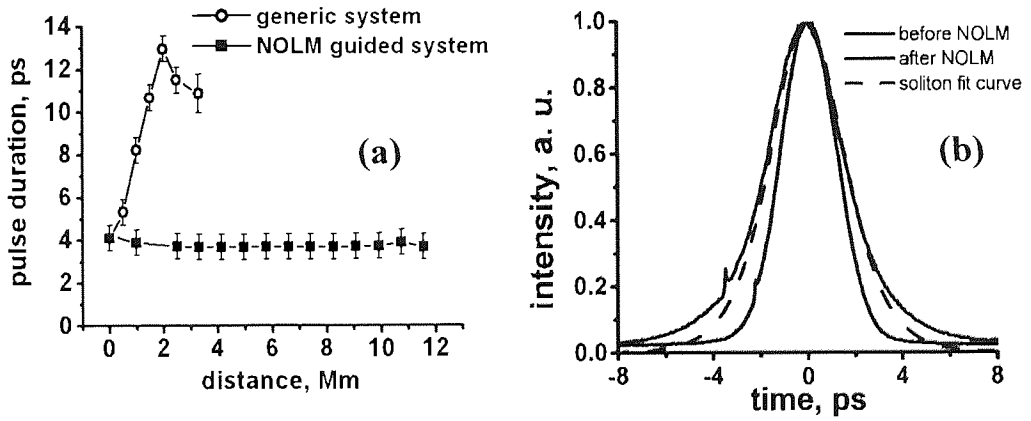

Figure 7.9 Stabilization of the pulse duration at 20Gbit/s in the NOLM guided system compared to the generic system (a). Autocorrelation traces taken before and after the NOLM (b).

The RMS timing jitter taken at 20Gbit/s, shown in Figure 7.10 was measured on the DSO. As can be seen there is a dramatic improvement in the timing jitter from the generic system to that of the NOLM guided system. The timing jitter rate of accumulation is 0.16ps/Mm, with a core linear element of timing jitter arising from PMD, the rate of PMD

accumulation can be approximated at 0.05ps/Mm. This improvement in jitter was due to the reduction of ASE that leads to Gordon-Haus timing jitter and dispersive wave radiation elimination by the intensity filtering properties of the NOLM. This is in agreement with the results obtained at 10Gbit/s. At data rate of 20Gbit/s and higher there is additional timing jitter attributed to ISI, due to the strong dispersion map. The timing jitter in the NOLM guided system with the BPF added, shows a stabilization of the jitter, and the overall rate of timing jitter accumulation is reduced to 0.11ps/Mm which is slightly greater than that at 10Gbit/s obtained in Section 7.3, where the extra jitter is arising from ISI.

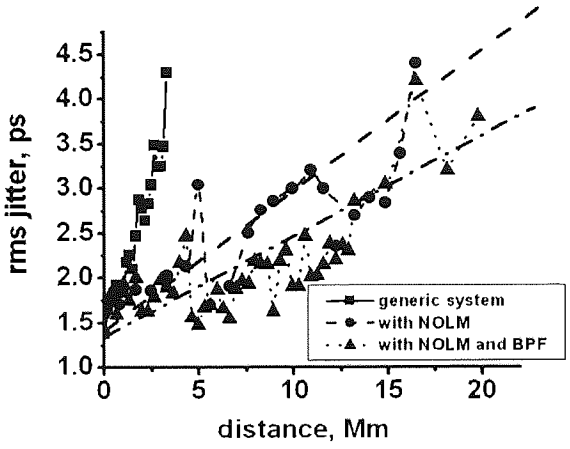

Figure 7.10 The RMS timing jitter in the generic system (squares), in the NOLM guided system (circles), and in the NOLM guided system with the band pass filter (triangles).

The benefit of this stabilization and jitter reduction rate is illustrated in Figure 7.11, which shows in the generic system, the BER reaches 10^{-9} at 2500km total transmission distance (SMF plus DCF). For the NOLM guided system, the 10^{-9} BER floor was reached at 8900km total transmission distance. But the stabilization of the transmission system was evident in NOLM guided system with the BPF, where the BER stays at 10^{-9} beyond 20Mm. The values that drift away from the error free floor arise from timing problems and general polarization optimization.

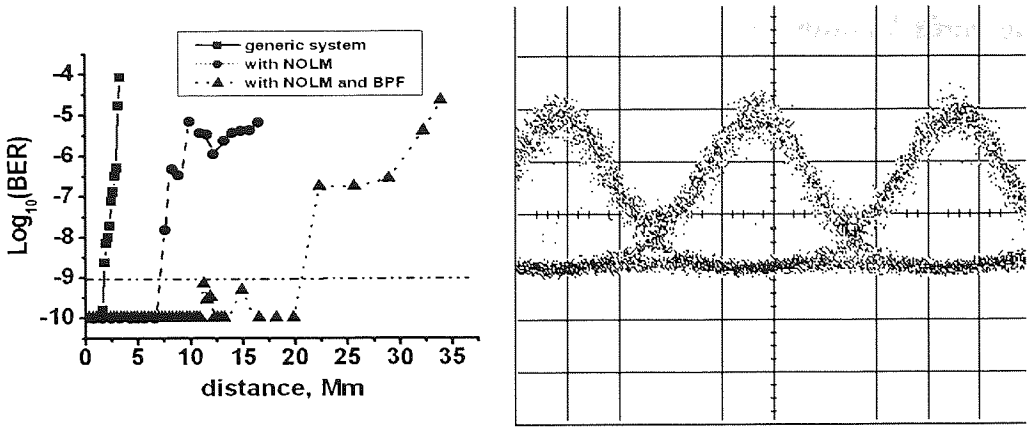

Figure 7.11 Shows the BER in the three different systems. The demultiplexed eye after 20Mm of propagation in the NOLM guided system with the BPF.

This result agrees with the result given in section 7.3, and is in correlation with previous studies [178], [179].

7.5 Summary

In section 7.3, propagation of a 10Gbit/s data stream over a practically unlimited distance in a strongly dispersion-managed, standard fibre system has been observed using passive, NOLM based 2R regeneration. Physically limited, error free (Q>15.6dB) data transmission over a distance in excess of 100Mm of standard fibre with 80km amplifier spacing has been achieved without re-timing.

In section 7.4, propagation of a 20Gbit/s data stream over a practically unlimited distance in a strongly dispersion-managed, standard fibre system has been observed using passive, NOLM based 2R regeneration. A physically limited, error free data transmission over a distance in excess of 20Mm of standard fibre with 80km amplifier spacing has been achieved without re-timing, thus giving a bit-rate distance product of 400Gbit/sMm. The propagation distance at 20Gbit/s is limited by a combination of ISI and PMD.

Chapter 8 The effects of passive 2R regeneration on optical time division multiplexed propagation

8.1 Introduction

In this chapter the importance of keeping the optical power in each of the data channels uniform, in an optically time division multiplexed system is examined. In section 8.3 the experimental set-up is explained. The results are discussed in section 8.4 and finally in section 8.5 the chapter is summarized.

8.2 Transmission of non-uniform OTDM channels in a non-linearly-guided dispersion-managed fibre system

Optical time division multiplexing (OTDM) is an important technique in high-capacity optical communications. At ultrahigh speeds of 80Gb/s and above, it is currently the only way to form optical data streams. Due to the finite accuracy of channel equalisation techniques, some variation of amplitude between the constituent channels is inevitable in OTDM transmitters. Other fundamental effects, including phase noise from the laser source and interferometric noise, also contribute to these variations [197]. On the other hand, it is sometimes advantageous, from the system point of view, to introduce some degree of channel inequality deliberately in order either to reduce pulse-to-pulse interactions [198], or to simplify the task of clock recovery [199].

All 2R regenerators, including non-linear optical fibre loop mirror (NOLM) [200], [201], [202], possess non-linear transmission response characteristics. Therefore, OTDM channels of different amplitudes will experience different transformations when switched in a 2R device. This is an important factor in a 2R-supported data transmission link. In this research, we investigate how the channel inequality affects non-linear signal switching in a

NOLM-based 2R regenerator, and the data transmission at a speed of 40Gbit/s in a non-linear switch-guided system.

8.3. Experimental set-up

The experimental arrangement (Figure 8.1) was similar to that used in previous recirculating loop experiments using the in-line NOLM as a 2R element [202]. A mode-locked fibre laser generated Gaussian-shaped 3.5ps pulses with an extinction ratio higher than 33dB. The pulses were modulated at 10Gbit/s by a pseudo-random bit stream (PRBS) with a length of 2^{31}-1 and were subsequently optically multiplexed to form a single-polarization, 40Gbit/s OTDM data stream by using a two-stage fibre delay line. It was possible to vary the amplitudes of the four OTDM channels in the 40Gbit/s signal individually by adjusting the polarization states within the delay line.

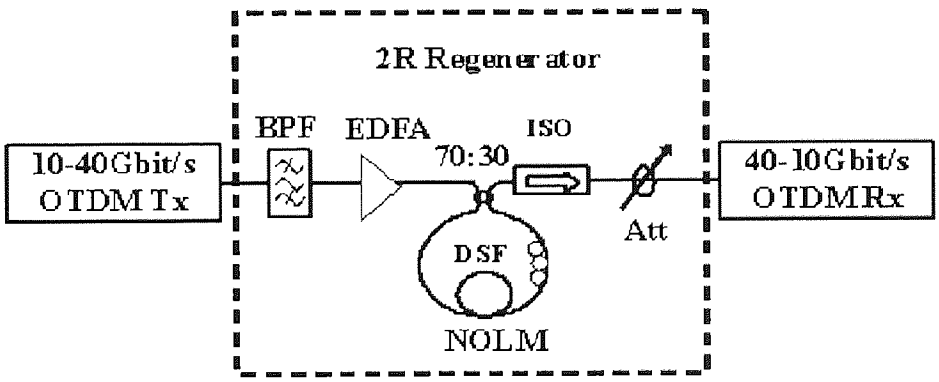

Figure 8.1. Experimental set-up

At the receiver, the 40Gbit/s signal was optically demultiplexed to 10Gbit/s using an electro-absorption modulator. The NOLM comprised a 70:30 fibre coupler and 2.3km of dispersion-shifted fibre with an anomalous dispersion of +2.8ps/(nm·km) at a wavelength of 1550nm. The recirculating loop comprised two spans of standard single mode fibre (SMF), 82 and 83km long, respectively, and two slope-compensating fibre dispersion

compensators. The average dispersion in the system was set to be slightly anomalous, at approximately +0.003ps/(nm·km) at the operating wavelength.

8.4. Results and discussion

Figure 8.2. Shows the measured transmission of the NOLM as a function of the average power of the input 40Gbit/s signal. The shaded area indicates the input optical power range that usually provides the best switching and noise suppression performance [200], [201], [202].

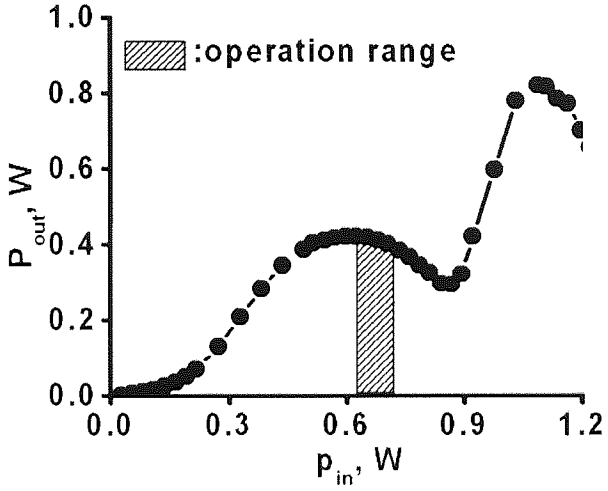

Figure 8.2 Switching curve of NOLM at 40Gbit/s.

Firstly, the switching behaviour of the 40Gbit/s OTDM signal was investigated by using histogram analysis of the eye diagrams taken on a 50GHz digital sampling oscilloscope equipped with a 32GHz photodetector. The signals were measured before and after the 2R regenerator. The relative standard deviation of amplitude, ΔV, was used as a measure of inter-channel non-uniformity. The mean voltage value V_i (i = 1, 2, 3, 4) of the marks in each individual eye determined the amplitude of the corresponding channel. The effective inter-

channel amplitude difference was defined as $\Delta V = \sigma/\mu$, where σ is the standard deviation of V measured channel-to-channel, and μ is the averaged value of V over the four channels.

The input value of ΔV was varied by adjustment of the OTDM multiplexer. The average power at the NOLM input was optimized to minimize the ΔV of the signal at the NOLM output. The average power arriving at the photodetector was maintained constant. Figure 8.3 shows the output ΔV as a function of that at the regenerator input. One can see that the inter-channel amplitude variation is always reduced by the NOLM, but that the effect weakens as the input signal becomes less uniform.

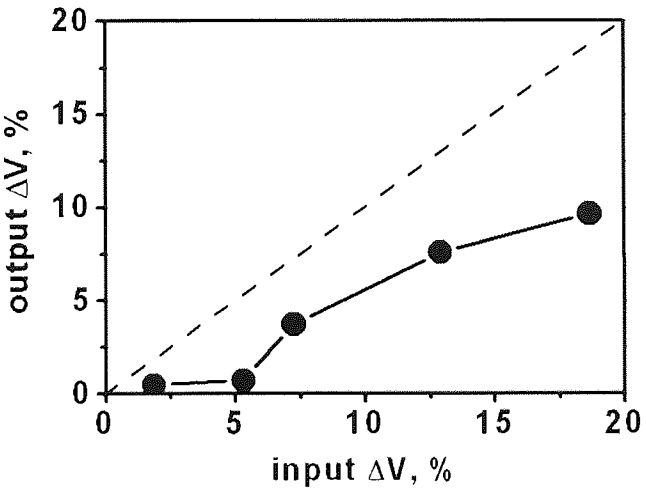

Figure 8.3. Inter-channel amplitude variation, ΔV, before and after the 2R regenerator.

The dynamics of another important parameter were studied, the random fluctuation of amplitude. This was characterized by $du = (S\rho_i)/4$, where ρ_i was the measured standard deviation of the amplitude within each channel. Figure 8.4. shows two dependencies of du on the input amplitude difference, ΔV, one measured before and the other after the regenerator. The height of the error bar indicates the difference between the minimum and

maximum ρ_i measured in the most stable and in the noisiest of the four channels, respectively.

One can see that the effect of the input channel non-uniformity on the amplitude noise suppression is significant. When the input amplitudes are relatively uniform (ΔV less than 5% in the experiment), the NOLM efficiently suppresses the amplitude fluctuations in all channels. However, when the input channels become considerably unequal (ΔV larger than 10%), the efficiency of the amplitude noise suppression varies strongly among the channels: as a result, the overall quality of the switched signal deteriorates. In fact, a signal comprising very non-uniform OTDM channels actually experiences an amplitude noise increase as a result of switching in the NOLM.

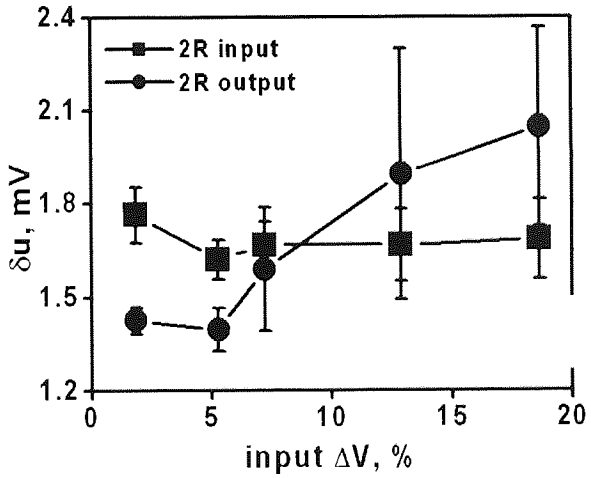

Figure 8.4. Random amplitude fluctuations du before (squares) and after (circles) the 2R regenerator, as functions of the input ΔV.

Non-uniformity of the input signal is likely to affect the data transmission in any system employing NOLMs as in-line 2R regenerators. If the format of the input signal is such that the amplitude fluctuations in some channels increase in the first NOLM, these channels might subsequently deteriorate during propagation through subsequent 2R elements, probably resulting in unstable propagation of corresponding channels.

The effect of channel non-uniformity on the data transmission was studied by monitoring the eye diagrams and Q-factor of a digital signal propagating in the recirculating loop. The 2R regeneration was performed after every 200km of fibre [202]. Figure 8.5 shows the eye diagrams measured back-to-back and after propagating over 2500km of SMF. The initial amplitude difference, ΔV, was set at a level of either 15% (Figure 8.5(a, b)) or 5% (Figure 8.5(c, d)) for this experiment.

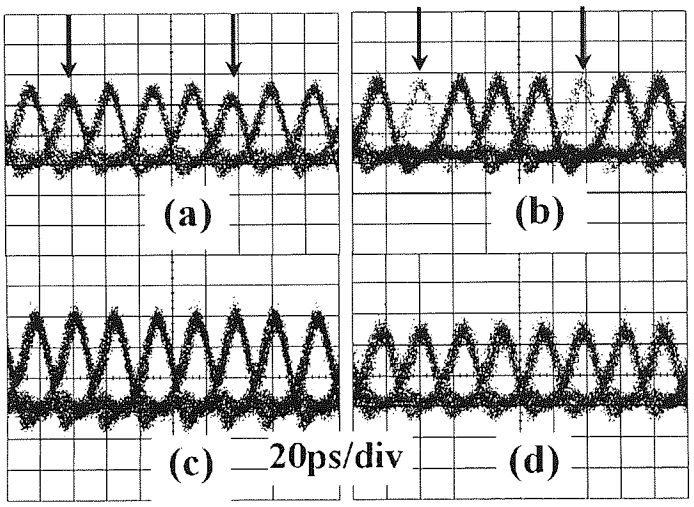

Figure 8.5 Eye diagrams. a) Initial ΔV = 15%, back-to-back. b) ΔV = 15%, measured after 2,500km. c) ΔV = 5%, back-to-back. d) ΔV = 5%, after 2,500km.

With an initial ΔV of 15% (Figure 8.5(a)), the signal considerably deteriorated during transmission, showing drop-out of the selected channel after propagating over 2,500km (Figure 8.5(b)). The overall bit-error-rate of the 40Gbit/s data stream increased dramatically during the first several hundred kilometres of transmission.

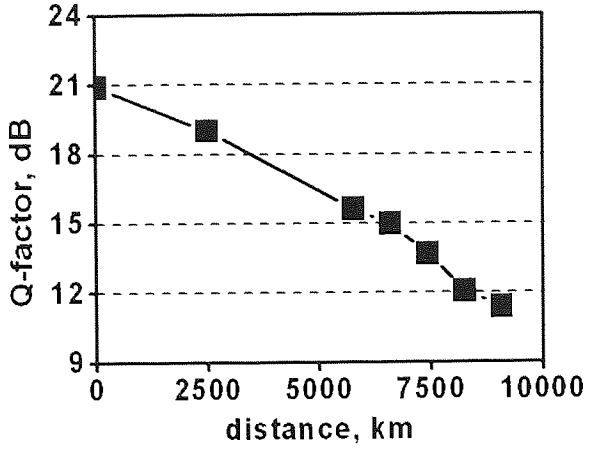

Figure 8.6 Q-factor vs. transmission distance.

The higher quality signal with an initial ΔV of 5% (Figure 8.5(c)) propagated in a totally different manner. Channel non-uniformity was eliminated after multiple transmissions through the 2R element, resulting in a virtually perfectly uniform OTDM data stream observed after 2,500km of propagation (Figure 8.5(d)). The estimated Q-factor was as high as 19dB after 2500km of SMF (Figure 8.6) and the error-free propagation (Q ~ 15.6dB) distance was estimated to be in excess of 5800km.

8.5 Summary

Channel-to-channel amplitude differences in OTDM data streams were shown to have a strong impact on the switching behaviour of individual channels in a 2R-regenerator. Depending on the inter-channel amplitude difference, the optical pulses in different channels experience either suppression of the amplitude noise, or a noise increase.

The results given in this chapter show that if there is as much as a 15% deviation of the pulse amplitude then there is pulse 'drop out' when propagated. However, with a deviation of 5% the 2R-regenerator can then overcome this and go on to eliminate channel non-uniformity to sustain a stable propagation regime. This was verified by taking the Q factor

that showed the propagation of the pulse up to 5,800km before falling below the accepted level.

Appropriate control of the channel uniformity in the OTDM transmitters is necessary in order to support stable long-haul transmission in 2R-regenerated systems.

Chapter 9 Conclusion

The work described in this thesis has experimentally examined the viability of using several techniques for high-speed long haul optical communications. Before any such system could be considered for implementation, issues regarding stability, cost and practicality must all be addressed. Using current technologies, a practical insight to what is possible in terms transmission has been considered.

Chapter 2 presents the underlying theory to optical propagation and Chapter 3 describes the experimental details.

In Chapter 4, the optimization of the dispersion map and Raman amplification was considered; this is of importance as there is a continual need for greater bandwidth and propagation distance, to be extracted from single mode fibre. Single mode fibre (SMF) represents the majority of fibre laid in the ground, so any method that exploits this is of interest. Placement and amplification of the dispersion compensators is critical if the optimum transmission distance to be reached, as too much signal power will lead to increased non-linear effects. Distributed amplification is most likely the future of optical amplification, where Raman amplification provides high gain and a relatively flat gain bandwidth, making it suitable to both wavelength division multiplexing (WDM) and optical time division multiplexing (OTDM). In the experiment demonstrated in this thesis the Raman amplification was optimized for the individual dispersion maps, with degradation of the signal arising from double Rayleigh backscattering (DRBS) that leads to multi-path interference (MPI).

The degradation of the signal was monitored by two means to highlight the effects of Multi Path Interference (MPI); these were Optical Signal to Noise Ratio (OSNR) and Q factor measurements. The amplifier spacing used throughout was between 75 to 90km, which are mostly adopted in long-haul communications (such distance is not an ideal choice, but based on economical consideration). The signal in each of the four dispersion maps was monitored with increasing pump power, and type A yielded the best overall

values for OSNR and Q factors. This was corroborated with the bit error ratio (BER) test, which also showed that dispersion map A was the best. This then led to an error free propagation of over 2000km of total fibre at 40Gbit/s in dispersion map A. Optimization of the amplification regime and the dispersion map yielded significant improvements, delivering system performance similar to the theoretically limited one.

The work described in chapter 5, signal propagation in a Raman amplified system with transoceanic amplifier spacing and strong dispersion map has been studied. A direct comparison of transmission performance has been carried out in a regenerated system and an equivalent non-regenerated system.

A 2R regenerator was utilized to extend propagation distance, whilst stabilizing the pulse into a novel DM autosoliton propagation regime at 10, 40 and 80Gbit/s. The use of a non-linear loop mirror (NOLM), as a saturable absorber has virtually eliminated noise build up arising from amplified spontaneous emission (ASE) and dispersive wave radiation as shown in the results obtained. In addition, the NOLM initiates in standard fibre, a DM autosoliton propagation regime even with a large dispersion map strength. The experiments demonstrate that the DM autosoliton is achieved by using the local non-linearity of the NOLM, as NOLMs are not as susceptible to changes in the input parameters, unlike dispersion-managed solitons (DMS).

The DM autosoliton in comparison to a DMS system can be set up within a transmission system designed for linear DM RZ pulses, as the DM autosoliton for the majority of the propagation time spends it in the quasi-linear regime, where it undergoes significant temporal dispersion. The use of the NOLM periodically provides the nonlinearity to the pulse to provide the distinction between the DM autosoliton and linear DM pulses. As the NOLM provides the nonlinearity the system needs to propagate in the DM autosoliton regime, the pulse exiting the NOLM is a soliton, the optical power of which is then attenuated to that of a linear DM pulse this maintains the quasi-linear propagation. This is in comparison to DMS systems where the inputted pulse has a power enhancement to maintain the balance between the path average dispersion and the nonlinearity of the fibre producing

a soliton, and at no point along the fibre span does the pulse resemble that of a quasi-linear DM pulse.

After the initialisation of the DM autosoliton propagation regime, stable propagation where the pulse integrity remains visible was observed over 17,000km at 10Gbit/s, over 10,000km for 40Gbit/s and over 3,500km at 80Gbit/s. A BER test at 10Gbit/s gave an error-free data transmission distance of over 10,000km and at 40Gbit/s a distance of over 5,800km.

Chapter 6 discussed the timing jitter in a Raman amplified system with transoceanic amplifier spacing and strong dispersion map has been studied. A direct comparison of transmission performance has been carried out in a regenerated system and an equivalent non-regenerated system.

Timing jitter is of importance as it is the limiting factor to transmission distance in the optics industry, when loss and dispersion are fully compensated for. Therefore, a better understanding of the timing jitters involved in transmission systems is imperative. The timing jitter in this chapter was measured on a gated autocorrelator which unlike many digital sampling oscilloscopes (DSO), it is unaffected by amplitude jitter.

Optical transmission systems that are amplified with optical amplifiers, will suffer from Gordon-Haus jitter and in the generic system, as described above, this was the limiting factor.

Timing jitter after propagation in the 2R regenerated systems is considerably suppressed by the reduction of ASE to minimal amounts and a much-reduced ISI. The NOLM itself adds timing jitter to the system and this was one of the limiting factors at lower data rates, and at higher rates ISI. The rate of timing jitter accumulation was accessed and as the bit rate increases the rate of timing jitter increase becomes non-linear, which is indicative of non-linear interactions due to ISI.

In the NOLM guided system at 10Gbit/s, where the noise has been intensity filtered and inter symbol interference (ISI) is at a minimum, the limiting factor is a combination of polarization mode dispersion (PMD) and jitter added by the NOLM.

The experiments described in Chapter 7, show that signal propagation in a Raman amplified system with transoceanic amplifier spacing and strong dispersion map has been studied. A direct comparison of transmission performance has been carried out in a regenerated system and an equivalent non-regenerated system yielding a further demonstration of the DM autosoliton regime at 10 and 20Gbit/s. A band pass filter (BPF) was placed after the NOLM and this offered greater stabilization to the DM autosoliton propagation, making it physically limited at 10Gbit/s and giving an error free propagation over 100Mm. This result was also confirmed at 20Gbit/s where an error free distance of 20Mm was achieved.

Finally, in Chapter 8, the dropping of OTDM channels in long haul communications was considered in a 2R regenerator based on a saturable absorber was investigated. 2R regenerators and how they perform in telecommunications are of great interest, especially information on how intensity dependent switches react with any channel non-uniformity when concatenated over long distances.

This experiment uses the same set-up as described previously, using the NOLMs to non-linearly guide the signal. The signal was then monitored on the DSO, and the intra channel amplitude variation was taken before and after the NOLM. Depending on the inter-channel amplitude difference, the optical pulses in different channels experienced either suppression of the amplitude noise, or a noise increase. Appropriate control of the channel uniformity in the OTDM transmitters is necessary in order to support stable long-haul transmission in 2R-regenerated systems.

In conclusion, the use of NOLMs as a concatenated 2R regenerator is valid and initiates the DM autosoliton propagation regime that until now was not observed in optical fibre communications. The use of numerical simulations would have been useful in verifying the work carried out and expanding on the results, by taking all the system parameters and input parameters more insight could have been attained in how and what direction to take the experimental work. With the miniaturization of components, the NOLM will become one of the important devices in optical transmission.

9.1 Further Work

Any future research, could investigate making the NOLM more efficient to enable lower pump powers that initiate switching to be used, this would then enable the observation of propagation at higher data rates.

The optimization of the dispersion map is also of interest, such as longer/shorter maps to enable the best propagation distance to be reached. A 40Gbit/s demultiplexer with an appropriate switching window would enable up to 160Gbit/s transmission to be checked on the 10Gbit/s BERT.

To ascertain whether use of NOLM and a broadband amp if it is possible to regenerate multiple signals from Wavelength Division Multiplexed (WDM) transmission system. Also, if multiple NOLMs are used on a WDM transmission system the possibility to regenerate the signals individually, as S. Boscollo et al have shown theoretically. In both of these cases if the NOLM could be constructed from highly non-linear fibre or photonic crystal fibre this would greatly aid stabilization.

A comparison of the work described in this thesis with numerical simulation could be carried out, this could highlight better ways to improve propagation.

Further studies of the timing jitter and the NOLMs effect on it would be beneficial as would any work to enable the distribution of the jitter to be determined as some theoretical work by Leclerc et al, has indicated the distribution is Gaussian rather than Lorentzian when 2R regenerators are used. The effect on PMD by the NOLM could also provide some useful insight.

REFERENCES

[1] J.M. Senior, 'Optical fibre communications', Prentice Hall, Europe, pp. 12-159 (1992).

[2] G.P. Agrawal, 'Fibre-optic communication systems', John Wiley & Sons Ltd, Canada, pp. 24-74 (1997).

[3] I.S. Grant and W.R. Phillips, 'Electromagnetism', John Wiley & Sons Ltd, UK, pp. 379-383 (1990).

[4] G.P. Agrawal, 'Non-linear fibre optics', Academic Press, UK, pp. 7-12 (1995).

[5] L.J. Greenstein and A.A.M. Saleh, 'Optical equalization to combat the effects of laser chirp and fibre dispersion', *IEEE Journal of lightwave technology*, Vol. 8-5 (1990).

[6] A.M. Vengsarkar and W.A. Reed, 'Dispersion compensating single mode fibres: efficient designs for first and second order compensation', *Opt. Lett.*, Vol. 18-11, pp. 924-926 (1993).

[7] U. Eriksson, P. Blixt, and J.A. Tellefson Jr, 'Design of fibre gratings for total dispersion compensation', *Opt. Lett.*, Vol. 19-14 (1994).

[8] L. F. Mollenauer and J. P. Gordon, 'Birefringence mediated timing jitter in soliton transmission', *Opt. Lett.*, Vol. 19-6 pp. 375-377 (1994).

[9] D. Cotter, 'Optical non-linearity in fibres: A new factor in systems design', *British Telecom Technology Journal*, Vol. 1-2, pp. 17-19 (1983).

[10] D. Cotter, K.I. White, K.J. Blow and N.J. Doran, 'Optical pulse compression using fibres', *IEE Colloquium (Digest)*, n 1983/60, pp. 6. 1-6. 3 (1983).

[11] Y. Li and G. Li, '2R Regeneration and Simultaneous Wavelength Conversion Using a Fibre Parametric Amplifier and a Semiconductor Optical Amplifier', *Conference on Optical Fiber Communication, Technical Digest Series*, Vol. 86, pp. 349-350 (2003).

[12] P.O. Hedekvist, P.A. Andrekson, 'Demonstration of fibre four-wave mixing optical demultiplexing with 19 dB parametric amplification', *Electron. Lett.*, Vol. 32-9, pp. 830-831 (1996).

[13] R.H. Stolen and J.E. Bjorkholm, 'Parametric amplification and frequency conversion in optical fibres', *IEEE Journal of Quantum Electronics*, Vol. 18-7, pp. 1062-1072 (1982).

[14] R.H. Stolen, L.F. Mollenauer and W.J. Tomlinson, 'Observation of pulse restoration at the soliton period in optical fibres', *Opt. Lett.*, Vol 8-3, pp. 186-188 (1983).

[15] Y.R. Shen, 'The principles of non-linear optics', Wiley-Interscience, USA (1984).

[16] J. Wilson and J. Hawkes, 'Optoelectronics an introduction', Prentice Hall, UK, pp. 119-120, (1998).

[17] G.P. Agrawal, 'Non-linear fibre optics', Academic Press, UK (1995).

[18] A. Ghatak and K. Thyagaranajan, 'Introduction to fibre optics', Cambridge University Press, USA, pp. 339-359.

[19] C.G. Someda and G. Stegeman, 'Anisotropic and non-linear waveguides', Elsevier, Netherlands, pp. 159-183 (1992).

[20] G.P. Agrawal, 'Non-linear Fibre Optics', Academic Press, USA, pp. 60-87 (1995).

[21] G.P. Agrawal, 'Fibre-Optic Communication Systems', John Wiley and Sons. Inc., USA, pp. 475-486 (1997).

[22] P.N. Butcher and D. Cotter, 'The elements of non-linear optics', Cambridge University Press, USA, pp. 236-245 (1990).

[23] G.P. Agrawal, 'Non-linear fibre optics', Academic Press, USA, pp. 89-132 (1995).

[24] T. Widdowson, 'Ultra-long haul optical fibre transmission systems', PhD Thesis, Aston University, pp. 18-19 (1995).

[25] A. Hasegawa and F. Tappert, 'Transmission of stationary non-linear optical pulses in dispersive dielectric fibres', *Appl. Phys. Lett.*, Vol. 23, pp. 142 (1973).

[26] C.F. Mollenauer, R.H. Stolen, and J.P. Gordon, 'Experimental observation of picosecond pulse narrowing and solitons in optical fibres', *Phys. Rev. Lett.*, Vol. 45, pp. 1095 (1980).

[27] J.R. Taylor, 'Optical Solitons – Theory and Experiment', Cambridge Studies In Modern Optics N° 10, Cambridge University Press, UK, pp. 30-60 (1992).

[28] G.P. Agrawal, 'Non-linear fibre optics', Academic Press, USA, pp. 133-192 (1995).

[29] C.S. Gardner, J.M. Green, M.D. Kruskal, and R.M. Miura, 'Method for Solving the Korteweg-deVries Equation', *Phys. Rev. Lett.*, Vol. 19-6, pp. 1065-1097 (1967).

[30] V.E. Zakharov, A.B. Shabat, 'Exact theory of two-dimensional self-focusing and one-dimensional self-modulation of waves in nonlinear media', *Sov. Phys.*, JETP 34-1, pp. 62-69 (1972).

[31] M. Jain and N. Tzoar, 'Non-linear pulse propagation in optical fibre', *Opt. Lett.*, Vol. 3-5, pp. 202-204 (1978).

[32] T. Widdowson, 'Ultra-long haul optical fibre transmission systems', PhD Thesis, Aston University, pp. 18-19 (1995).

[33] A. Hasegawa and Y. Kodama, 'Amplification and reshaping of optical solitons in glass fibre – 1', *Opt. Lett.*, Vol. 7-6, pp.285-287 (1982).

[34] L. F. Mollenauer, J. P. Gordon, and M. N. Islam, 'Soliton propagation in long fibres with periodically compensated loss', *IEEE J Quant. Electron.*, Vol. 22-1, pp. 157-173 (1986).

[35] R. J. Mears, L. Reekie, I. M. Jauncey, and D. N. Payne, 'Low-noise erbium-doped fibre amplifier operating at 1.54 μm', *Electron. Lett.*, Vol. 23-19, pp. 1026-1028 (1987).

[36] M. Nakazawa, Y. Kimura, and K. Suzuki, 'Soliton amplification and transmission with Er/sup 3+/-doped fibre repeater pumped by GaInAsP diode', *Electron. Lett.*, Vol. 25-3, pp. 199-200 (1989).

[37] Y.W.A. Lee, 'Advanced optical techniques for high capacity transmission', PhD Thesis, Aston University, pp. 37-38 (2003).

[38] K.J. Blow and N.J. Doran, 'Average soliton dynamics and the operation of soliton systems with lumped amplifiers', *IEEE Photon. Tech. Lett.*, Vol. 3-4, pp. 369-371 (1991).

[39] A. Hasegawa, 'Numerical study of optical soliton transmission amplified periodically by the stimulated Raman process', *Appl. Opt.*, Vol. 23-19, pp. 3302-3309 (1984).

[40] D.M. Patrick and A.D. Ellis, '10Ghz pulse train derived from a CW DFB laser using cross phase modulation in an optical fibre', *Electron. Lett.*, Vol. 29-15, pp. 1391-1392 (1993).

[41] D.M. Patrick and A.D. Ellis, 'Demultiplexing using cross phase modulation-induced spectral shifts and Kerr polarization rotation', *Electron. Lett.*, Vol. 29-2, pp. 227-228 (1993).

[42] T. Widdowson, D.J. Malyon, A.D. Ellis, K. Smith and K.J. Blow, 'Soliton shepherding: all active transmission control over global distances', *Electron. Lett.*, Vol. 30-12, pp. 990-991 (1994).

[43] P. N. Butcher and D. Cotter, 'Elements of non-linear optics', Cambridge University Press, UK, pp. 216 (1990).

[44] M. Jinno and T. Matsumoto, 'Non-linear sagnac interferometer switch and its applications', *IEEE J Quantum Electron.*, Vol. 28-4. pp. 875-882 (1992).

[45] R.W. Hellwarth, 'Theory of phase-conjugation by four-wave mixing in a waveguide', *IEEE J Quantum Electron.*, Vol. 15-2, pp. 101-109 (1979).

[46] G.P. Agrawal, 'Fibre-optic communication systems', Wiley-Interscience, Canada, pp. 63-64 (1997).

[47] S. Watanabe and T. Chikama, 'Highly efficient conversion and parametric gain of non-degenerate forward four-wave mixing in a single mode fibre', *Electron. Lett.*, Vol. 30-2, pp. 163-164 (1994).

[48] Y. Li, C. Kim; G. Li; K. Croussore, 'All-optical 2R regeneration using data-pumped fibre parametric amplification', *Electron. Lett.*, Vol. 39-17, pp. 1263-1264 (2003).

[49] R.G. Waarts and R.P. Braun, 'System limitations due to four-wave mixing in single mode optical fibres', *Electronics Letters*, Vol. 22-16, pp. 873-875 (1986).

[50] G.P. Agrawal, 'Non-linear fibre optics', Academic Press, 2nd Ed., 1989, pp. 370-399.

[51] E.J. Woodbury, Ng W K *Proc. IRE.*, Vol. 50, pp. 2347 (1962).

[52] N. Bloembergen, 'The stimulated Raman effect', *Am. J. Phys.*, Vol. 35, pp. 989-1023 (1967).

[53] G.P. Agrawal, 'Non-linear fibre optics', Academic Press, 2nd Ed., 1989, pp. 316-369.

[54] R.H. Stolen, E.P. Ippen, and A.R. Tynes, 'Raman Oscillation in Glass Optical Waveguide', *Appl. Phys. Lett.*, Vol. 20-2, pp. 62-64 (1972).

[55] R.G. Smith, 'Optical power handling capacity of low loss optical fibres as determined by stimulated Raman and Brillouin scattering', *Appl. Opt.*, Vol. 11-11, pp. 2489-2494 (1972).

[56] R. Shuker and R.W. Gammon, 'Raman-Scattering Selection-Rule Breaking and the Density of States in Amorphous Materials', *Phys. Rev. Lett.*, Vol. 25-4, pp. 222-225 (1970).

[57] Y. Aoki, 'Properties of fibre raman amplifiers and their applicability to digital optical communication systems', *J of Lightwave Tech.*, Vol. 6-7, pp. 1225-1239 (1988).

[58] J.P. Pocholle, J. Rafty, M. Papuchon, and E. Desurvire, 'Raman and four photon mixing amplification in single mode fibres', *Optical Engineering*, Vol. 24-4, pp. 600-608 (1985).

[59] L.C. Blank, E.G. Bryant, A. Lord, J.M. Boggis, and W.A. Stallard, '150 km optical fibre transmission network experiment with 2 Gbit/s throughput', Electron. Lett., Vol. 23-19, pp. 977-978 (1987).

[60] L.F. Mollenauer, S.G. Evangelides, and J.P. Gordon, 'Wavelength division multiplexing with solitons in ultra-long distance transmission using lumped amplifiers', Journ. of Lightwave Tech., Vol. 9-3, pp. 362-367 (1991).

[61] Y. Yamamoto, 'Coherent optical fibre transmission systems', IEEE Journal of Quantum Electronics, Vol. 17-6, pp. 919-935 (1981).

[62] A.R. Chraplyvy, A.H. Gnauck, R.W. Tkach, and R.M. Derosier, '8x10GB/s transmission through 280km of dispersion-managed fibre', IEEE Photon. Tech. Lett., Vol. 5-10, pp.1233-1235 (1993).

[63] A. Yariv, 'Signal to noise considerations in fibre links with periodic or distributed amplification', Opt. Lett., Vol. 15-19, pp. 1064-1066 (1990).

[64] C.R. Giles, 'Propagation of signal and noise in concatenated erbium-doped fibre optical amplifiers', Jour. Lightwave Tech., Vol. 9-2, pp. 147-154 (1991).

[65] G.P. Agrawal, 'Fibre-Optic Communication Systems', John Wiley and Sons. Inc., USA, pp. 475-486 (1997).

[66] G.P. Agrawal, 'Non-linear fibre optics', Academic Press, USA, pp. 316-362 (1995).

[67] Y.Aoki, 'Properties of fibre raman amplifiers and their applicability to digital optical communication systems', J Lightwave Tech., Vol. 6, pp. 1225-1239 (1988).

[68] R. Hainberger, J. Kumasako, K. Nakamura, T. Terahara, and H. Onaka, 'Optimum span configuration of Raman amplified dispersion managed fibres', OFC 2001, Anaheim, CA, USA, paper MI5 (2001).

[69] T. Okoshi, 'Recent advances in coherent optical fibre communication systems' Jour. of Lightwave Tech., Vol. 5-1, pp. 44-52 (1987).

[70] R.A. Linke, B.L. Kasper, N.A. Olsson, R.C. Alferness, L.L. Buhl, and A.R. McCormick, 'Coherent lightwave transmission over 150 km fiber lengths at 400 Mb/s and 1 Gb/s data rates using DPSK modulation', IOOC-ECOC '85., Vol. 3, pp. 35-38 (1985).

[71] M.J. Adams, A.G. Steventon, W.J. Delvin, and I.D. Henning, 'Semiconductor lasers for long wavelength optical fibre', Peter Peregrinus, IEE Materials & Devices 4, UK (1987).

[72] G.M. Carter, J.M. Jacob, C.R. Menyuk, E.A. Golovchenko, and A.N. Pilipetskii, 'Timing-jitter reduction for a dispersion-managed soliton system: experimental evidence', Opt. Lett., Vol. 22-8, pp. 513-15 (1997).

[73] G.M. Carter, J.M. Jacob, E.A. Golovchenko, A.N. Pilipetskii, and C.R. Menyuk, 'Experimental measure of the timing jitter in dispersion-managed soliton transmission at 10 Gbit/s up to 20,000 km', Conference on Lasers and Electro-Optics Europe - Technical Digest, Vol. 11, pp. 347-348 (1997).

[74] G.P. Agrawal, 'Fibre-Optic Communication Systems', John Wiley and Sons. Inc., USA, pp. 475-486 (1997).

[75] J.H.B. Nijhof, N.J. Doran, W. Forysiak and A.Berntson, 'Energy enhancement of dispersion managed solitons and WDM', Electron. Lett., Vol. 34-5, pp.481-482 (1998).

[76] T. Hirooka and M.J. Ablowitz, 'Analysis of timing jitter and amplitude jitter due to intra-channel dispersion-managed pulse interactions', IEEE Photon. Tech. Lett., Vol. 14-5, pp. 633-635 (2002).

[77] L.J. Richardson, V.K. Mezentsev and S.K. Turitsyn, 'Limitations of 40Gbit/s based dispersion managed WDM transmission: solitons versus quasi-linear propagation regime', OFC 2001. Optical Fibre Communication Conference and Exhibit. Technical Digest Postconference Edition, Vol.1, pt. 1, pp. MF5/1-3 (2001).

[78] H.N. Ereifej, R. Holzlöhner, G.M. Carter and C.R. Menyuk, 'Intersymbol interference and timing jitter measurements in a 40Gbit/s long-haul dispersion-managed soliton system', IEEE Photon. Tech. Lett., Vol: 14-3, pp. 343-345 (2002).

[79] J.P. Gordon and H.A. Haus, 'Random walk of coherently amplified solitons in optical fiber transmission', Opt. Lett., Vol. 11-10, pp. 665-667 (1986).

[80] E. Poutrina and G.P. Agrawal, 'Effect of distributed Raman amplification on timing jitter in dispersion-managed lightwave systems', IEEE Photon. Tech. Lett., Vol. 14-1, pp. 39-40 (2002).

[81] L.F. Mollenauer, J.P. Gordon, and S.G. Evangelides, 'The sliding-frequency guiding filter: an improved form of soliton jitter control', Opt. Lett., Vol. 17-22, pp. 1575-1577 (1992).

[82] L.F. Mollenauer, P.V. Mamyshev, and M.J. Neubelt, 'Measurement of timing jitter in filter-guided soliton transmission at 10Gbits/s and achievement of 375Gbits/sMm, error-free, at 12.5 and 15 Gbits/s', Opt. Lett., Vol. 19-10, pp. 704-706 (1994).

[83] N.J. Smith and N.J. Doran, 'Pico-second soliton transmission using concatenated non-linear optical loop-mirror intensity filters', Jour. Opt. Soc. Am. B., Vol. 12-6, pp. 1117-1125 (1995).

[84] T. Georges and B. Charbonnier, 'Pre-chirping and dispersion compensation for long-haul 20Gbit/s soliton transmission at 1.55-mum on non-dispersion-shifted fibres', Conference on Optical Fibre Communications. Technical Digest. Postconference Edition. 1997 OSA Technical Digest Series., Vol.6, pp. 144-145 (1997).

[85] W. Forysiak, K.J. Blow, and N.J. Doran, 'Reduction of Gordon-Haus jitter by post-transmission dispersion compensation', Electron. Lett., Vol. 29-13, p 1225-1226 (1993).

[86] B.J. Eggleton, T.N. Nielsen, J.A. Rogers, P.S. Westbrook, T.A. Strasser, P.B. Hansen, and K.F. Dreyer, 'Dispersion compensation in 20Gbit/s dynamic nonlinear lightwave systems using electrically tunable chirped fibre grating', Electron. Lett., Vol. 35-10, pp. 832-833 (1999).

[87] N.S. Bergano, J. Aspell, C.R. Davidson, P.R. Trischitta, B.M. Nyman, and F.W. Kerfoot, 'Bit error rate measurements of 14,000 km, 5Gbit/s fibre amplifier transmission system using recirculating loop', Electron. Lett., Vol. 27-21, pp.1889-1890 (1991).

[88] N.S. Bergano and C.R. Davidson, 'Circulating loop transmission experiments for the study of long-haul transmission systems using erbium doped fibre amplifiers', IEEE J. Lightwave Tech., Vol. 13-5, pp. 879-888 (1995).

[89] D. Marcuse, 'Calculation of bit-error probability for a lightwave system with optical amplifiers and post-detection Gaussian noise', IEEE J. Lightwave Tech., Vol. 4-4, pp. 505-513 (1991).

[90] L.F. Mollenauer, M.J. Neubelt, S.G. Evangelides, J.P. Gordon, J.R. Simpson and L.G. Cohen, 'Experimental study of soliton transmission over more than 10,000km in dispersion shifted fibre', Opt. Lett., Vol. 15-21, pp. 1203 –1205 (1990).

[91] N.S. Bergano, J. Aspell, C.R. Davidson, P.R. Trischitta, B.M. Nyman and F.W. Kerfoot, 'Bit-error rate measurements of 14,000km 5Gbit/s fibre-amplifier transmission system using circulating loop', Electron. Lett., Vol. 27-21, pp.1889-1890 (1991).

[92] N.S. Bergano and C.R. Davidson, 'Circulating loop transmission experiments for the study of long-haul transmission systems using erbium-doped fibre amplifiers', J. Lightwave Tech., Vol. 13-5, pp. 879-888 (1995).

[93] I.S. Penketh, P. Harper, S.B. Alleston, A.M. Niculae, I. Bennion and N.J. Doran, '10Gbit/s dispersion-managed soliton transmission over 16,500km in standard fibre by reduction of soliton interactions', Opt. Lett., Vol. 24-12, pp.802-804 (1999).

[94] M. Nakazawa, E. Yamada, H. Kubota, and K. Suzuki, '10Gbit/s soliton transmission over one million kilometers', Electron. Lett., Vol. 27, pp. 1270-1272 (1991).

[95] J.P. Curtis and J.E. Carroll, 'Autocorrelation systems for the measurement of picosecond pulses from injection lasers', Int. J. Electron., Vol: 60-1, pp. 87-111 (1986).

[96] J.A. Armstrong, 'Measurement of picosecond laser pulse widths', Appl. Phys. Lett., Vol: 10, pp. 16-18 (1967).

[97] http://www.physics.gatech.edu/gcuo/Tutorial/Autocorrelation.html

[98] E.P. Ippen and C.V. Shank, 'Techniques for measurment. Ultrashort light pulses', Berlin: Springer-Verlag, pp.83-122 (1977).

[99] J. Dörring, G.B. Tudury, A. Lenihan, G.M. Carter andY.J. Chen, 'All-optical timing jitter measurements on 40Gbit/s pseudorandom RZ data after long-haul transmission in dispersion-managed soliton system', Electron. Lett., Vol. 38-14, pp. 727-728 (2002).

[100] A. Gray, Z. Huang, Y.W.A. Lee, I. Khrushchev, I. Bennion, 'Experimental observation of autosoliton propagation in a dispersion managed system guided by non-linear optical loop mirrors', Opt. Lett., Vol. 29, pp. 926-928 (2004).

[101] A. Gray, Z. Huang, I. Khrushchev, I. Bennion, 'Autosoliton propagation at 80Gbit/s using concatenated non-linear loop switches in standard fibre', Electron. Lett., Vol. 40, pp. 498-500 (2004).

[102] A. Gray, Z. Huang, I. Khrushchev, I. Bennion, 'Evolution of Timing Jitter in Non-linearly Guided, Dispersion Managed Transmission Systems', We4.P.117, ECOC, Stockholm, Sweden 2004.

[103] D. S. Govan, W. Forysiak and N. J. Doran: 'Long-distance 40Gbit/s soliton transmission over standard fibre by use of dispersion management', Opt. Lett., Vol. 23-19, pp.1523-1525 (1998)

[104] P. Harper, S. B. Alleston, I. Bennion, and N. J. Doran, '40 Gbit/s dispersion managed soliton transmission over 1160 km in standard fibre with 75 km span length', Electron. Lett., Vol. 35-24, pp. 2128-2130 (1999).

[105] T.Schafer, E.W. Laedke, M. Gunkel, C. Karle, A. Posth, K.H. Spatschek, and S.K. Turitsyn, 'Optimization of dispersion managed optical fibre lines', J Lightwave tech., Vol. 20, pp. 946-952 (2002).

[106] A.Sahara, T. Inui, T. Komukai, H. Kubota, and M. Nakazawa, '40Gb/s RZ transmission over a transoceanic distance in a dispersion managed standard fibre using a modified inline synchronous modulation method', J Lightwave Tech., Vol. 18, pp. 1364-1373 (2000).

[107] I. Morita, K. Tanaka, N. Edagawa and M. Suzuki: '40Gbit/s single-channel transmission over standard single mode fibre using distributed Raman amplification', Electron. Lett., Vol. 36-25, pp. 2084-2085 (2000).

[108] Y. Zhu, W. S. Lee, C. Scahill, C. Fludger, D. Watley, M. Jones, J. Homan, B. Shaw, A. Hadjifotiou, '1.28 Tbit/s (32x40Gbit/s) transmission over 1000 km NDSF employing distributed Raman amplification and active gain flattening', Electron. Lett., Vol. 37-1, pp. 43-45 (2001).

[109] R. Hainberger, J. Kumasako, K. Nakamura, T. Terahara, and H. Onaka, 'Optimum span configuration of Raman amplified dispersion managed fibres', OFC 2001, Anaheim, CA, USA, paper MI5 (2001).

[110] M.Vasilyev, B. Szalabofka, S. Tsuda, J.M. Grochocinski, and A.F. Evans, 'Reduction of Raman MPI and noise figure in dispersion managed fibre', Electron Lett., Vol. 38-6, pp. (2002).

[111] Y. Zhu, I. Hardcastle, W.S. Lee, C.R.S. Fludger, A. Hadjifotiou, C. Li, D. Qiao, H. Sun, K.T. Wu, J. McNicol, 'Experimental comparison of Raman-amplified dispersion-managed fibre types using 16×40 Gbit/s transmission over 500 km', Electron. Lett., Vol. 38-16, pp. 895-896 (2002).

[112] G.P. Agrawal, 'Non-linear fibre optics', Academic Press, USA, pp. 316-362 (1995).

[113] G.P. Agrawal, 'Fibre-Optic Communication Systems', John Wiley and Sons. Inc., USA, pp. 475-486 (1997).

[114] M.Vasilyev, B. Szalabofka, S. Tsuda, J.M. Grochocinski, and A.F. Evans, 'Reduction of Raman MPI and noise figure in dispersion managed fibre', Electron Lett., Vol. 38-6, pp. (2002).

[115] Y.Zhu, C.R.S. Fludger, W.S. Lee, P. Lobb, T.Schilhabel, and A. Hadjifotiou, 'Experimental comparison of all-Raman and Raman/EDFA hybrid amplifications using 40 Gb/s based transmissions over 400km TW-RS fibre', Electron Lett., Vol. 38-16, pp. (2002).

[116] M.Nakazawa, 'Rayleigh backscattering theory for single mode optical fibres', J Opt. Soc. Am. B., Vol. 73-9, pp. (1983).

[117] C.R.S.Fludger, Y. Zhu, V. Handerek, and R.J. Mears, 'Impact of MPI and modulation format on transmission systems employing distributed Raman amplification', Electron Lett., Vol. 37-15, pp. (2001).

[118] Y.Aoki, 'Properties of fibre raman amplifiers and their applicability to digital optical communication systems', J Lightwave Tech., Vol. 6, pp. 1225-1239 (1988).

[119] Z. Huang, A. Gray, Y. W. A. Lee, I. Y. Khrushchev, and I. Bennion, 'All-Raman amplified transmission at 40Gbit/s in standard single mode fibre', in Proceedings of the Conference on Lasers and Electro-Optics, CLEO/Europe 2003, Munich, Germany, paper CJ4-4-TUE.

[120] D. Rouvillain, P. Brindel, F. Seguineau, L. Pierre, O. Leclerc, H. Choumane, G. Aubin, and J.L. Oudar, 'Optical 2R regenerator based on passive saturable absorber for 40 Gbit/s WDM long-haul transmissions', Electron. Lett., Vol. 38-19, pp. 1113-1114 (2002).

[121] N. J. Smith and N. J. Doran, 'Picosecond soliton transmission using concatenated nonlinear optical loop-mirror intensity filters', J. Opt. Soc. Am. B., Vol. 12-6, pp. 1117-1125 (1995).

[122] S. Boscolo, J.H.B. Nijhof, and S.K. Turitsyn, 'Autosoliton transmission in dispersion-managed systems guided by in-line nonlinear optical loop mirrors', Opt. Lett., Vol. 25-17, pp. 1240-1242 (2000).

[123] S. Boscolo, S. K. Turitsyn, and K. J. Blow, 'All-optical passive regeneration of 40 Gbit/s soliton data stream using dispersion management and in-line NOLMs', Electron. Lett., Vol. 37-2, pp. 112-113 (2001).

[124] V. S. Filho, F. Kh. Abdullaev, A. Gammal, L. Tomio, 'Autosolitons in trapped Bose-Einstein condensates with two- and three-body inelastic processes', Phys. Rev. A., Vol. 63-5, pp. 053603/1 (2001).

[125] N.J. Doran and D. Wood, 'Non-linear optical loop mirror', Opt. Lett., Vol. 13-1, pp. 56-58 (1988).

[126] K. J. Blow, N. J. Doran, and B. K. Nayar, 'Experimental demonstration of optical soliton switching in anall-fiber nonlinear Sagnac interferometer', Opt. Lett., Vol. 14-14, pp. 754-756 (1989).

[127] M. N. Islam, E. R. Sunderman, R. H. Stolen, W. Pleibel, and J. R. Simpson, 'Soliton switching in a fiber nonlinear loop mirror', Opt. Lett., Vol. 14-15, pp. 811-813 (1989).

[128] K. Smith, N. J. Doran, and P. G. J. Wigley, 'Pulse shaping, compression, and pedestal suppression employing a non-linear optical loop mirror', Opt. Lett., Vol. 15-22, pp. 1294-1296 (1990).

[129] M. E. Fermann, F. Haberl, M. Hofer, and H. Hochreiter, 'Nonlinear amplifying loop mirror', Opt. Lett., Vol. 15-13, pp. 752-754 (1990).

[130] W. S. Wong, S. Namiki, M. Margalit, H. A. Haus, and E. P. Ippen, 'Self-switching of optical pulses in dispersion-imbalanced non-linear loop mirrors', Opt. Lett., Vol. 22-15, pp. 1150-1152 (1997).

[131] D. A. Pattison, W. Forysiak, P. N. Kean, I. Bennion, and N. J. Doran, 'Soliton switching using cascaded non-linear optical loop mirrors', Opt. Lett., Vol. 20-1, pp.19-21 (1995).

[132] N. Finlayson, B. K. Nayar, and N. J. Doran, 'Switch inversion and polarization sensitivity of the nonlinear-optical loop mirror', Opt. Lett., Vol. 17-2, pp. 112-114 (1992).

[133] J. P. Gordon, 'Theory of the soliton self-frequency shift', Opt. Lett., Vol. 11-10, pp. 662-664 (1986).

[134] F. M. Mitschke, and L. F. Mollenauer, 'Discovery of the soliton self-frequency shift', Opt. Lett., Vol. 11-10, pp. 659-661 (1986).

[135] K. J. Blow, N. J. Doran, and D. Wood, 'Suppression of the soliton self-frequency shift by bandwidth-limited amplification', J. Opt. Soc. Am. B, Vol. 5-6, pp. 1301-1304 (1988).

[136] V. S. Grigoryan, 'Autosoliton in a fibre with distributed saturable amplifiers', Opt. Lett., Vol. 21-23, pp. 1882-1884 (1996).

[137] Z. Huang, A. Gray, Y.W.A. Lee, I. Khrushchev, I. Bennion, '40Gb/s Transmission over 4000km of standard fibre using in-line nonlinear optical loop mirrors', ECOC 2003, paper Mo4.6.3.

[138] L. F. Mollenauer, E. Lichtman, M. J. Neubelt, and G. T. Harvey, 'Demonstration, using sliding-frequency guiding filters, of error-free soliton transmission over more than 20 Mm at 10 Gbit/s, single channel, and over more than 13 Mm at 20 Gbit/s in a two-channel WDM', Electron. Lett., Vol. 29-10, pp. 910-911 (1993).

[139] S. Penketh, P. Harper, S. B. Alleston, A. M. Niculae, I. Bennion, and N. J. Doran, '10Gbit/s dispersion-managed soliton transmission over 16,500 km in standard fiber by reduction of soliton interactions', Opt. Lett., Vol. 24-12, pp. 802-804 (1999).

[140] H. N. Ereifej, V. Grigoryan, and G. M. Carter, '40 Gbit/s long-haul transmission in dispersion-managed soliton system using Raman amplification', Electron. Lett., Vol. 37-25, pp. 1538-1539 (2001).

[141] J. H. B. Nijhof, N.J. Doran, W. Forysiak, and A. Berntson, 'Energy enhancement of dispersion-managed solitons and WDM', Electron. Lett., Vol. 34-5, pp. 481-482 (1998).

[142] E. Poutrina and G. P. Agrawal, 'Design rules for dispersion-managed soliton systems', Opt. Comm., Vol. 206-1(3), pp. 193-200 (2002).

[143] J. Dörring, G. B. Tudury, A. Lenihan, G. M. Carter, and Y. J. Chen, 'All-optical timing jitter measurement on 40Gbit/s pseudorandom RZ data after long-haul transmission in dispersion-managed soliton system', Electron. Lett., Vol. 38, pp. 727 (2002).

[144] J. Inoue, H. Sotobayashi, W. Chujo and H. Kawaguchi, '80Gbit/s OTDM signal transmission over 208km standard fibre using midspan optical phase conjugation based on four wave mixing in semiconductor amplifiers', Electron. Lett., Vol. 38, pp.819 (2002).

[145] Y.Su, G.Raybon, R.J.Essiambre, L.Wickham, '80Gbit/s single-channel transmission over 1200 km of nonzero dispersion shifted fibre', Electron. Lett. Vol.38, (2002).

[146] M. Nakazawa, K. Suzuki and H. Kubota, 'Single channel 80Gbit/s soliton transmission over 10000km using in-line synchronous modulation', Electron. Lett., Vol. 35, pp.162, (1999).

[147] Z. Huang, A. Gray, Y.W.A. Lee, I. Khrushchev, I. Bennion, '40Gb/s Transmission over 4000km of standard fibre using in-line nonlinear optical loop mirrors', ECOC 2003, paper Mo4.6.3.

[148] S. Boscolo, J.H.B. Nijhof, and S.K. Turitsyn, 'Autosoliton transmission in dispersion-managed systems guided by in-line nonlinear optical loop mirrors', Opt. Lett., Vol. 25, pp.1240 (2000).

[149] J. Dörring, G. B. Tudury, A. Lenihan, G. M. Carter, and Y. J. Chen, 'All-optical timing jitter measurement on 40Gbit/s pseudorandom RZ data after long-haul transmission in dispersion-managed soliton system', Electron. Lett., 38, pp.727-728 (2002).

[150] G. M. Carter, J. M. Jacob, C. R. Menyuk, E. A. Golovchenko, and A. N. Pilipetskii, 'Timing jitter reduction for a dispersion-managed soliton system: experimental evidence', Opt. Lett., Vol. 22-8, pp. 513-515 (1997).

[151] L. F. Mollenauer, M. J. Neubelt, S. G. Evangelides, J. P. Gordon, J. R. Simpson, and L. G. Cohen, 'Experimental study of soliton transmission over more than 10,000km in dispersion shifted fibre', Opt. Lett., Vol. 15-21, pp. 1203-1205 (1990).

[152] L. F. Mollenauer, P. V. Mamyshev, and M. J. Neubelt, 'Measurment of timing jitter in filter-guided soliton transmission at 10Gbit/s and achievement of 375Gbit/sMm, error free, at 12.5 and 15Gbit/s', Opt. Lett., Vol. 19-10, pp. 704-706 (1994).

[153] N. J. Smith, W. Forysiak, and N. J. Doran, 'Reduced Gordon-Haus jitter due to enhanced power solitons in strongly dispersion managed systems', Electron. Lett., Vol. 32-22, pp. 2085-2086 (1996).

[154] E. Poutrina and G. P. Agrawal, 'Effect of distributed Raman amplification on timing jitter in dispersion-managed lightwave systems', IEEE Photon. Tech. Lett., Vol. 14-1, pp. 39-40 (2002).

[155] E. Poutrina and G. P. Agrawal, 'Timing jitter in dispersion-managed soliton systems with distributed, lumped, and hybrid amplification', J. Lightwave Tech., Vol. 20-5, pp. 790-797 (2002).

[156] S. Kumar and F. Lederer, 'Gordon-Haus effect in dispersion-managed soliton systems', Opt. Lett., Vol. 22-24, pp. 1870-1872 (1997).

[157] W. Forysiak, K. J. Blow, and N. J. Doran, 'Reduction of Gordon-Haus jitter by post-transmission dispersion compensation', Electron. Lett., Vol. 29-13, pp. 1225-1226 (1993).

[158] A. Mecozzi, J. D. Moores, H. A. Haus, and Y. Lai, 'Soliton transmission control', Opt. Lett., Vol. 16-23, pp. 1841-1843 (1991).

[159] L. F. Mollenauer, J. P. Gordon, and S. G. Evangelides, 'The sliding-frequency guiding filter: an improved form of soliton jitter control', Opt. Lett., Vol. 17-22, pp. 1575-1577 (1992).

[160] A. Mecozzi, M. Midrio, and M. Romagnoli, 'Timing jitter in soliton transmission with sliding filters', Opt. Lett., Vol. 21-6, pp. 402-404 (1996).

[161] T. Yu, E. A. Golovchenko, A. N. Pilipetskii, and C. R. Menyuk, 'Dispersion-managed soliton interactions in optical fibres', Opt. Lett., Vol. 22-11, pp. 793-795 (1997).

[162] J. Martensson, A. Berntson, M. Westlund, A. Danielsson, P. Johannisson, D. Anderson, and M. Lisak, 'Timing jitter owing to intrachannel pulse interactions in dispersion-managed transmission systems', Opt. Lett., Vol. 26-2, pp. 55-57 (2001).

[163] H. N. Ereifej, R. Holzlöhner, G. M. Carter, and C. R. Menyuk, 'Intersymbol interference and timing jitter measurements in a 40Gb/s long-haul dispersion managed soliton system', IEEE Photon. Tech. Lett., Vol. 14, pp. 343-345 (2002).

[164] E. M. Dianov, A. V. Luchnikov, A. N. Pilipetskii, and A. N. Starodumov, 'Electrostriction mechanism of soliton interaction in optical fibers', Opt. Lett., Vol. 15, pp. 314-316 (1990).

[165] L. F. Mollenauer, and J. P. Gordon, 'Birefringence-mediated jitter in soliton transmission', Opt. Lett., Vol. 19, pp. 375-377 (1994).

[166] J. Dörring, G. B. Tudury, A. Lenihan, G. M. Carter, and Y. J. Chen, 'All-optical timing jitter measurements on 40Gbit/s pseudorandom RZ data after long-haul transmission in dispersion managed soliton system', Electron. Lett., Vol. 38, pp. 727-729 (2002).

[167] J. P. Gordon and H. A. Haus, 'Random walk of coherently amplified solitons in optical fiber transmission', Opt. Lett., Vol. 11, pp. 665-668 (1986).

[168] L. F. Mollenauer, E. Lichtman, M. J. Neubelt, and G. T. Harvey, 'Demonstration, using sliding-frequency guiding filters, of error-free soliton transmission over more than 20Mm at 10Gbit/s single channel, and over more than 13Mm at 20Gbit/s in a two-channel WDM', Electron. Lett., Vol. 29, pp. 910-911 (1993).

[169] M. Nakazawa, E. Yamada, H. Kubota, and K. Suzuki, '10Gbit/s soliton transmission over one million kilometers', Electron. Lett., Vol. 27, pp. 1270-1272 (1991).

[170] A. Gray, Z. Huang, Y. W. A. Lee, I. Y. Khrushchev, and I. Bennion, 'Experimental observation of autosoliton propagation in a dispersion-managed system guided by nonlinear optical loop mirrors', Opt Lett., Vol. 29, pp. 926-928 (2004).

[171] Y. Kodama, and A. Hasagawa, 'Generation of asymptotically stable optical solitons and suppression of the Gordon-Haus effect', Opt. Lett., Vol. 17, pp. 31-33 (1992).

[172] S. Boscolo, S. K. Turitsyn, K. J. Blow, and J. H. B. Nijhof, 'Passive regeneration in 40Gbit/s based WDM dispersion-managed RZ transmission systems by in-line NOLMs', Opt. Fibre Technol., Vol. 8, pp. 313-318 (2002).

[173] F.X. Kartner, D. J. Dougherty, H. A. Haus, and E. P. Ippen, 'Raman noise and soliton squeezing', J. Opt. Soc. Am. B, Vol. 17-7, pp. 1267-1276 (1994).

[174] D. Levandovsky, M. Vasilyev, and P. Kumar, 'Soliton Sqeezing in a highly transmissive non-linear optical loop mirror', Opt. Lett., Vol. 24-2, pp. 89-91 (1999).

[175] D. Krylov and K. Bergman, 'Amplitude-squeezed solitons from an asymmetric fiber interferometer', Opt. Lett., Vol. 23-17, pp. 1390-1392 (1998).

[176] I. S. Penketh, P. Harper, S. B. Alleston, I. Bennion, and N. J. Doran, '10Gbit/s dispersion managed soliton transmission over 16,500km in standard fiber by reduction of soliton interactions', Opt. Lett., Vol. 24, pp. 802-804, Jun. 1999.

[177] J. M. Jacob, and G. M. Carter, 'Error-Free Transmission of Dispersion-Managed Solitons at 10Gbit/s over 24,500 km without Frequency Sliding', Electron. Lett., Vol. 33, pp. 1128-1129, Jan. 1997.

[178] M. Matsumoto, H. Ikeda, and A. Hasegawa, 'Suppression of noise accumulation in bandwidth-limited soliton transmission by means of non-linear loop mirrors', Opt. Lett., Vol. 19, pp.183-185, Feb. 1994.

[179] D. Atkinson, W. H. Loh, V.V. Afanasjev, A. B. Grudinin, A. J. Seeds, and D. N. Payne, 'Increased amplifier spacing in a soliton system with quantum-well saturable absorber and spectral filtering', Opt. Lett., Vol. 19, pp. 1514-1516, Oct. 1994.

[180] M. Nakazawa, E. Yamada, H. Kubota, and K. Suzuki, '10Gbit/s soliton data transmission over one million kilometres', Electron. Lett., Vol. 27, pp. 1270-1272, Jul. 1991.

[181] M. Pantouvaki, M. J. Fice, R. Feced, E. P. Burr, R. Gwilliam, A. B. Krysa, J. S. Roberts, and A. J. Seeds, '10Gb/s All-Optical 2R Regeneration Using an MQW Fabry–Pérot Saturable Absorber and a Nonlinear Fiber', IEEE Photon. Technol. Lett., Vol. 16, pp. 617-619, Feb. 2004

[182] N. J. Doran, and D. Wood, 'Nonlinear optical loop mirror', Opt. Lett., Vol. 13, pp. 56-58, Jan. 1988.

[183] N. J. Smith, and N. J. Doran, 'Picosecond soliton transmission using concatenated nonlinear optical loop-mirror intensity filters', J. Opt. Soc. Am. B, Vol. 12, pp. 1117-1125, Jun. 1995.

[184] T. Yamamoto, E. Yoshida, and M. Nakazawa, 'Ultrafast nonlinear optical loop mirror for demultiplexing 640 Gbit/s TDM signals', Electron. Lett., Vol. 34, pp. 1013-1014, May 1998.

[185] C. M. Weinert, A. Sizmann, R. Ludwig, C. Schubert, U. Feiste, and H. G. Weber, 'Nonlinear optical intensity filters: experiment and design rules', ECOC 2001, Amsterdam, Holland, 2001, Paper We. L. 1. 4

[186] N. Chi, B. Carlsson, and P. Jeppesen, '2R regeneration based on dispersion-imbalanced loop mirror and its applications in WDM systems', J. of Lightwave Technol., Vol. 20, pp. 1809-1817, Oct. 2002.

[187] A. Gray, Z. Huang, Y. W. A. Lee, I. Y. Khrushchev, and I. Bennion, 'Experimental observation of autosoliton propagation in a dispersion managed system guided by nonlinear optical loop mirrors', Opt. Lett., Vol. 29-9, pp. 926-928 (2004).

[188] The actual simulation work was carried out by Z. Huang and is included only for comparison purposes.

[189] A. Naka, T. Matsuda, and S. Saito, 'Optical RZ single straight line transmission experiments with dispersion compensation over 5520km at 20Gbit/s and 2160km at 2x20Gbit/s', Electron. Lett., Vol. 32-18, pp. 1694-1695 (1996).

[190] M. Nakazawa, K. Suzuki, E. Yamada, and Y. Kimura, '20Gbit/s soliton transmission over 200km using erbium-doped fibre repeaters', Electron. Lett., Vol. 26-19, pp.1592-1593 (1990).

[191] F. Favre and D. LeGuen, '20Gbit/s soliton transmission over 19Mm using sliding-frequency guiding filters', Electron. Lett., Vol. 31-12, pp. 991-992 (1995).

[192] S. Bigo, P. Brindel, O. Leclerc, E. Brun-Maunand, and E. Desurvire, 'Error-free soliton transmission at 20Gbit/s over 7150km through all-optical synchronous phase modulation', Elecron. Lett., Vol. 33-6, pp.449-450 (1997).

[193] G. Aubin, E. Jeanney, T. Montalant, J. Moulu, F. Pirio, J. B. Thomine, and F. Devaux, "20Gbit/s soliton transmission over transoceanic distances with a 105km amplifier span", Electron. Lett., Vol. 31-13, pp.1079-1080 (1995).

[194] F. Seguineau, D. Rouvillain, H. Choumane, G. Aubin, J. L. Oudar, P. Brindel, B. Lavigne, and O. Leclerc, 'Regeneration capabilities of passive saturable absorber-based optical 2R in 20Gbit/s RZ DWDM long-haul transmissions', Electron. Lett., Vol. 39-11, pp. 857-858 (2003).

[195] A. Gray, Z. Huang, I. Khrushchev, I. Bennion, 'Autosoliton propagation at 80 Gbit/s using concatenated nonlinear loop switches in standard fibre', Electron. Lett., Vol. 40-8, pp. 498-500 (2004).

[196] Z. Huang, A. Gray, I. Y. Khrushchev, and I. Bennion, '10Gbit/s transmission over 100Mm of standard fibre using 2R regeneration in an optical loop mirror', Photon. Tech. Lett., to be published November 2004

[197] Khrushchev, I.Y., Phillips, I.D., Ellis, A.D., Manning, R.J., Nesset, D., Moodie, D.G., Penty, R.V., and White, I.H., 'OTDM applications of dispersion-imbalanced fibre loop mirror', Electron. Lett., 1999, 35, pp. 1183-1185.

[198] Agrawal, G. P., Nonlinear Fiber Optics, Academic Press, London, 1989, pp. 130-133.

[199] Gnauck, A. H., Raybon, G., Bernasconi, P. G., Leuthold, J., Doerr, C. R., and Stulz, L. W., '1Tb/s (6×170.6Gbit/s) transmission over 2000km NZDF using OTDM and RZ-DPSK format', IEEE Photon. Technol. Lett., 2003, 15, pp. 1618-1620

[200] Smith, N. J., and Doran, N. J., 'Picosecond soliton transmission using concatenated non-linear optical loop-mirror intensity filters', J. Opt. Soc. Am. B, 1995, 12, pp. 1117-1125.

[201] Matsumoto, M., Ideka, H., and Hasegawa, A., 'Suppression of noise accumulation in bandwidth-limited soliton transmission by means of non-linear loop mirrors', Opt. Lett., 1994, 19, pp. 183-185.

[202] Huang, Z., Gray, A., Khrushchev, I. Y., and Bennion, I., '40Gb/s transmission over 4000km of standard fibre using in-line non-linear optical loop mirrors', 29th European Conference on Optical Communication (ECOC2003), Rimini, Italy, 2003, Paper Mo4.6.3

APPENDIX A PUBLISHED PAPERS

"All-Raman amplified transmission at 40Gbit/s in standard single mode fibre", Z. Huang, A. Gray, Y.W.A. Lee, I.Y. Khrushchev, I. Bennion, CJ4-4-Tue, CLEO/Europe, Munich, Germany (2003).

"40Gbit/s transmission over 4000km of standard fibre using in line non-linear optical loop mirrors", Z. Huang, A. Gray, Y.W.A. Lee, I. Khrushchev, I. Bennion, Mo4.5.3, ECOC, Rimini, Italy (September 2003).

"Experimental observation of autosoliton propagation in a dispersion managed system guided by non-linear optical loop mirrors", A. Gray, Z. Huang, Y.W.A. Lee, I. Khrushchev, I. Bennion, OSA Opt. Lett., Vol. 29, pp. 926-928, May 2004.

"Autosoliton propagation at 80Gbit/s in standard fibre using in-line non-linear loop switches", A. Gray, Z. Huang, I. Khrushchev, I. Bennion, *CThQ, CLEO/IQEC, San Francisco, California, USA (May 2004).*

"Autosoliton propagation at 80Gbit/s using concatenated non-linear loop switches in standard fibre", A. Gray, Z. Huang, I. Khrushchev, I. Bennion, *IEE Electron. Lett.*, Vol. 40, pp. 498-500, April 2004.

"10Gbit/s Transmission over Unlimited Distance in Standard Fibre Using 2R Regeneration", Z. Huang, A. Gray, I. Khrushchev, I. Bennion, Th3.5.5, ECOC, Stockholm, Sweden (September 2004).

"Evolution of Timing Jitter in Non-linearly-Guided, Dispersion Managed Transmission Systems", A. Gray, Z. Huang, I. Khrushchev, I. Bennion, We4.P.117, ECOC, Stockholm, Sweden (September 2004).

"10Gbit/s Transmission over 100Mm of Standard Fibre using 2R Regeneration in an Optical Loop Mirror", Z. Huang, A. Gray, I. Y. Khrushchev, I. Bennion, Accepted IEEE Photonics Technology Letters 7/04, to be published 11/04.

"Propagation of unequal OTDM data channels in 2R regenerated system", Z. Huang, A. Gray, I. Y. Khrushchev, I. Bennion, OpNeTec 2004, Pisa, Italy (October 2004).

"Transmission of non-uniform OTDM channels in a nonlinearly-guided dispersion-managed fibre system", Z. Huang, A. Gray, I. Y. Khrushchev, I. Bennion, accepted IEE Electronics Letters 6/04.

"Unequal OTDM Channels in a 2R Regenerated, Dispersion Managed Transmission System", Z. Huang, A. Gray, I. Y. Khrushchev, I. Bennion, OME66, OFC 2005, Anaheim, California, USA (March 2005).